AD-A051 851 HUGHES AIRCRAFT CO EL SEGUNDO CALIF SPACE AND COMMUN--ETC F/G 10/2
GAAS CONCENTRATOR PHOTOVOLTAIC POWER SYSTEM FEASIBILITY INVESTI--ETC(U)
DEC 77 S KAMATH, R C KNECHTLI, S SCHWARTZ F33615-76-C-2142
UNCLASSIFIED SCG-70392P AFAPL-TR-77-80 NL

1 OF 2
AD
A051851

AFAPL-TR-77-80

GaAs CONCENTRATOR PHOTOVOLTAIC POWER SYSTEM FEASIBILITY INVESTIGATION

Hughes Aircraft Company
Space and Communications Group
El Segundo, California

Contract No. F33615-76-C-2142

DECEMBER 1977

FINAL REPORT 15 JUNE 1976 – 30 SEPTEMBER 1977

Air Force Aeropropulsion
Air Force Wright-Aeronautical Laboratories
Air Force Systems Command
Wright-Patterson Air Force Base, Ohio 45433

NOTICE

When Government drawings, specifications, or other data are used for any purpose other than in connection with a definitely related Government procurement operation, the United States Government thereby incurs no responsibility nor any obligation whatsoever; and the fact that the Government may have formulated, furnished, or in any way supplied the said drawings, specifications, or other data, is not to be regarded by implication or otherwise as in any manner licensing the holder or any other person or corporation, or conveying any rights or permission to manufacture, use, or sell any patented invention that may in any way be related thereto.

This report has been reviewed by the Information Office (OI) and is releasable to the National Technical Information Service (NTIS). At NTIS, it will be available to the general public, including foreign nations.

This technical report has been reviewed and is approved for publication.

Lowell D. Massie
LOWELL D. MASSIE
Project Engineer

R. R. Barthelemy
R.R. BARTHELEMY
Actg Ch, Energy Conversion Branch

FOR THE COMMANDER

James D. Reams
JAMES D. REAMS
Chief, Aerospace Power Division

AFAPL/POE

"If your address has changed, if you wish to be removed from our mailing list or if the addressee is no longer employed by your organization please notify AFAPL/POE , Wright-Patterson Air Force Base, Ohio 45433 to help us maintain a current mailing list".

Copies of this report should not be returned unless return is required by security considerations, contractual obligations, or notice on a specific document.

AIR FORCE/56780/1 March 1978 — 250

SECURITY CLASSIFICATION OF THIS PAGE (When Data Entered)

REPORT DOCUMENTATION PAGE

READ INSTRUCTIONS BEFORE COMPLETING FORM

1. REPORT NUMBER: AFAPL-TR-77-80
2. GOVT ACCESSION NO.
3. RECIPIENT'S CATALOG NUMBER

4. TITLE (and Subtitle)
GaAs CONCENTRATOR PHOTOVOLTAIC POWER SYSTEM FEASIBILITY INVESTIGATION

5. TYPE OF REPORT & PERIOD COVERED
Final Report.
15 Jun 76 - 30 Sep 77

6. PERFORMING ORG. REPORT NUMBER
SCG-71392P

7. AUTHOR(s)
S. Kamath, R. C. Knechtli, S. Schwartz, G. Wolff

8. CONTRACT OR GRANT NUMBER(s)
F33615-76-C-2142

9. PERFORMING ORGANIZATION NAME AND ADDRESS
Hughes Aircraft Company
Space and Communications Group
El Segundo, California 90245

10. PROGRAM ELEMENT, PROJECT, TASK AREA & WORK UNIT NUMBERS
Program Element: 63401F
Project: 682J Task: 68233
W.U.: 682J0403

11. CONTROLLING OFFICE NAME AND ADDRESS
Air Force Aero Propulsion Laboratory (POE)
Air Force Wright - Aeronautical Laboratories (AFSC) WPARB, OH 45433

12. REPORT DATE
Dec 77

13. NUMBER OF PAGES
95

14. MONITORING AGENCY NAME & ADDRESS (if different from Controlling Office)

15. SECURITY CLASS. (of this report)
Unclassified

15a. DECLASSIFICATION/DOWNGRADING SCHEDULE

99 p.

16. DISTRIBUTION STATEMENT (of this Report)
APPROVED FOR PUBLIC RELEASE;
DISTRIBUTION UNLIMITED

17. DISTRIBUTION STATEMENT (of the abstract entered in Block 20, if different from Report)

18. SUPPLEMENTARY NOTES

19. KEY WORDS (Continue on reverse side if necessary and identify by block number)
Advanced GaAs Solar Cells, Solar Energy Conversion, Space Power, Radiation Effects, Temperature Coefficients, Sunlight Concentrators, Welded Interconnects

20. ABSTRACT (Continue on reverse side if necessary and identify by block number)
A number of GaAs Solar Cells for high sunlight intensity operation were fabricated and experimentally evaluated. I-V characteristics were determined for 1, 5, and 9 solar constants. Temperature coefficients of OCV, SCC, and Pmax were determined for one sun GaAs cells by measuring cell electrical performance at 50C steps from -190 C to +250 C. Results of 1 Mev electron irradiation to 1 x 10^{16} Mev equivalent electrons/cm^2 and welded interconnect investigations are presented.

10 to the 16th
sq. cm.

DD FORM 1 JAN 73 1473 EDITION OF 1 NOV 65 IS OBSOLETE

UNCLASSIFIED
SECURITY CLASSIFICATION OF THIS PAGE (When Data Entered)

SUMMARY

This report covers the work performed on Contract No. F33615-76-C-2142 from the Air Force Aero Propulsion Laboratory (AFAPL) to study GaAs solar cells for a concentrator space power system from June 1976 to October 1977.

The objective of the program was to fabricate GaAs solar cells optimized for space applications at low solar concentration ratios and to design a concentrator for optimum performance. Because of the critical importance of radiation damage characteristics of the cell for space use, the goals of the program were modified during the sixth month to emphasize this aspect of the solar cell characteristics. Further, the interconnect problem for array fabrication was added to study the methods for improving mechanical integrity of the package. The various sections of this report cover the work performed on all aspects of the program. Section II describes the cell optimization effort, the different concentrator designs tried, and their relative merits. Section III deals with the radiation testing and the significant progress made in this area by cell optimization. Section IV details the welding studies – the problems posed by various aspects of array fabrication, and the solutions achieved. Conclusions concerning overall program objectives are presented in Section V. An appendix is attached that discusses in detail the temperature behavior of the GaAs cells, especially under solar concentrations, using the concentrator designs proposed.

TABLE OF CONTENTS

LIST OF ILLUSTRATIONS

LIST OF TABLES

SECTION I

PROGRAM OBJECTIVES

The objective of this effort was to investigate the feasibility of a concentrating GaAs solar cell space power system. Cell development for concentration, cell characterization, and a concentrator design study were a part of this effort.

1.1 ORIGINAL OBJECTIVES

The technical plan proposed for meeting the objectives outlined above divided the work of the program into six discrete tasks:

Task I	Modify/optimize existing Hughes Research Laboratories (GaAl) As/GaAs solar cells as required for operation up to 20 suns.
Task II	Fabricate 20 of these cells.
Task III	Electrically characterize the cells fabricated.
Task IV	Design and analytically evaluate a reflector type (Cassegrain) and a Fresnel lens type concentrator and assess the feasibility of applying concentrator-cells technology to earth orbiting spacecraft.
Task V	Provide a Fresnel lens and assemble a laboratory test unit along with two 5 cell strings of GaAs solar cells produced under Task II.
Task VI	Test the unit produced in Task V.

A detailed description of each of these tasks, including the analytical and testing approaches proposed, was developed and submitted AFAPL in July 1976 as the program Technical Plan.

1.2 MODIFIED PROGRAM OBJECTIVES

During the sixth month of the program, with the completion of the cell optimization for multisun application phase (Task I), the status of all program tasks was reviewed and stood as follows:

Task I	Complete.

Task II	Twelve of twenty cells fabricated.
Task III	One cell of the final design electrically characterized at 25°C and at 1, 5, and 9 suns illumination.
Task IV	Fresnel lens and reflector type concentrator designs completed; some preliminary aspects of the space systems investigation completed.
Task V	Fresnel lens concentrator system assembled and some initial efforts in the development of a welded interconnect technique completed.
Task VI	Not initiated.

Air Force and Hughes' concern at this time with the radiation resistant characteristics of GaAs solar cells for 1 sun application, and with the adequacy of existing cell interconnect techniques, suggested a modification of the program Technical Plan as the most desirable method of facilitating the orderly development of these cells. Previous electron irradiation testing of GaAs solar cells had determined the necessity of modifying these cells to provide increased radiation resistance. Revision of the program task descriptions would provide the means of conducting the testing necessary to verify the suitability of the envisioned cell modifications within the near term. In addition, the ability to pursue the development of suitable interconnection methods for such cells would provide increased confidence in the integrity of the cells being developed.

As a result of these considerations, and subsequent to a Hughes-AFAPL meeting of 15 December 1976, Hughes proposed the following modifications to the original program task descriptions:

Task I	No change.
Task II	Reduce the required number of cells fabricated for multisun applications from 20 to 12. Fabricate 8 cells designed for 1 sun application for additional electron irradiation testing. In addition, fabricate 15 cells to be used for studies of various cell interconnect techniques.
Task III	Delete any further testing of cells under multisun illumination. Determine the temperature coefficients of current and voltage at 1 sun illumination for the GaAs cell. The temperature range is to be -160° to +250°C with temperature steps of approximately 50°C.
Task IV	Suspend.
Task V	Delete fabrication of two 5 cell strings and their installation onto the assembled concentrator. Continue the development of the cell welded interconnect technique on 1 sun designed cells, and investigate alternate interconnection methods. Fifteen cells fabricated under Task II (1 sun optimized) would be employed for this development.

Task VI Delete all testing of the concentrator/cell system. Add radiation damage testing of cells optimized for 1 sun application. This testing to employ eight cells (1 sun optimized) fabricated under Task II.

With AFAPL approval, the above changes were incorporated into the program Technical Plan.

SECTION II

CONCENTRATOR SYSTEM DEVELOPMENT

2.1 CELL MODIFICATION, FABRICATION, and CHARACTERIZATION

2.1.1 General

Cell Modification

The solar cells used in this program were (GaAl) As-GaAs cells of the type developed by the Hughes Research Laboratories (HRL) and schematically illustrated in Figure 1. Representative performance of such a cell is illustrated in Figure 2 for AMO illumination (unity concentration ratio); these data show an AMO efficiency of 14.7 percent for that cell.

During this effort, two areas were investigated for feasibility of improving the cell: 1) cell contact, and 2) cell window. The (GaAl) As-GaAs solar cells made at HRL and illustrated above were designed for a unity solar concentration ratio. The HRL solar cell had therefore to be modified for use at higher concentration ratios. Such ratios produce higher current densities in the solar cell and put a premium on minimizing series resistance. For this reason, the contact geometry had to be redesigned, and the thickness and surface resistance of the GaAlAs window layer reoptimized.

The preferred type of junction selected was p on n, with the p-n junction within the GaAs, as illustrated in Figure 1. One reason for this selection was that in this configuration, the (GaAl)As/GaAs heterojunction is a p-p junction, has an ohmic characteristic (no potential barrier to majority carrier flow, no discontinuity in valence band energy), and provides the desired potential barrier to minority carrier (electron) flow from the GaAs to the (GaAl)As in the cell structure. This results from the fact that the sum of bandgap plus electron affinity is nearly constant in $Ga_{1-x}Al_xAs$, independently of the value of x. If an n on p configuration had been selected, the conduction band discontinuity at the n-GaAlAs/N-GaAs heterojunction might have led to a non-ohmic junction characteristic with potential barrier inhibiting the flow of both minority and majority carriers.

The (GaAl)As window determines the amount of incident solar energy reaching the junction area. (GaAl)As has an optical absorption coefficient which varies with photon energy h in the manner illustrated in Figure 3. The bandgap of the material is a function of the aluminum concentration, as

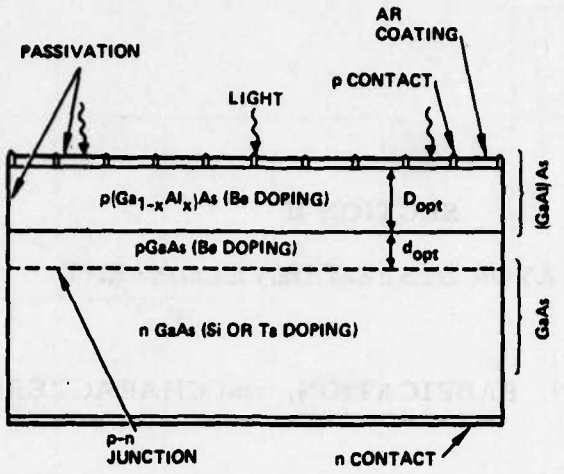

70392-1

FIGURE 1. SOLAR CELL DESIGN

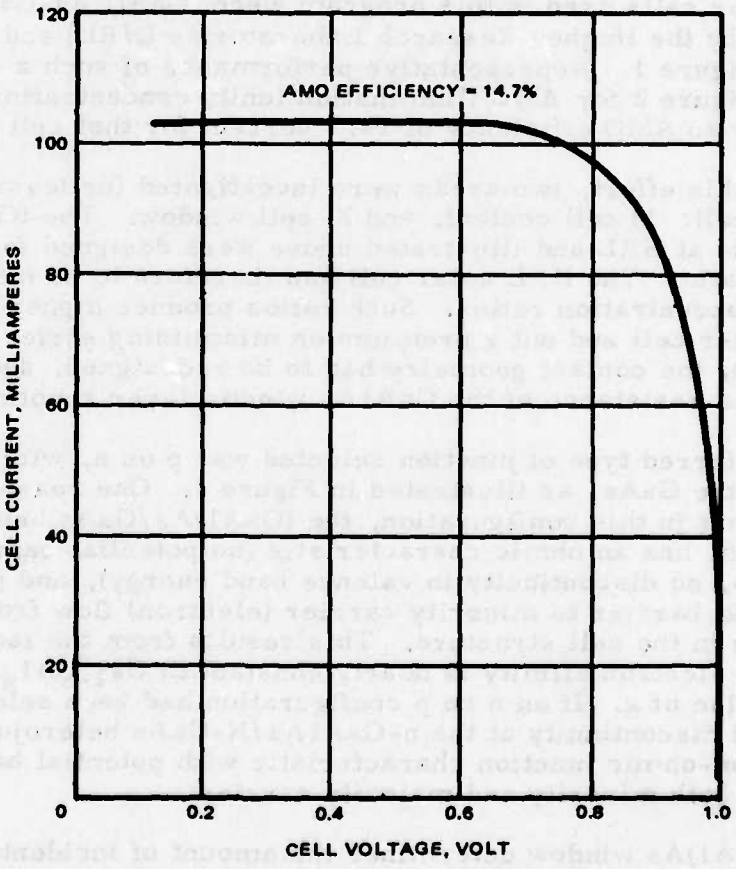

70392-2

FIGURE 2. SOLAR CELL AMO PERFORMANCE

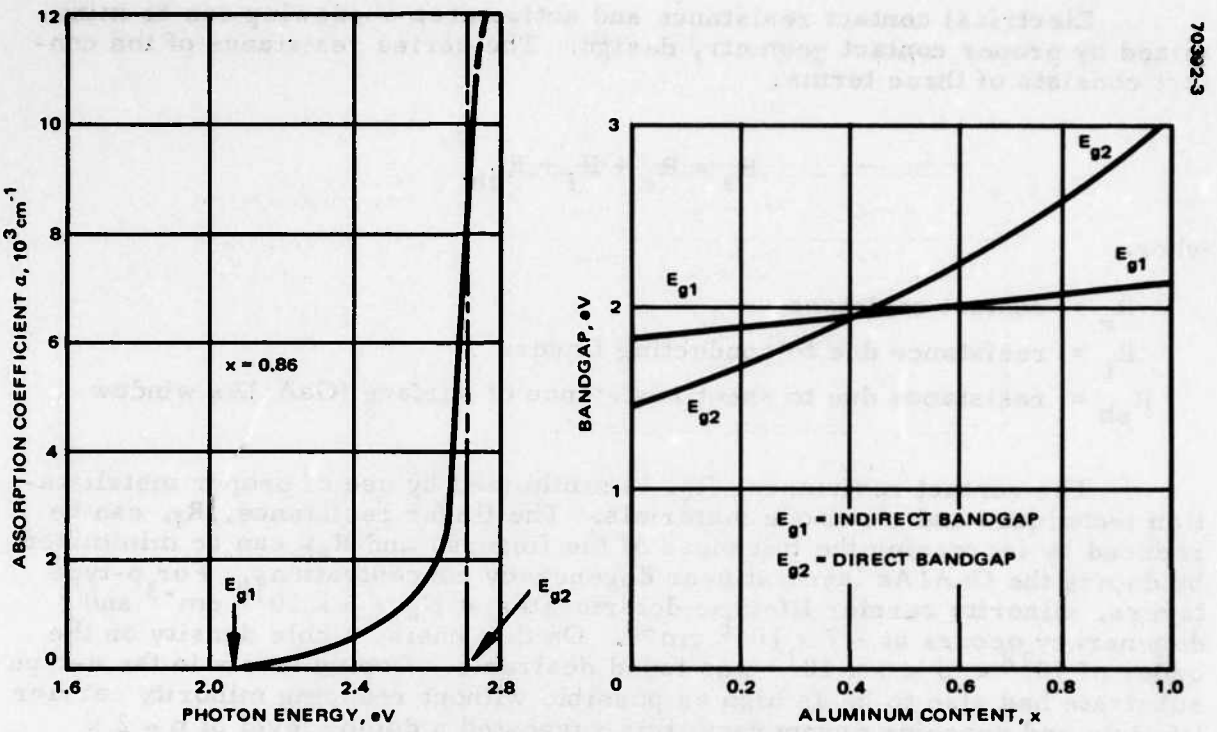

FIGURE 3. ABSORPTION COEFFICIENT AND BANDGAP FOR (GaAl)As SYSTEM

also shown in Figure 3. Photons absorbed in the surface (GaAl)As layer cannot reach the junction area; this results in a corresponding loss of cell output and efficiency. To minimize absorption in the (GaAl)As layer, the value of Eg_2 of the direct bandgap had to be as large as possible. Direct bandgap can be seen from Figure 3 to be maximized when the aluminum concentration is maximized. Hughes experience indicated no major problem in growing $(Ga_{1-x}Al_x)As$ layers with $x > 0.8$.

Light transmission was also planned to be increased by minimizing the (GaAl)As window thickness, D. With values of α between 10^4 and 10^5 cm^{-1}, and $h_\nu > E_{g2}$, absorption noticeably decreases with decreasing D, for $D < 1\mu$. In the region $E_{g1} < h_\nu < E_{g2}$, α can be as high as 10^3 cm^{-1}. Therefore, a value of 2 μm for D is an upper limit on the $Ga_{1-x}Al_xAs$ layer thickness to keep absorption losses acceptable. Cell output would be increased by up to 20 percent by letting $D \longrightarrow 0$.

Optimizing the window thickness D and making it reproducibly < 1 μm, was deemed feasible with the special technology developed at HRL and outlined below.

Electrical contact resistance and active area shadowing can be minimized by proper contact geometry design. The series resistance of the contact consists of three terms:

$$R_s = R_c + R_f + R_{sh}$$

where

R_c = contact resistance
R_f = resistance due to conducting fingers
R_{sh} = resistance due to sheet resistance of surface (GaAl)As window

The contact resistance, R_c, is minimized by use of proper metallization techniques and electrode materials. The finger resistance, R_f, can be reduced by increasing the thickness of the fingers, and R_{sh} can be minimized by doping the GaAlAs layer at near degeneracy concentrations. For p-type layers, minority carrier lifetime deteriorates at $N_a > 5 \times 10^{18}$ cm^{-3} and degeneracy occurs at $\sim 7 \times 10^{18}$ cm^{-3}. On this basis, a hole density on the order of $10^{18} < p < 5 \times 10^{18}$ was found desirable. Doping levels in the n-type substrate had also to be as high as possible without reducing minority carrier lifetime and reaching degeneracy; this suggested a doping level of $n \sim 2 \times 10^{-17}$ cm^{-3}. These factors were examined under the program to arrive at an optimum cell design.

Contact fabrication had heretofore been accomplished both by conventional masking techniques and by photolithography. The photolithography technique gave high resolution contact patterns capable of defining contact finger widths of 25 μm and less. Several contacting metal systems had been developed for both the p-type (GaAl)As layer and the n-type GaAs back contact. These metallizations resulted in the low resistance ohmic contacts necessary for high efficiency solar cells.

Cell Fabrication

The cells fabricated on this program were produced by the Hughes Research Laboratories developed method of reliably growing large area GaAs and GaAlAs layer by a modified infinite melt liquid phase epitaxy (LPE) process. The LPE system Hughes developed for its (AlGa)As solar cell fabrication is shown in Figure 4. It features an all quartz growth tube connected to a stainless steel entry chamber through a high vacuum valve. A saturated solution of high purity gallium arsenide dissolved in a mixture of 99.999 percent pure Ga and Al doped with Be serves as the growth matrix. The Al:Ga ratio can be adjusted to yield any desired value of Al in $Al_xGa_{1-x}As$. Once a specific solution for growth is prepared, it is maintained in an ambient of palladium-diffused hydrogen. During a long series of runs, all operations for layer growth, such as the introduction of the substrate, the seed or additional dopants, are performed by passing them through the entry chamber, which can be independently evacuated and flushed

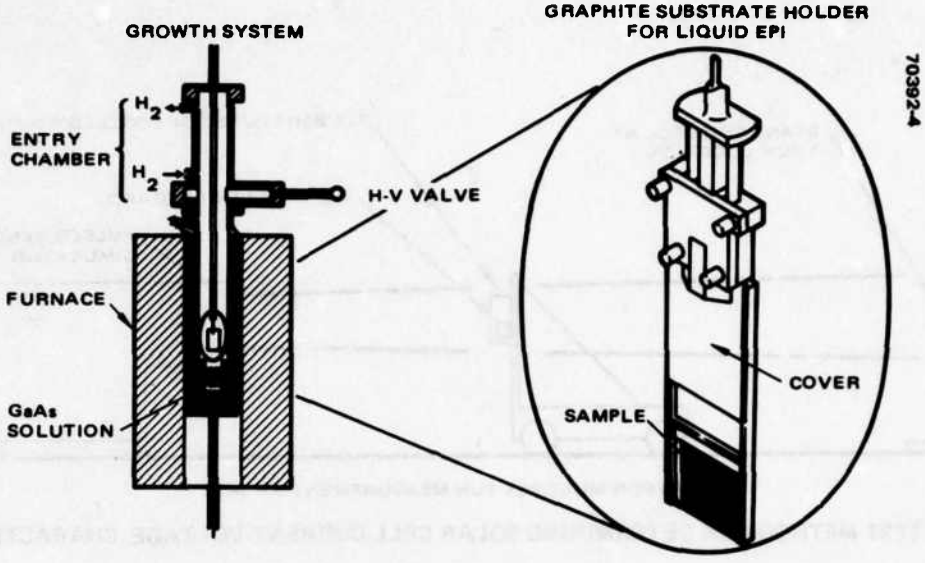

FIGURE 4. HUGHES LIQUID PHASE EPITAXY APPARATUS

with hydrogen before it is opened to the growth chamber. The capability of the system to handle large volumes of growth solution without danger of contamination from ambient gases, especially oxygen, can be seen from the fact that during a period of 2 years Hughes has grown more than (1000 layers) of $Al_{.95}Ga_{.05}As$ doped with Be from this system, with reproducible properties.

The layers grown have generally been 1 μm thick or less and show a variation in thickness of less than ±10 percent over substrates larger than 1 in^2 in area. The surfaces obtained are specular, and the layers are processed for solar cells without any further surface preparation.

This LPE system has also been used to grow tin doped n type GaAs layers on commercial n type substrates, since a high degree of variability in doping levels and crystal perfection in state of the art substrates has been observed. The LPE layers are much more reproducible in uniformity and homogeneity and have a lower dislocation density.

The major advantage of Hughes' LPE system is that it allows a long series of growth runs without loss of gallium and with a high yield in solar cells. Since one run only takes about an hour and several substrates can be processed simultaneously, the system can easily be adapted for large scale production, thus minimizing the cost of the solar cell.

Cell Electrical Characterization

Two solar cells selected from those fabricated under Task II were electrically characterized to determine a) temperature coefficients of current and voltage, and b) illumination level dependences of current and voltage.

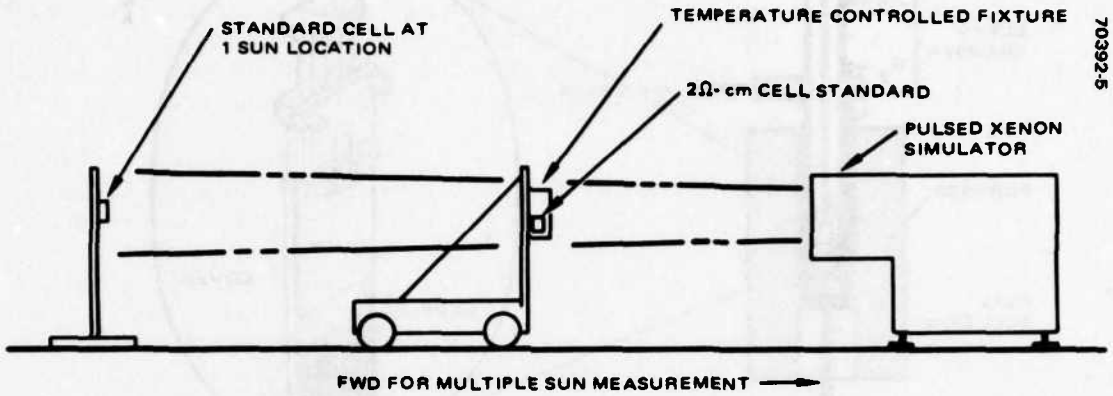

FIGURE 5. TEST METHOD FOR DETERMINING SOLAR CELL CURRENT-VOLTAGE CHARACTERISTICS

FIGURE 6. PULSED XENON SOLAR SIMULATOR (PHOTO ES25794)

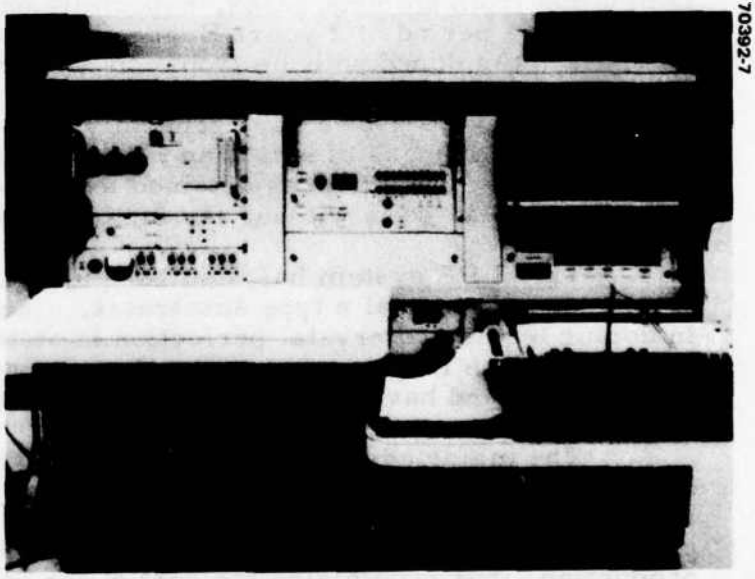

FIGURE 7. AUTOMATIC DATA ACQUISITION SYSTEM (PHOTO ES25058)

Parametric electrical data was obtained by generating current-voltage characteristics of the (GaAl)As solar cells over ranges of temperature and intensity of -160°C to +250°C and 1 to 20 suns respectively. Temperature steps were approximately every 50°C and intensity steps were approximately every 5 suns. Figure 5 shows the test method used for this investigation. A thermal-vacuum test chamber was employed in conjunction with the highly collimated Hughes pulsed xenon simulator, which approximates the spectrum and intensity of space sunlight.

The Hughes pulsed xenon solar simulator system is located in the solar panel manufacturing facility, a temperature-controlled clean room, and is used continuously in testing single solar cells, cell groups, and solar panels for flight spacecraft programs. The system (see Figure 6) yields an accuracy in solar simulation for testing solar cells and large solar panels not previously possible in the field of solar cell/panel testing. Test results are comparable of superior to high altitude ground based natural sunlight testing.

Cell characterization electrical data are obtained by simultaneously illuminating the test solar cells mounted in the thermal-vacuum fixture, an intensity reference test cell located adjacent to and in the thermal-vacuum fixture test plane, and a cell standard located at the 1 solar constant (135.3 mw/cm^2 intensity) test place. The test intensity is increased by moving the vacuum test fixture and reference cell closer to the simulator.

The automatic data acquisition system (Figure 7) simultaneously records the electrical performance of the solar cells on magnetic tape and on an x-y graph. From this data, a computer program analytically summarizes the solar cell performance characteristics.

The advantage of this test approach is that it allows accurate and precise data acquisition for single cells at high intensity levels by permitting testing in a controlled thermal environment without the thermal problems (heat flux) inherent with multisun steady state simulation; i.e., the bulk cell temperature is constant and controlled by the backs de-heating/cooling block of the test fixture.

To reduce the effects of spectral mismatch with AMO, the Hughes test technique uses specially selected standard cells. Hughes maintains a solar cell calibration system traceable to JPL balloon flown standard cells and routinely recalibrates all secondary cells used for electrical performance testing. For new type of cells which have not been flown, such as standard (GaAl)As, standards are created using Hughes established methods for absolute spectral response. Integration of absolute spectral response over the NASA standard AMO spectrum with this method has been shown to be within ±2 percent of JPL balloon flight, which corresponds to the precision of the actual balloon flights (i.e., flight to flight).

The multicell test fixture is a thermal-vacuum chamber with a highly transparent Suprasil II quartz window. The chamber test sample capacity is six 2 x 2 cm solar cells. The minimum usable temperature range is -170°

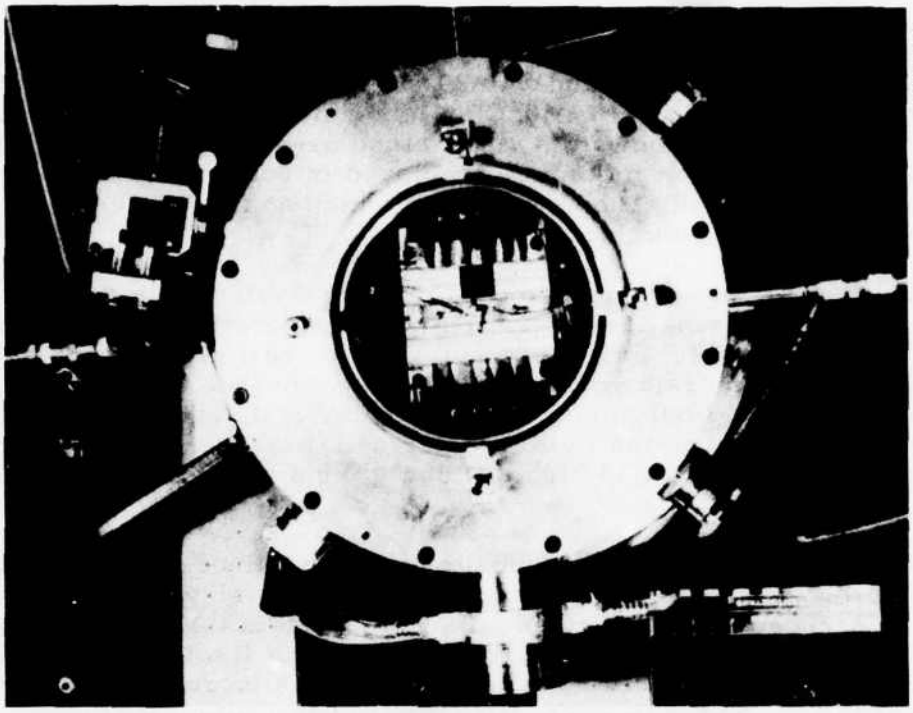

a) SHOWING INTENSITY REFERENCE CELL (PHOTO 4B00599)

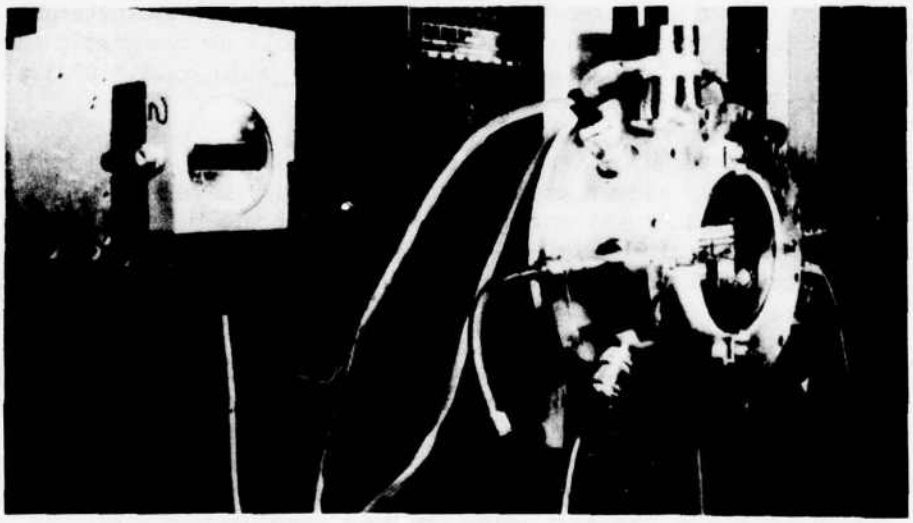

b) SHOWING SECONDARY STANDARD CELL (PHOTO 4B00600)

FIGURE 8. SOLAR CELL THERMAL-VACUUM TEST CHAMBER

to +250°C. In the chamber is a thermally controlled test block where the solar cells are mounted. The test block is temperature controlled by flowing LN_2 through the block and by electrical cartridge heaters mounted in the block. Thermocouples sense the test block and cell temperature. The solar cells are held to the block by positive tension spring probes which are the electrical contact for the top contact of the cell. Electrical and thermal contact to the cells is made to the back of the cells by pressure contact to the test block.

The thermal-vacuum chamber with the intensity reference cell in the test plane is shown in Figure 8a; in Figure 8b, the secondary standard cell is shown with the thermal-vacuum test chamber.

The intensity reference cell mounted in the same test plane as the test cells is a 2 ohm-cm cell. The 2 ohm-cm cell short circuit current (I_{SC}) output is linear as a function of intensity and therefore was used as the intensity reference for the test cells to a 10 sun level.

2.1.2 Task Development

Cell Modification, Fabrication

Cell Contact Geometry. Initial effort on the cell modification task was devoted to redesign of cell contact geometry. In a first step, the number of grid lines per cell was increased from 18 to 24. This, together with a decrease in grid line width, improved the spreading resistance in the GaAl As layer without increasing the area of the metallic contacts.

Subsequently, the number of grid lines was increased to 36. By this method the series resistance of the cell was decreased, without an increase in voltage loss, by keeping the shadowing ratio constant.

Front contact grid geometry can be defined on a solar cell by means of either a metal evaporation mask or by photolithography. The common technique at HRL employs a metallic shadow mask since it requires the fewest number of process steps.

HRL has available grid configurations of 18 lines, 24 lines, and 36 lines. The 18-line mask defines a conductive finger 0.003 inch wide by 0.745 inch long on 0.043 inch spacings. The 24-line finger dimension is 0.0015 inch wide by 0.765 inch long on 0.032 inch center-to-center spacings, and the 36-line finger measures 0.0015 inch wide by 0.765 inch long on 0.021 inch centers. The reason for increasing the number of grid lines on a solar cell becomes apparent when we compare the series resistance of the three types of cells.

The major contributor to series resistance in any cell is the sheet resistance of the front surface of the cell. For any value of sheet resistance

$R\square$, the series resistance R_{sr} can be expressed as $R_{sr} = \frac{R}{8} \left(\frac{b}{a}\right)^2$, where "b" is the line spacing dimension and "a" is the length of the fingers. We have then:

$$R_{sr_{18}} = \left[(1.06 \times 10^{-4})\, R\square\right]\Omega$$

$$R_{sr_{24}} = \left[(5.58 \times 10^{-5})\, R\square\right]\Omega$$

$$R_{sr_{36}} = \left[(2.42 \times 10^{-5})\, R\square\right]\Omega$$

where $R\square$ is any value of sheet resistance. The series resistance can be seen to be reduced by a factor of four in going from 18 to 36 grid lines.

The next parameter to be considered is the voltage drop along the grid line. This voltage can be expressed as:

$$\Delta V_f = j \cdot \left(\frac{b}{w}\right) \frac{a^2 \rho_f}{3h}$$

where j = current flowing in finger

b = spacing of fingers

w = width of finger

a = length of finger

ρ_f = conductivity of finger metal

h = height of finger

and $\left(\frac{w}{b}\right)$ is commonly defined as the shadowing ratio. We have:

$$\Delta V_{f_{18}} = 14.C$$

$$\Delta V_{f_{24}} = 21.3C$$

$$\Delta V_{f_{36}} = 14.C$$

if we include all the common parameters in a constant term. The ΔV_f for both the 18 and 36 grid lines is the same due to identical $\frac{W}{b}$ ratios. The ΔV_f

for the 24 line cell can be made compatible by increasing the height of the finger by 50 percent.

This simple treatment of front contact series resistance and voltage loss shows the attractiveness of having a greater number of grid lines. A more rigorous examination of these parameters leads to tapered grid lines for optimum high current operations. Tapered line masks are being designed for use at HRL and are expected to aid in increasing fill factor of the next generation of cells.

While aware of the limitations of the 24 and 36 finger masks, we decided to use them to determine the mechanical problems that arise when finger grid lines with close spacings are used. We had noticed in earlier work that the narrower fingers tend to have difficulties in establishing good uniform ohmic contacts and also tend to have random variations in thickness. For concentrated applications, these irregularities would not be tolerable.

Masks to make contacts with 24 and 36 fingers were obtained. The decreased finger width (1.5 mils) for which these masks were designed was, however, more demanding as far as control of the finger deposition process is concerned. The sputter-deposition and evaporation systems heretofore used for our contact fabrication were shared with other projects, a factor that interfered with the quality control required to go reproducibly to the desired larger number of narrower contact fingers. To obviate these difficulties, an independent contact fabrication system assigned exclusively to the GaAs solar cells was set up. This was an interim measure needed for the present project until a new solar cell fabrication laboratory (set up independently of this contract) became available to make cells for this contract. This latter lab, which includes a dedicated E-beam evaporation system for contact fabrication, became available in November 1976.

Cell Window Improvement. In parallel with the cell contact geometry effort, the influence of the thickness of the window layer on the power conversion efficiency of the cell was also studied. A number of GaAs wafers with $(Al_x Ga_{1-x})As$ window layers of the desired thickness (1/2, 1, 2, and 5 μm) for 1 μm were made for fabrication of the solar cells required for this contract. The key step still needed to complete these cells was the fabrication of a high quality 24 finger ohmic contact.

It had been hoped that the interim contact fabrication system mentioned above would be suitable for this purpose. Inadequate control over the oxide layer present on the (AlGa)As surface prior to evaporation in this system produced a more serious obstacle than originally anticipated. To make the required cells, the evaporation system was improved by incorporation of an ion gun for sputter-cleaning of the (AlGa)As surface prior to evaporation. Alternately, and as a backup, we also reverted to the sputter-deposition technique for the fabrication of a number of 24 finger cells, in parallel with cell fabrication in the improved evaporation system. Figure 9 shows a dark I-V curve for a typical cell with 24 fingers on 2 cm by 2 cm as

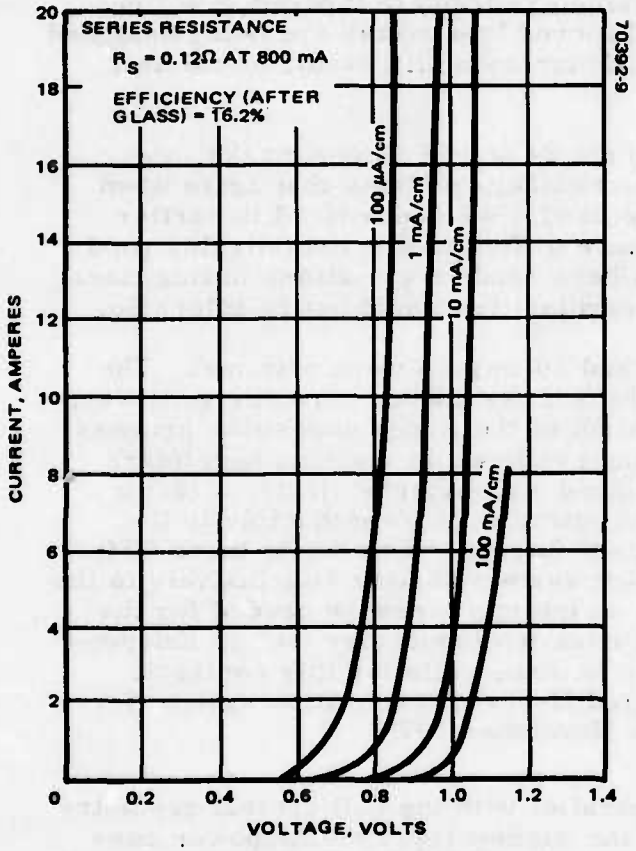

FIGURE 9. I-V CHARACTERISTICS (DARK) FOR TYPICAL 24 FINGER CELL

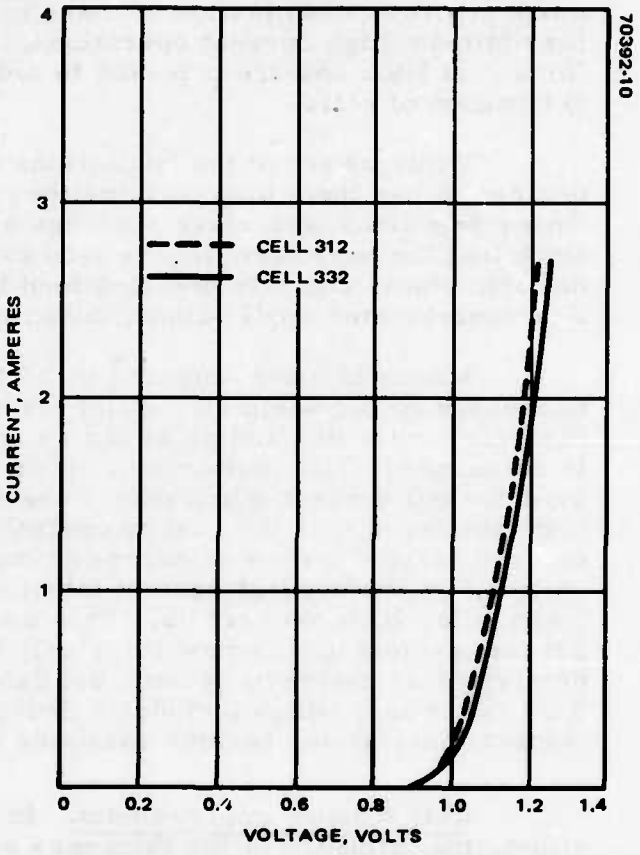

FIGURE 10. DARK I-V CURVES FOR CELLS 312 AND 332

fabricated today. The resistance of the cell at 800 mA current level has been calculated to be 0.12 ohms. Under concentration in the range of 10 suns, the current level will exceed 1 ampere, and the resistance of the cell should decrease even more. Further improvement contact geometry may result from optimization of the junction.

Cell Welding. In order to provide for ultimate cell operation to 250°C, it was found necessary to weld cell interconnects onto the cell contacts. Development of the proper weld technique for such interconnection was initiated. The selected cell interconnect was the Hughes GPD 1 mil thick silver interconnect. The basic technique employed was an ultrasonic rolling seam weld. Several iterations on the proper weld schedule for the GaAs cell were made with satisfactory welds being achieved. Difficulties in obtaining completely satisfactory welds seemed traceable to lack of sufficient contact adhesion to the GaAs substrate. This apparently resulted from the presence of an oxide layer on the wafer surface prior to contact deposition as discussed above.

Cell Characterization

The initial series of individual cell testing was used to determine the optimum window thickness for the 10 to 20 sun intensity level and to verify the satisfactory performance of the 24 finger ohmic front contact. This test series included testing cells at 5, 10, and 15 sun intensity levels at 25 and 50°C operating temperatures.

Initial emphasis was on making measurements of cell characteristics under small concentrations up to 8 suns. The two cells chosen were cells 312 and 332. Both have nominal 0.5 μm gallium aluminum arsenide window layers and an area of 4 cm^2 with 24 and 18 fingers, respectively, for the bar contacts on the p window layer. 312 had a cover glass and 332 none. Other parameters for the cells are given in Table 1. The experiment was designed to determine the practical limitations in using the thinnest window layer possible for the concentrator with a contact geometry that is simple and economical. Some loss of cell efficiency from increased optical loss was expected with increased window layer thickness, as a tradeoff against lower series resistance loss. The experiment was designed to give us a baseline reading with a thin window layer of 0.5 μm.

The dark I-V characteristics of the cell are shown in Figure 10. The series resistance of the cells is seen to be in the range of 0.063 ohm for the two cells. Figures 11 and 12 show the variation of the cell characteristics as a function of concentration. The curve factor for cell 312 seems to go down faster than for cell 332. We felt the main difference here may have been in thickness of the (GaAl)As window layer. Cell 312 probably has a somewhat thinner layer, as evidenced by the higher power conversion efficiency at low-concentration ratio.*

*The variance in cell efficiency indicated in Figure 10 and in Figures 11 and 12 arises from differences in simulators and test arrangements at HRL and at Hughes SCG.

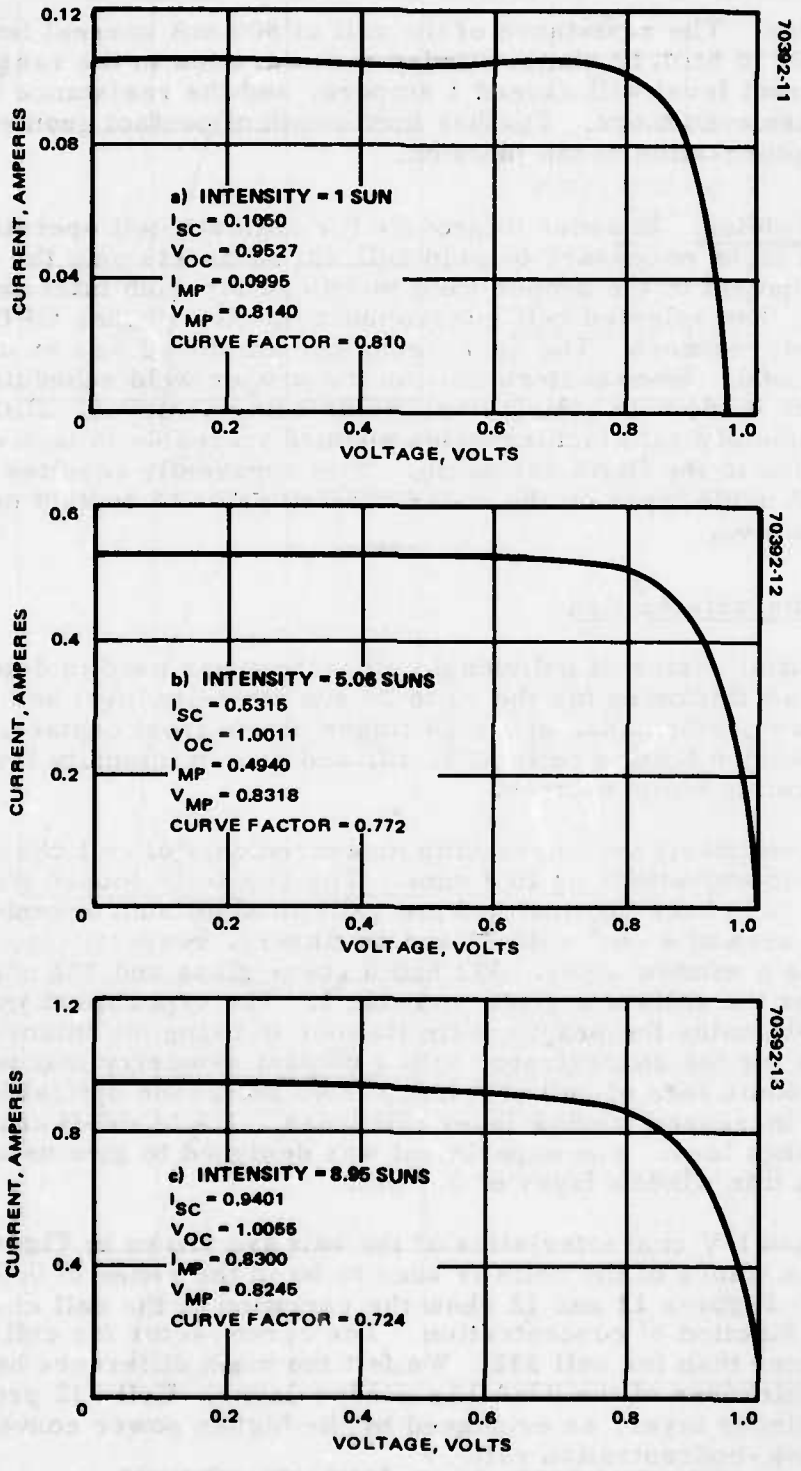

FIGURE 11. CELL PROFILE – 12 LINES/CM (CELL 312)

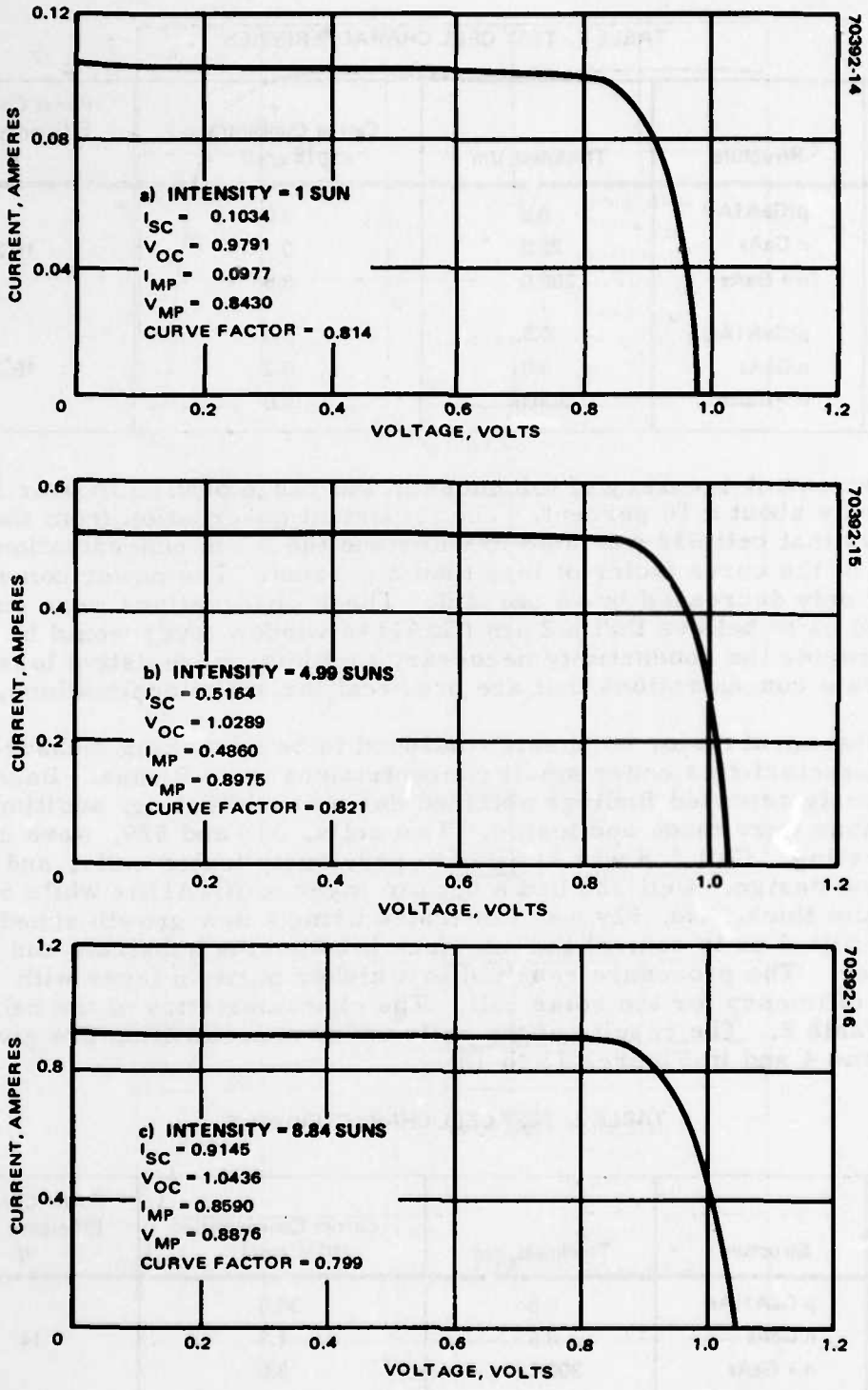

FIGURE 12. CELL PROFILE -- 9 LINES/CM (CELL 332)

TABLE 1. TEST CELL CHARACTERISTICS

Cell No.	Structure	Thickness, μm	Carrier Concentration x10^{18} cm^{-3}	Power Conversion Efficiency (AMO), η
	p(GaA1As)	0.5	3.0	
312	n GaAs	22.0	0.1	16.2
	n + GaAs	300.0	3.0	
	p(GaA1As)	0.5	3.0	
332	n GaAs	9.0	0.2	15.3
	n + GaAs	300.0	3.0	

The measurement accuracy of thickness in the range of 0.5 μm over large areas is only about ± 10 percent. The important observation from the experiments was that cell 332 was able to withstand the 8 sun concentration with a reduction of the curve factor of less than 2 percent. The power conversion efficiency only decreased by ~6 percent. These observations were encouraging and led us to believe that a 2 μm (GaA1)As window layer would be sufficient to provide the conductivity necessary to minimize resistive losses in the moderate concentrations that are practical for space applications.

Subsequent major emphasis continued to be on making measurements of cell characteristics under small concentrations up to 9 suns. Based upon the previously reported findings obtained during such testing, additional cell modifications were made and tested. Two cells, 328 and 529, were chosen for this testing. Cell 328 was similar to previously tested cells, and 529 was of the latest design. Cell 328 had a 0.5 μm layer of (GaA1)As while 529 had a layer 2 μm thick. No. 529 was fabricated using a new growth schedule which permitted us to control the interface between the substrate and the n buffer layer. The procedure resulted in a higher purity n layer with improved efficiency for the solar cell. The characteristics of the cells are given in Table 2. The results of the cells under concentration are given in Tables 3 and 4 and in Figures 13 to 18.

TABLE 2. TEST CELL CHARACTERISTICS

Cell No.	Structure	Thickness, μm	Carrier Concentration x10^{17} cm^{-3}	Power Conversion Efficiency (AMO), η
	p GaA1)As	0.5	30.0	
328	n GaAs	9.5	1.3	14
	n + GaAs	300.0	3.0	
	p GaA1) As	2.0	40.0	
529	n GaAs	12.0	0.3	16
	n + GaAs	300.0	7.0	

TABLE 3. MULTISUN TEST SCHEDULE: S/N 328

Tape	XEN019,	Temperature = 25°C
	Run No.	Intensity
	1	1 sun
	2	1 sun
	3	1 sun
	4	1 sun
	5	1 sun
	6	1 sun
	7	1 sun
Tape	XEN020,	Temperature = 25°C
	Run No.	Intensity
	1	5 suns
	2	5 suns
	4	9 suns
	5	9 suns

TABLE 4. MULTISUN TEST SCHEDULE: S/N 529

Tape	XEN024,	Temperature = 25°C
	Run No.	Intensity
	1	1 sun
	2	1 sun
	3	1 sun
	4	1 sun
	5	1 sun
	6	1 sun
	7	1 sun
Tape	XEN025,	Temperature = 25°C
	Run No.	Intensity
	1	5 suns
	2	5 suns
	3	9 suns
	4	9 suns
	5	9 suns

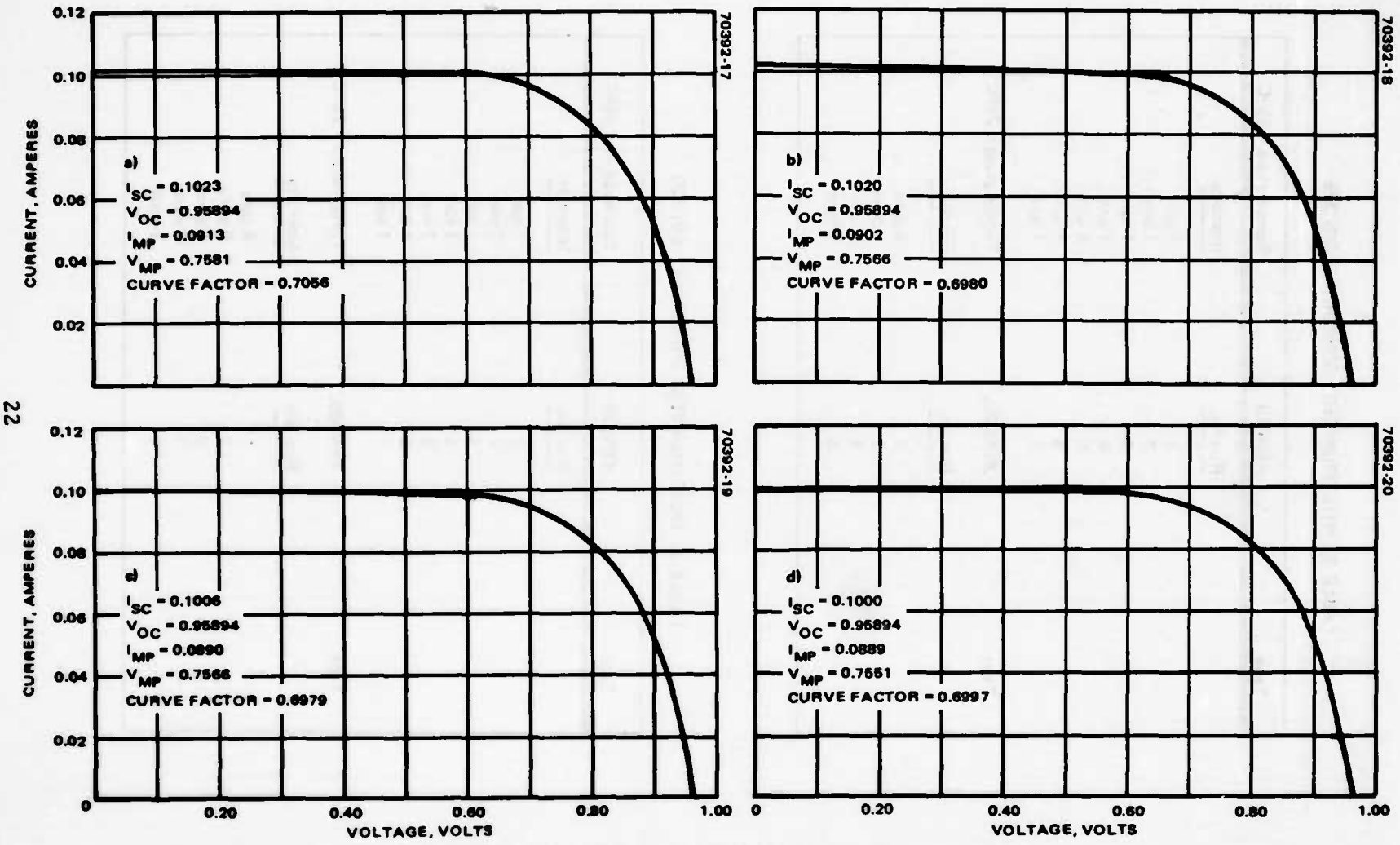

FIGURE 13. GaAs MULTISUN TEST: S/N 328 AT 1 SUN INTENSITY

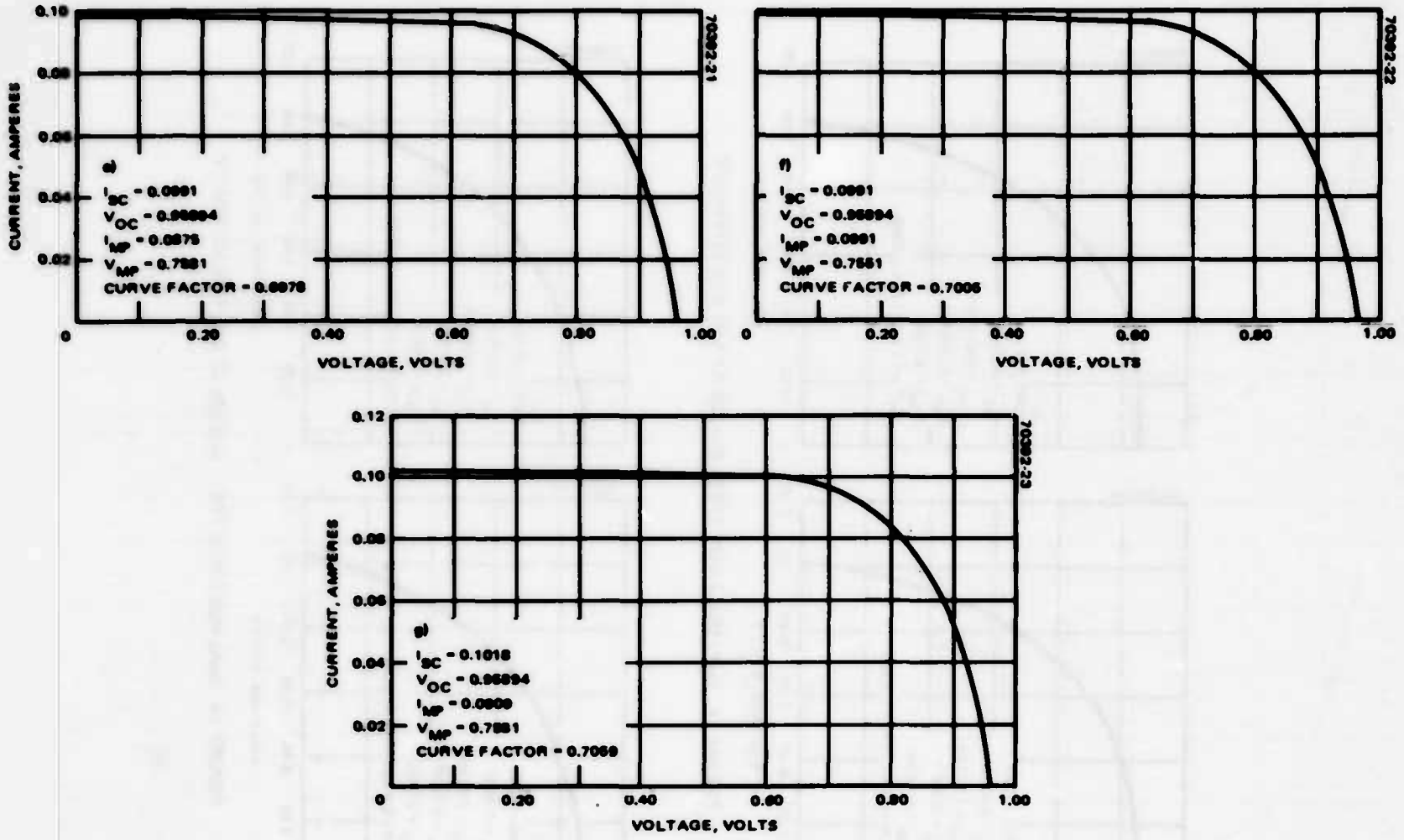

FIGURE 13 (CONTINUED). GaAs MULTISUN TEST: S/N 328 AT 1 SUN INTENSITY

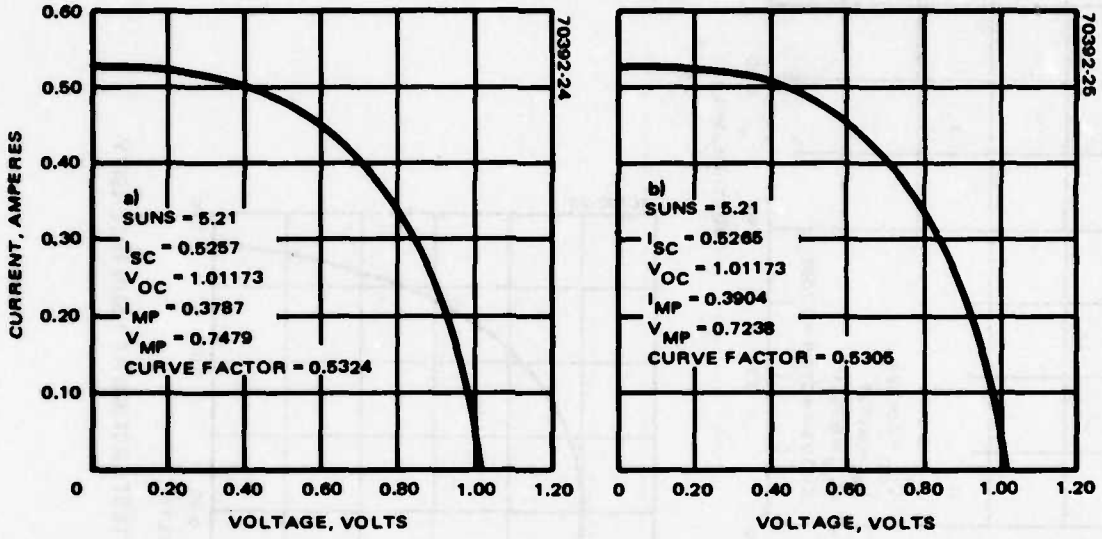

FIGURE 14. GaAs MULTISUN TEST: S/N 328 AT 5.21 SUN INTENSITY

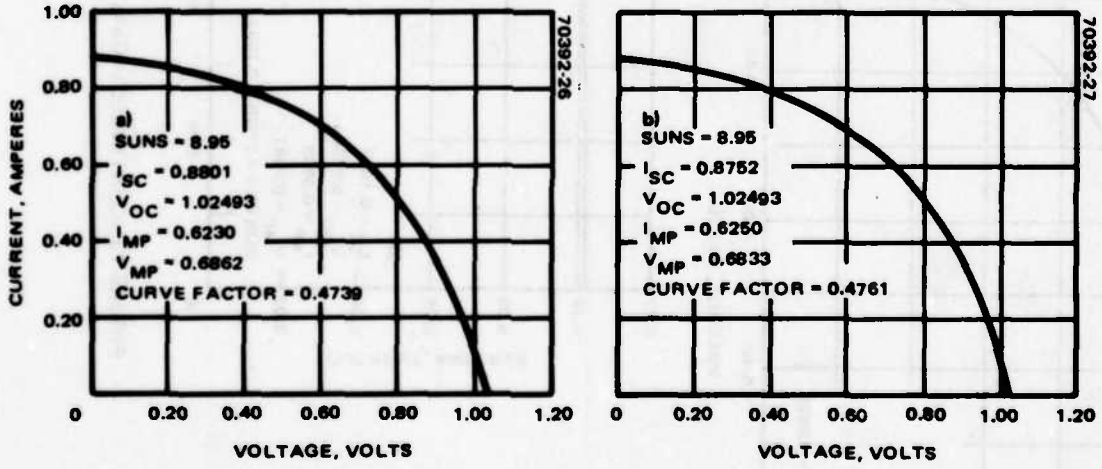

FIGURE 15. GaAs MULTISUN TEST: S/N 328 AT 8.95 SUN INTENSITY

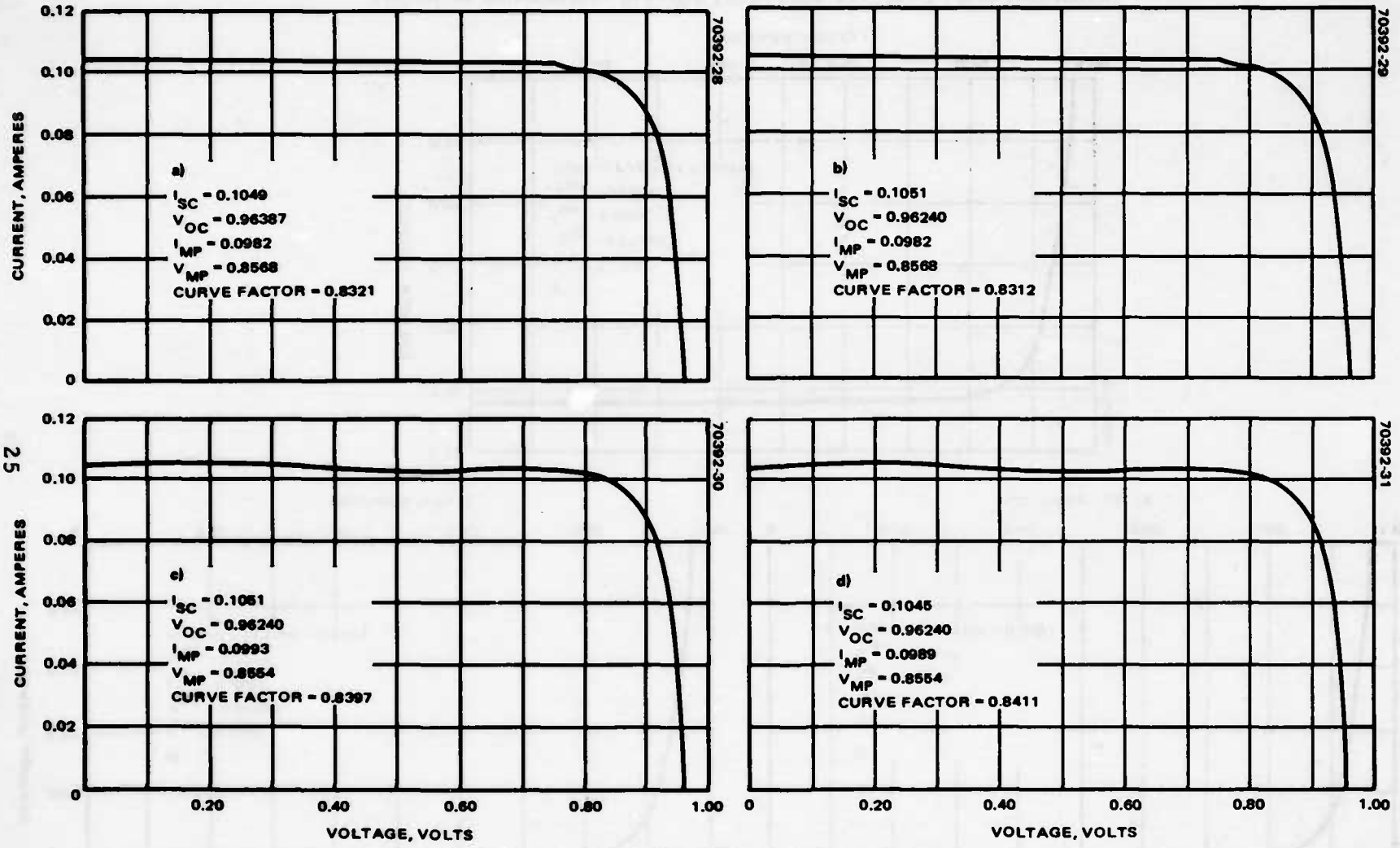

FIGURE 16. GaAs MULTISUN TEST: S/N 529 AT 1 SUN INTENSITY

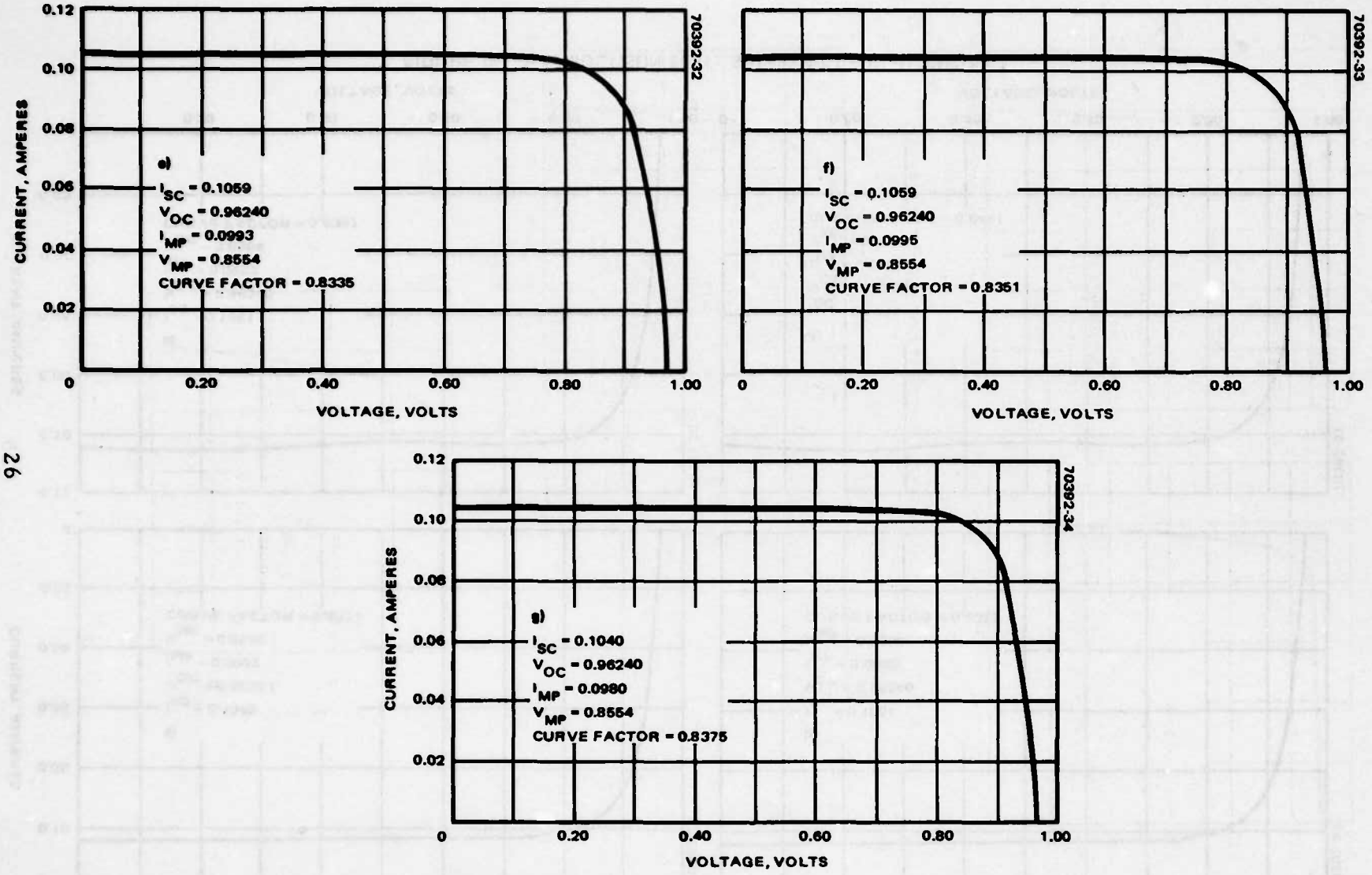

FIGURE 16 (CONTINUED). GaAs MULTISUN TEST: S/N 529 AT 1 SUN INTENSITY

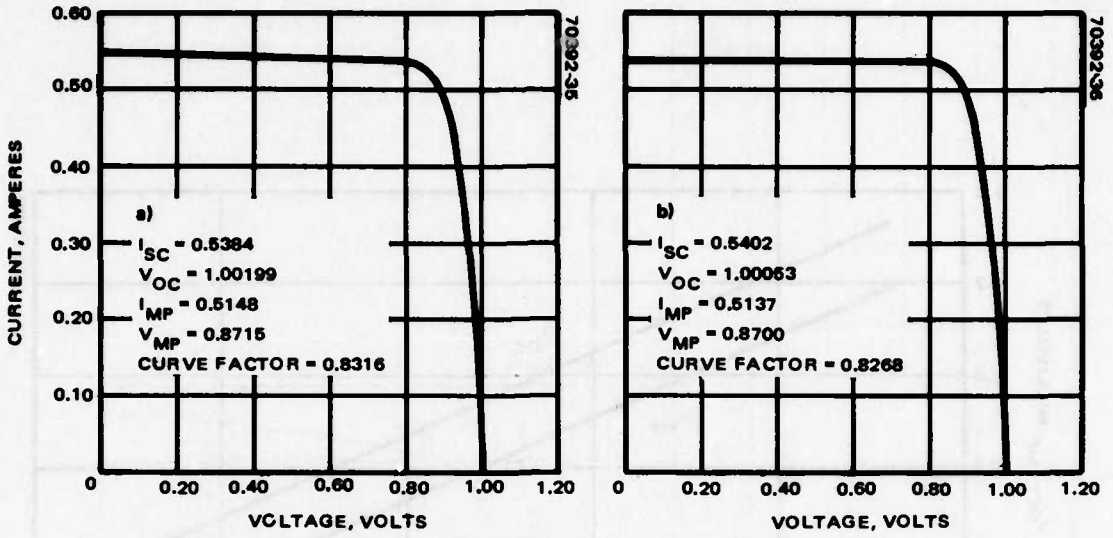

FIGURE 17. GaAs MULTISUN TEST: S/N 529 AT 5.07 SUN INTENSITY

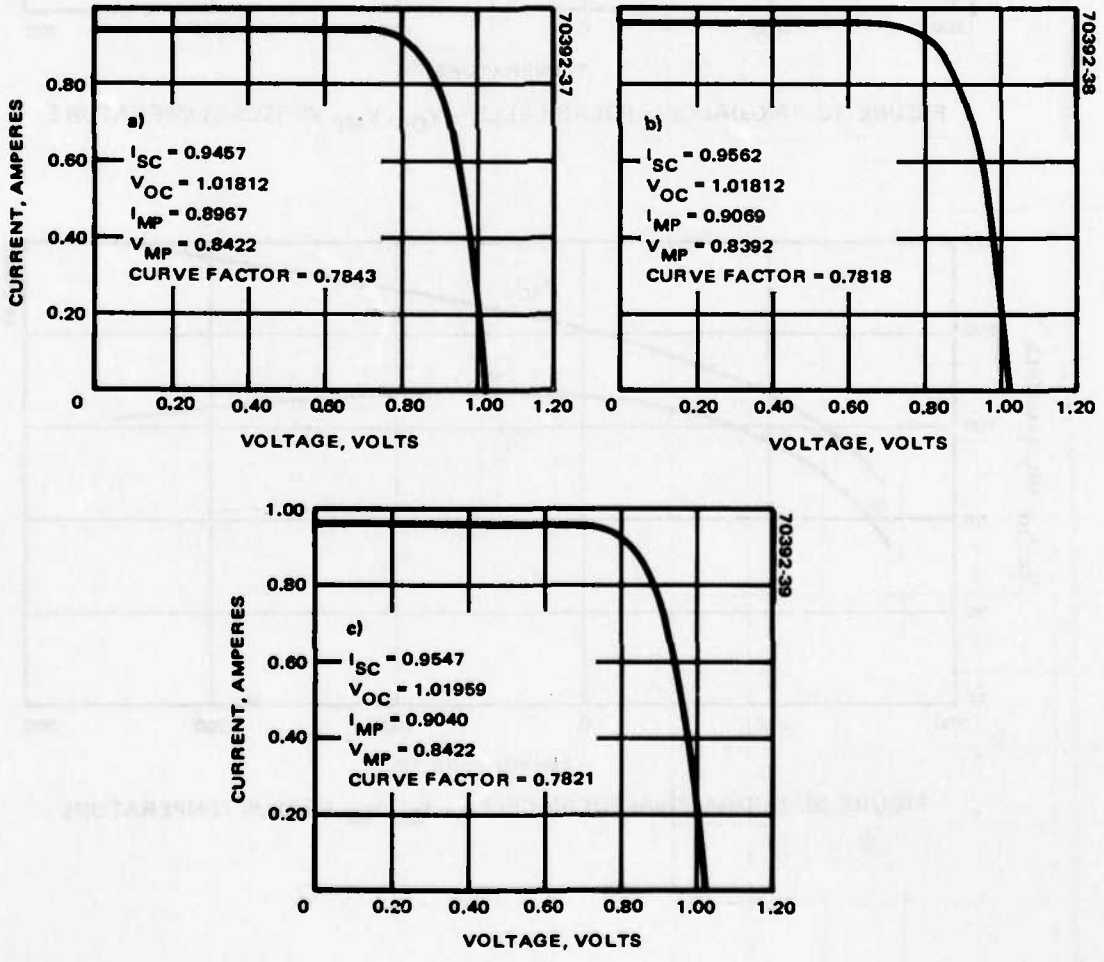

FIGURE 18. GaAs MULTISUN TEST: S/N 529 AT 9.08 SUN INTENSITY

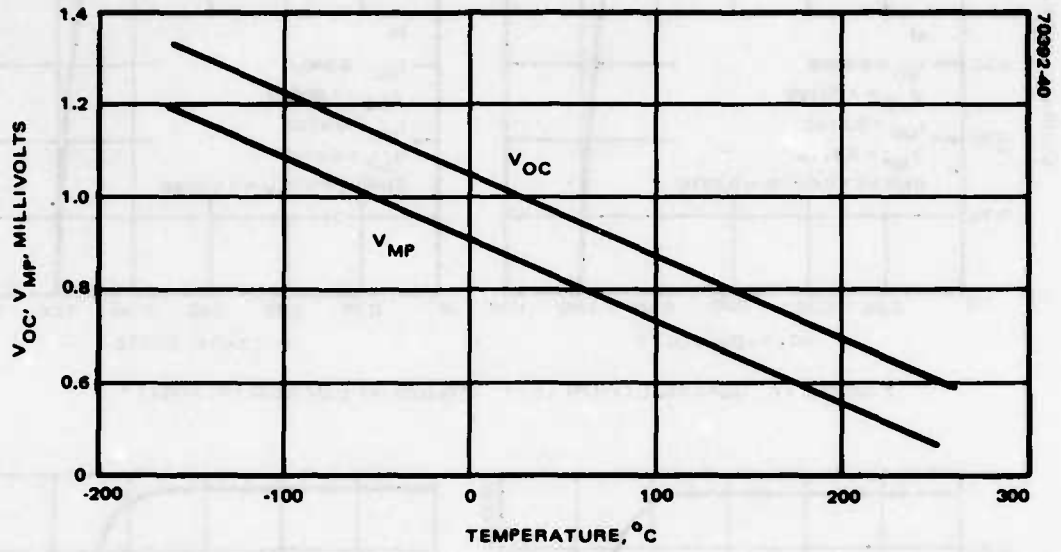

FIGURE 19. (AlGa)As/GaAs SOLAR CELLS – V_{OC}, V_{MP} VERSUS TEMPERATURE

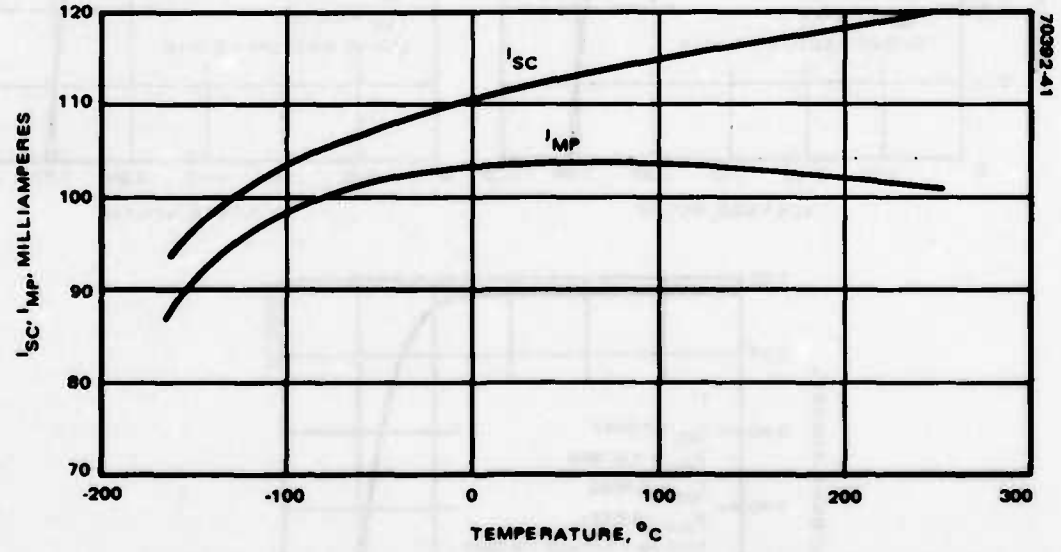

FIGURE 20. (AlGa)As/GaAs SOLAR CELLS – I_{SC}, I_{MP} VERSUS TEMPERATURE

The results confirmed our previous findings that a 2 μm layer of (GaAl)As is satisfactory for relatively low concentrations. While testing of cells with window layers of 1.3 μm and 3.0 μm was performed, these cells were damaged during handling, and reliable data were not obtained. However, the successful operation of the cell with the 2 μm window resulted in no requirement for retesting cells with other window thicknesses.

We subsequently manufactured an additional group of 10 cells with 2 μm windows for a total of 12 such cells, and analyzed their characteristics. These cells were used in the performance of the final testing required in this program, and thereafter delivered to AFAPL.

2.1.3 Cell Development Under Revised Program Plan

Cell Fabrication, Characterization

Under the revised program plan (See subsection 1.2), program enphasis was shifted to the replacement of the 12 cells produced for temperature coefficient testing with 12 new cells of more favorable construction. As previously noted, the first batch of cells prepared for use in space concentrators turned out to have problems in metallization for the contacts. Due to the fact that the sputtering system used previously for contact depositions was undergoing repairs and was thus unavailable, an electron beam system was used for contact evaporation. In addition, the parameters for etching, and the thickness of the zinc and gold, turned out to be more critical than at first assumed. As a result, the cells produced were unsatisfactory for the scheduled testing. Therefore, a replacement set of cells was made and metallized using the repaired sputtering system previously used. The cells have efficiencies in excess of 15 percent at AMO even with (GaAl)As window layers thicker than 1 to 2 μm. Measurements of I-V characteristics and spectral response were made on these cells, and they were remeasured after having gone through the temperature coefficient measurements. All the cells used in the present study were made using the new growth schedule which resulted in a buffer n-type epitaxial layer without significant substrate etching; this gave improved performance over solar cells grown previously.

The first 6 of the 12 replacement cells were delivered to Hughes, El Segundo for temperature coefficient testing. These tests were performed under the pulsed xenon solar simulator at an illumination level of 1 sun. The cells have (GaAl)As window layers $\gtrsim 2$ μm. They have AMO quantum efficiencies in excess of 15 percent and fill factors of over 0.80. Typical I-V and spectral response measurements were taken on these cells before they underwent testing at El Segundo. The measurements indicated that the cells are quite reproducible and uniform in their electrical and optical characteristics.

These tests have shown the variation of both current and voltage with cell temperature at a 1 sun intensity level. The results of this testing are given in Tables 5 and 6 and in Figures 19 and 20. Of the 12 cells

TABLE 5. AVERAGE MEASURED CELL PARAMETERS

T, °C	I_{sc}	V_{oc}	I_{mp}	V_{mp}
250.00	120.25	596.40	99.89	457.68
200.00	118.60	694.80	103.35	568.80
150.00	116.93	778.13	103.85	626.75
100.00	114.25	873.20	102.77	729.31
50.00	112.00	965.20	105.05	803.60
25.00	110.52	1014.40	103.55	859.20
0.00	109.72	1061.60	102.70	915.60
- 50.00	108.62	1152.80	102.17	1012.00
-100.00	106.00	1236.40	100.22	1095.20
-160.00	93.62	1326.00	85.67	1167.05

delivered, 4 cells were selected for testing. The results obtained from the 4 cells were relatively uniform and consistent, thus avoiding the necessity of testing all 12 cells. Table 5 contains the average values of the measured cell parameters, I_{sc}, V_{oc}, I_{mp}, and V_{mp} versus cell temperature. Table 6 contains the results from each individual cell. Figures 19 and 20 show the average results graphically. The results indicate the excellent performance of the gallium arsenide cell over the wide temperature range tested. The 12 cells, along with the test data (Appendix A of this report), and a silicon control cell were delivered to AFAPL in April 1977.

Preparation for Cell Interconnect Welding and Radiation Testing

These efforts were temporarily delayed because of the inavailability of the desired high quality cells. However, 12 cells were obtained from the High Efficiency GaAs Cell Development program. These cells had poor curve shape but did have good quality contacts, and were accordingly used for the initial weld schedule setup.

The welding machine was upgraded and 10 of the 15 cells required for the interconnect technique development were produced. Curves for these cells are shown in Figure 21. The 8 cells required for the radiation tests were manufactured along with cells delivered on the High Efficiency GaAs Solar Cell Development program. Radiation testing was scheduled at JPL during the first week in September. The results of these efforts are reported in Sections III (radiation testing) and IV (interconnect welding) respectively.

2.2 CONCENTRATOR DESIGN/DEVELOPMENT

Under this task, a reflector type (Cassegrainian) concentrator and a Fresnel lens type concentrator for use on earth orbiting spacecraft were conceptually designed and assessed to define rough order of magnitude system

TABLE 6. (AlGa)As/GaAs INDIVIDUAL CELL DATA

	T,°C	I_{sc}	V_{oc}	I_{mp}	V_{mp}	P_{mp}
GAA576	250.0	122.70	576.00	94.17	446.72	42.07
GAA576	200.0	121.20	678.40	99.40	535.20	53.20
GAA576	150.0	118.90	776.00	104.20	625.60	65.19
GAA576	100.0	115.90	873.60	105.17	713.15	75.00
GAA576	50.0	113.40	963.20	106.50	793.60	84.52
GAA576	25.0	111.80	1012.80	104.70	851.20	89.12
GAA576	0.0	111.10	1059.20	104.00	905.60	94.18
GAA576	- 50.0	109.60	1153.60	103.30	1011.20	104.46
GAA576	-100.0	106.80	1235.20	100.60	1113.60	112.03
GAA576	-160.0	94.20	1326.40	88.30	1185.60	104.69
GAA144	250.0	165.80	87.20	81.64	48.92	3.99
GAA144	200.0	161.00	188.80	119.47	117.42	14.03
GAA144	150.0	164.60	300.00	128.50	216.00	27.76
GAA144	100.0	160.70	404.00	142.20	299.20	42.55
GAA144	50.0	156.50	516.00	140.33	417.54	58.59
GAA144	25.0	154.20	572.00	144.90	459.20	66.54
GAA144	0.0	153.20	624.00	144.10	516.80	74.47
GAA144	- 50.0	148.10	728.00	139.60	630.40	88.00
GAA144	-100.0	139.10	824.00	130.70	731.20	95.57
GAA144	-160.0	126.10	944.00	111.79	870.40	97.22
GAA578	250.0	123.00	601.60	98.60	467.20	46.07
GAA578	200.0	120.50	696.00	108.20	608.80	65.87
GAA578	150.0	119.30	771.20	105.50	608.00	64.14
GAA578	100.0	115.10	875.20	101.50	726.40	73.73
GAA578	50.0	114.00	961.60	106.80	780.80	83.39
GAA578	25.0	112.50	1011.20	105.20	840.00	88.37
GAA578	0.0	111.30	1057.60	104.60	891.20	93.22
GAA578	- 50.0	110.00	1148.80	103.60	990.40	102.61
GAA578	-100.0	107.30	1235.20	101.60	1084.80	110.22
GAA578	-160.0	94.60	1323.20	87.22	1148.58	100.18
GAA584	250.0	119.60	606.40	105.00	460.80	48.38
GAA584	200.0	118.40	708.80	104.80	571.20	59.86
GAA584	100.0	115.10	868.80	101.61	748.08	76.02
GAA584	50.0	111.90	969.60	104.90	817.60	85.77
GAA584	25.0	110.70	1017.60	103.70	867.20	89.93
GAA584	0.0	110.00	1065.60	102.80	931.20	95.73
GAA584	- 50.0	109.20	1155.20	102.80	1017.60	104.61
GAA584	-100.0	106.00	1236.80	100.40	1084.80	108.91
GAA584	-160.0	93.80	1326.40	83.40	1179.20	98.35
GAA594	250.0	115.70	601.60	101.80	456.00	46.42
GAA594	200.0	114.30	696.00	101.00	560.00	56.56
GAA594	150.0	112.60	787.20	101.84	646.64	65.85
GAA594	100.0	110.90	875.20	102.80	729.60	75.00
GAA594	50.0	108.70	966.40	102.00	822.40	83.88
GAA594	25.0	107.10	1016.00	100.60	878.40	88.37
GAA594	0.0	106.50	1064.00	99.40	934.40	92.88
GAA594	- 50.0	105.70	1153.60	99.00	1028.80	101.85
GAA594	-100.0	103.90	1238.40	98.30	1097.60	107.89
GAA594	-160.0	91.90	1328.00	83.75	1154.82	96.71

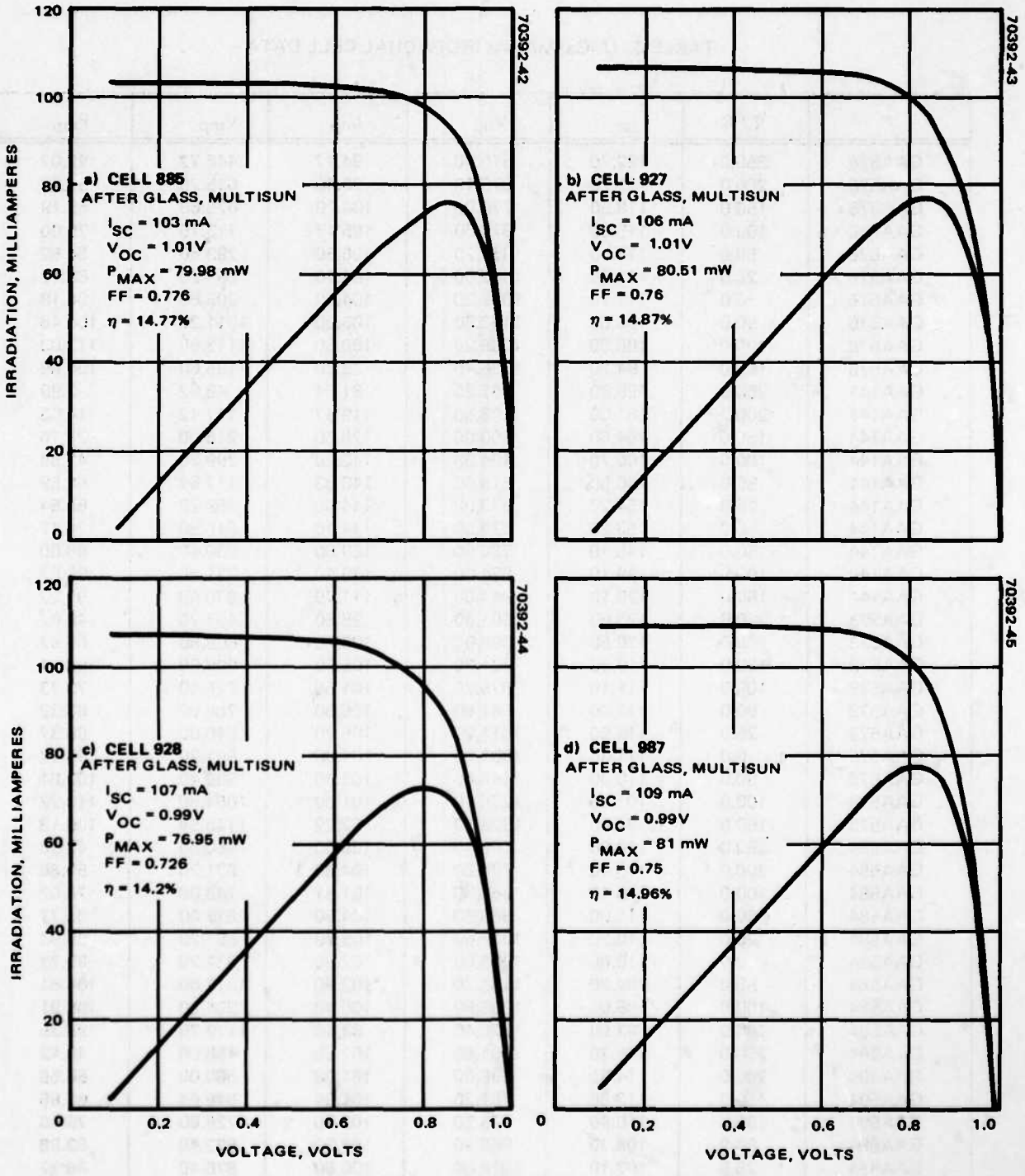

FIGURE 21. INTERCONNECT CELL CURVES

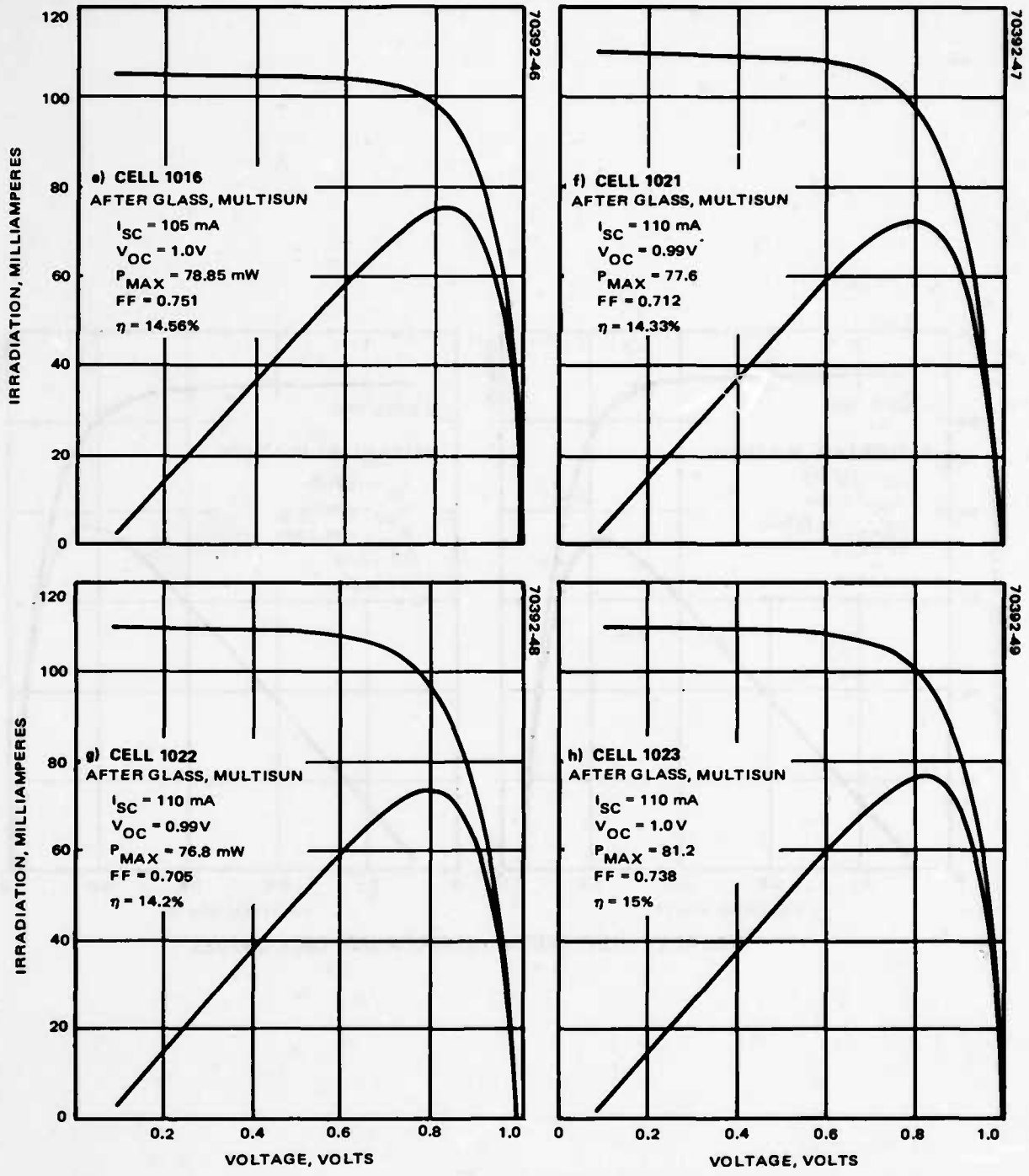

FIGURE 21 (CONTINUED). INTERCONNECT CELL CURVES

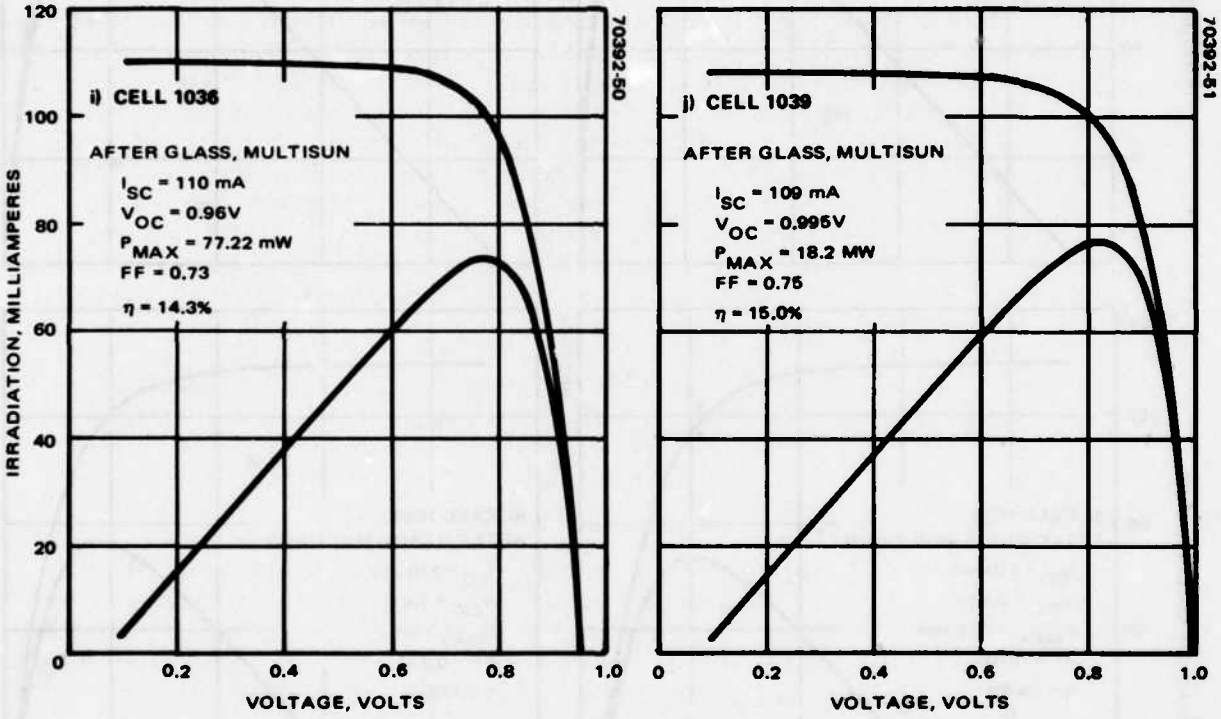

FIGURE 21 (CONTINUED). INTERCONNECT CELL CURVES

parameters to be used to indicate feasibility of the concepts. Specific system parameters estimated were watts per pound, system efficiency, and stored volume.

2.2.1 Fresnel Lens Concentrator

Work was inaugurated on this phase of the program with the purchase of Fresnel lenses from Randall Optics Co., Rostyn, New York. One 25 inch diameter lens of high quality was obtained and six 11 inch square lenses of somewhat lower quality were procured.

Two Fresnel lens holding fixtures were fabricated. One fixture holds a 6 inch by 37 inch cylindrical lens section designed to illuminate an assembly of five 2 cm^2 solar cells. The second fixture holds a 12 inch diameter circular lens designed to illuminate a single cell. It was decided to build two fixtrues because preliminary tests with the cylindrical lens obtained from Swedlow Plastics indicated that it was not capable of raising the temperature on each of the five cells as high as the circular lens could on one cell. Figure 22 shows the holding fixture made for the cylindrical lens; Figure 23 shows the similar fixture to be used for the circular lens. Both fixtures are designed to allow easy attachment and removal of the lens, variable focusing to allow increase or decrease of the line or spot size, and a tilting capability to follow the sun's declination.

The fixtures will be used to determine the efficiency of the GaAs cells at various temperatures. Thus, the cells will be mounted on a small, thermocouple-equipped heat sink block. Voltage and current measurements versus temperatures will be made to determine the cell efficiencies under various operating conditions.

It was also planned to determine the efficiency of a dichroic filter in reduction of IR radiation on the cell; the higher concentration ratio as given by the cylindrical lens makes these tests much more meaningful. Preliminary tests of this nature performed with a GaAs cell and a dichroic filter were conducted and the results reported in the document included here as Appendix B.

With the completion of the framework supports for the Fresnel lenses and the mounting of the solar cell, the Fresnel lens concentrator was assembled and shipped to WPAFB Aero Propulsion Laboratory in order to facilitate in-house testing by AFAPL personnel. The assembled concentrator is shown in Figure 24.

As proposed in the revised program plan, no further efforts were made to advance the concentrator design or development status. However, the reference data presented below were in preparation and are given here for future reference.

The weights shown in Table 7 were calculated for glass Fresnel lenses which have various concentration ratios. In determining the weights and concentration ratios, the following assumptions were made: 1) the solar

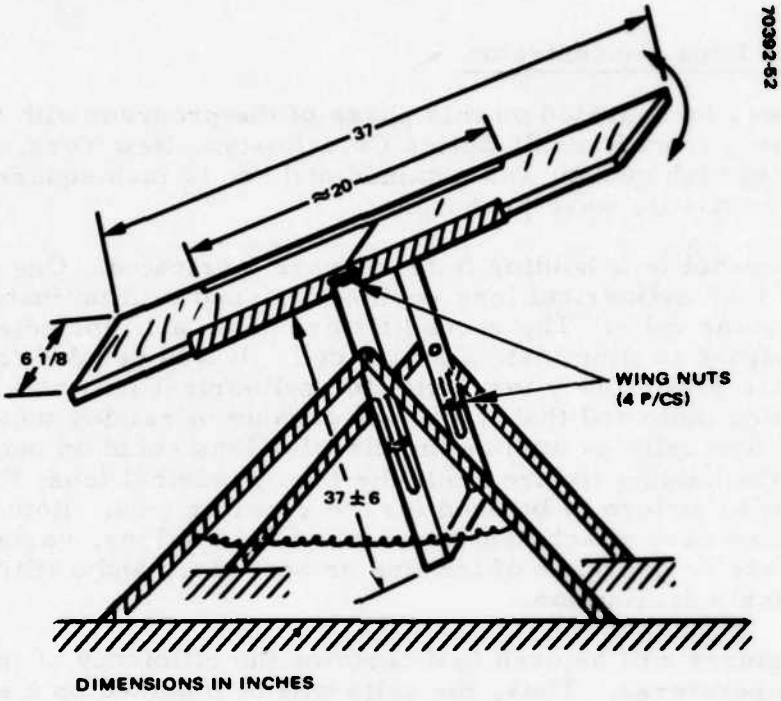

FIGURE 22. FRESNEL LENS STAND – CYLINDRICAL

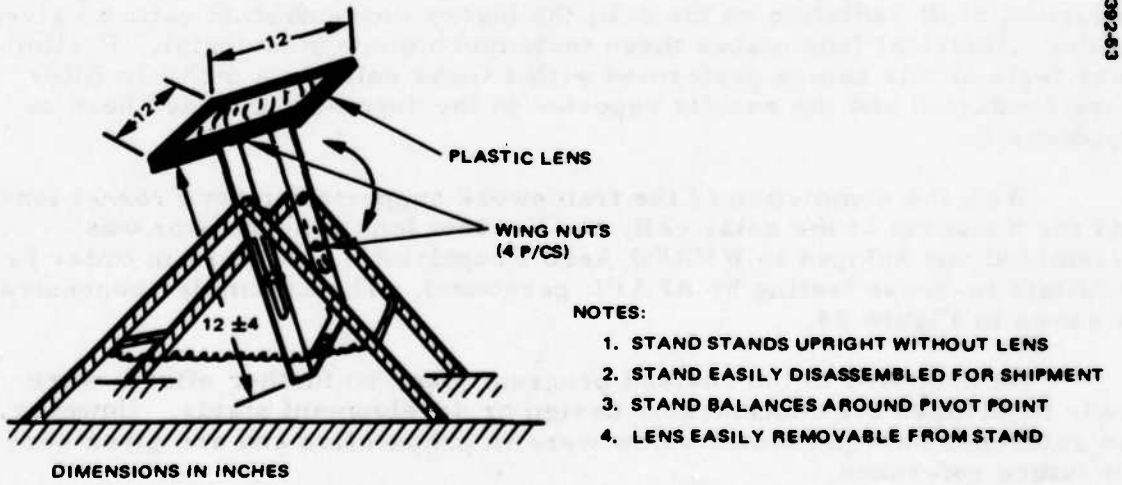

FIGURE 23. FRESNEL LENS STAND – CIRCULAR

cell area was composed of four 2 cm cells set in a square configuration, 4.2 cm on a side; 2) a glass of a specific gravity of 2.54 was used; 3) the concentrated spot was defocused to cover the area.

TABLE 7. CALCULATED WEIGHTS FOR GLASS FRESNEL LENSES

Lens Size		Area		Solar Cell Area		Concentration Ratio*	Weight, lh		
in.	cm	in^2	cm^2	in^2	cm^2		1/8 in.	3/16 in.	1/4 in.
12 x 12	30 x 30	144	929	2.73	17.7	32.6	1.65	2.47	3.3
12 dia	30 dia	113	730	2.73	17.7	25.8	1.29	1.94	2.6

*With the defocusing required to form a spot large enough to cover the solar cells, the radius of the spot will be approximately 3 cm. This will give a spot approximately 6 cm in diameter which will just cover the solar cell area. The concentration ratio is then calculated on the basis of the lens area divided by the spot area, not the cell area.

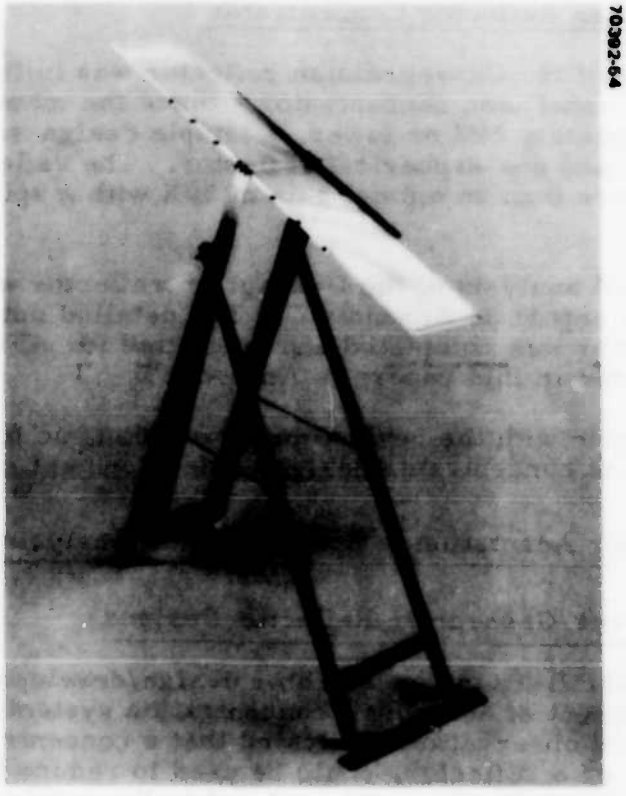

FIGURE 24. FRESNEL LENS CONCENTRATOR (PHOTO 4R47740)

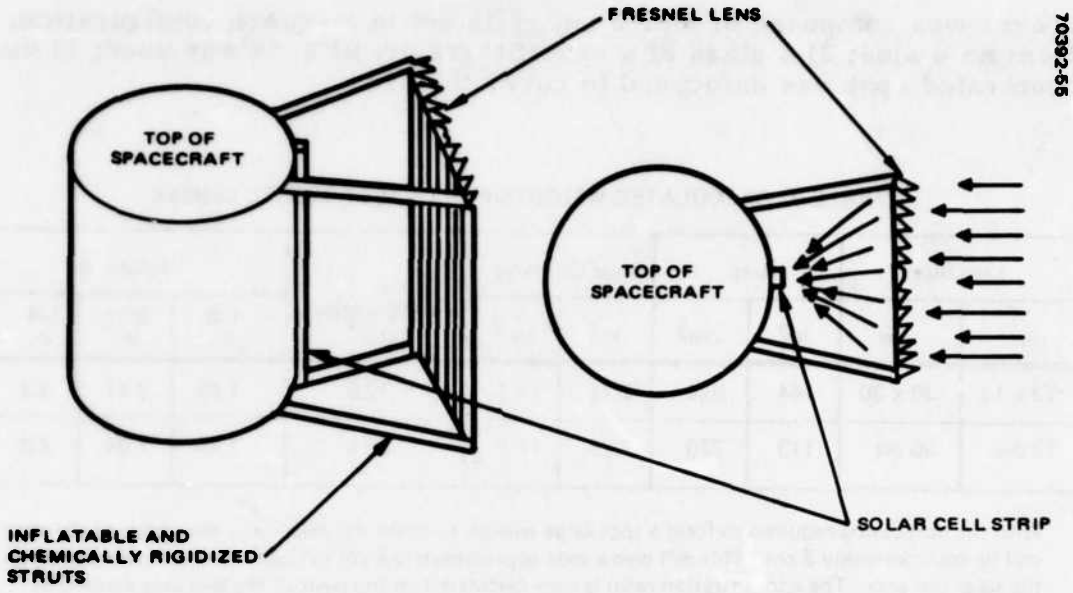

FIGURE 25. FRESNEL LENS ADAPTATION TO SPACECRAFT SCHEME

2.2.2 Cassegrainian Reflector Concentrator

The design of the Cassegrainian reflector was initiated in parallel with that of the Fresnel lens concentrator. Since the intensification had to be kept to approximately 20X or lower, a simple design was used, incorporating one spherical and one aspherical reflector. The reflector was designed to result in not more than an optical gain of 30X with a spillover of approximately 10 percent.

The thermal analysis of the Cassegrain reflector was completed and is included in this report as Appendix C. The detailed optical design of the Cassegrain reflector was completed and submitted for AFAPL review. This document is included in this report as Appendix D.

In accordance with the revised program plan, no further efforts were made to advance the concentrator design or development status.

2.2.3 Concentrator Adaptation to Space Systems Analysis

Fresnel Lens/Cassegrain Reflector Designs

An effort ancillary to concentrator design/development was initiated to examine the concept of adapting a concentration system to a full size spacecraft. Preliminary observations indicated that a concentrator, either the Fresnel lens type or a reflector, could be used to reduce the number of cells on a spacecraft by an amount roughly related to the concentrator efficiency. A high degree of tracking accuracy must be maintained to take full advantage of present concentrator designs. Alternate design concepts which alleviate this problem were also sought.

The first systems examined were those in which Fresnel lenses would be used to concentrate the light to approximately 20 to 50X on a band of cells on the spacecraft body, as shown in Figure 25. As shown in the figure, the struts would hold the lens at the correct focal distance and the energy would be concentrated on one row of cells. The obvious advantage is that a much smaller number of cells would be required to furnish power to the spacecraft. There are, however, some technical problems which might make such a system unattractive. First, the weight and complexity of the lens support system might be considerably more than the weight of the cells displaced, thus causing an immediate weight penalty, to any existent spacecraft design.

Possibly the most difficult problem to be solved would be the necessity to ensure accurate tracking (0.05° maximum) for the Fresnel lens (or a Cassegrainian reflector) to be utilized to maximum efficiency. Since Hughes spacecraft are currently spin stabilized, this would call for despin equipment to which the lens assembly would be attached. This would be similar to current despin techniques used for the antennas, except possibly larger and more powerful, since the lens and struts are outside the spacecraft, thus contributing a large moment of inertia. Other problems such as development of a suitable material which could be used, with no deterioration, for long periods as a lens, and techniques of dissipating the heat, all increase the complexity of development of such a system for solar cell efficiency enhancement.

With the preliminary analysis indicating that the 20 to 50X enhancement would present formidable problems, consideration was given to the possibility of developing other systems which might not be as efficient, but would weigh less and be less complicated. Several such systems have been conceived, and are considered worthy of further investigation.

Alternate Concentration Schemes

One of the major problems with concentrated solar cell arrays is the aiming accuracy needed. Several types of concentrators that do not have the high aiming accuracy requirement are considered the most easily implemented. The simplest of these concentrators is a trough with mirrors on the sides. Different concentration ratios and aiming requirements are obtained with different angles and sizes of the mirrors. The use of non-imaging plane surface reflectors means that light, inexpensive film type materials may be used. The tracking requirements are lax (5° to 10°) and, for certain geometries, totally passive nontracking concentrators may be used. Low concentration ratios (2 to 3) show the most promise.

Another type of concentrator has been conceived, but its feasibility has not yet been sufficiently evaluated. This method is entirely passive, i.e., nontracking, and it should be possible to get concentration ratios in the 20 to 50X range. The concentration comes from fluorescence and light piping of the downconverted radiation. Full utilization of this method depends on how small GaAlAs solar cells can economically be fabricated.

SECTION III

RADIATION TESTING

3.1 TEST DESCRIPTION

Eight cells designed for 1 sun application were irradiated with 1 MeV electrons at fluences varying between 5×10^{14} e/cm^2 and 1×10^{16} e/cm^2. Figure 26 shows the baseline structure of the solar cell used. The window layer (AlGaAs) thickness and the junction depth were kept slightly below 0.5μm, and a buffer layer of approximately 15μm was grown to minimize the effects of variations in substrate properties.

The irradiation was performed in collaboration with Dr. Bruce Anspaugh of Jet Propulsion Laboratories. The Dynamitron particle accelerator at JPL was used as the electron source; the irradiations were performed in vacuum using a JPL solar cell holder. The fixture holds up to eighteen 2 x 2 cm solar cells during an irradiation. A small amount of vacuum grease was placed on the back of each cell, permitting thermal control during irradiations. The uniformity over the test plane was ±4 percent with no areas of discontinuity. Fluxes and fluences were measured by means of a Farraday cup whose current was integrated to establish electron fluences and to automatically control termination of irradiation at the desired fluence levels. The cells were covered with 12 mil 7940 quartz cover glasses. The electrical characteristics of the eight cells used are given in Table 8.

TABLE 8. (AlGa)As/GaAs SOLAR CELL CHARACTERISTICS

Cell No.	I_{sc}, mA	V_{oc}, V	Fill Factor	P_{max}, mW	η, %
999	110	1.0	0.75	82.45	15.2
1047	112	0.99	0.74	82.0	15.2
1011	110	1.0	0.747	82.2	15.2
1008	115	0.99	0.739	81.6	15.1
1010	111	1.01	0.735	82.45	15.2
1020	111	1.0	0.735	81.59	15.1
1002	108	1.0	0.761	82.7	15.2
1006	111.5	1.01	0.732	82.41	15.2

TABLE 9. GaAs SOLAR CELL CHARACTERISTICS BEFORE AND AFTER 1 MeV ELECTRON IRRADIATION

Cell No.	Fluence Level, e/cm^2	I_{sc}, mA	V_{oc}, V	P_{mp}, mW	FF	η, %
999	0	110.0	1.0	82.45	0.75	15.2
	5×10^{14}	94.0	0.94	67.23	0.761	12.4
1047	0	112.0	0.99	82.00	0.74	15.2
	1×10^{15}	85.0	0.91	60.44	0.78	11.2
1008	0	111.5	0.99	81.60	0.74	15.1
	1×10^{15}	89.5	0.92	63.20	0.77	11.7
1011	0	110.0	1.0	82.2	0.747	15.2
	1×10^{15}	87.5	0.925	63.18	0.78	11.7
1010	0	111.0	1.01	82.45	0.735	15.2
	5×10^{15}	70.0	0.87	46.62	0.766	8.6
1020	0	111.0	1.0	81.6	0.735	15.1
	5×10^{15}	74.0	0.85	48.84	0.78	9.0
1006	0	111.5	1.01	82.41	0.732	15.2
	1×10^{16}	58.0	0.84	36.92	0.76	6.8
1002	0	108.0	1.0	82.2	0.76	15.2
	1×10^{16}	56.0	0.84	36.0	0.77	6.6

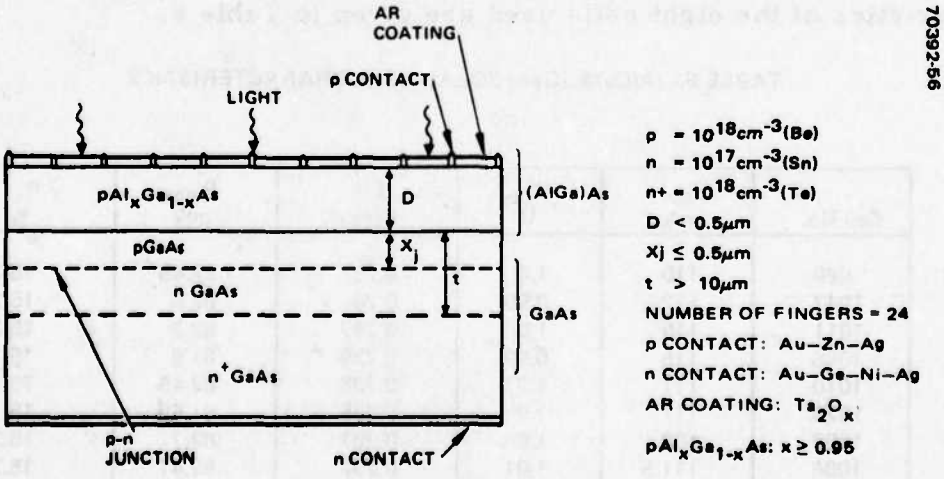

FIGURE 26. BASELINE GaAs SOLAR CELL STRUCTURE USED IN 1 MeV RADIATION DAMAGE STUDIES

3.2 RESULTS

Figures 27 through 34 show the photo I-V characteristics for these eight (AlGa)As/GaAs solar cells before and after irradiation. Table 9 gives the individual cell characteristics: short circuit current (I_{sc}), open circuit voltage (V_{oc}), fill factor (FF), maximum output power (P_{mp}) and power conversion efficiency (η).

3.2.1 Short Circuit Current

Figure 35 shows the measured short circuit current density after irradiation as a function of 1 MeV electron fluence. The solid line and the dotted line represent the measured short circuit current density for two different junction depths (0.5 μm and 1 μm). As expected from the theory, the shallow junction solar cells are more resistant to radiation than the ones with deeper junction. Figure 36 shows the short circuit current of the shallow junction (0.5 μm) solar cell compared with the theoretical short circuit current calculation by using a damage constant $K = 7 \times 10^{-8}$. Again, it is predicted that these GaAs solar cells can achieve much better radiation resistance by decreasing the junction depth to 0.2 μm.

3.2.2 Open Circuit Voltage

The open circuit voltage, V_{oc}, for a solar cell can be represented by the following equation:

$$V_{oc} = n \frac{KT}{q} \ln \left(\frac{I_{sc}}{I_o} + 1 \right) \qquad (1)$$

Figure 37 shows the measured V_{oc} as a function of the 1 MeV electron irradiation fluence. The open circuit voltage, V_{oc}, is found to decrease logarithmically with the electron irradiation fluence. This can be expected from the degradation of I_{sc} with the radiation fluence. The dark I-V characteristics for these cells after irradiation have also been measured (Figure 38). The n-factor is obtained from the slope of the dark log I-V plot; the value of the diode dark current at zero voltage yields the diode saturation current. These measured values are substituted in Equation 1 to calculate V_{oc}. The results are summarized in Table 10; it can be seen that there is good agreement between the measured V_{oc} obtained from the photo I-V measurement and the V_{oc} calculated using Equation 1.

3.2.3 Fill Factor

The fill factors (FF) of these eight cells seem to improve after irradiation (see Table 9). The fill factor is a convenient figure of merit that characterizes the knee of the diode I-V characteristics. Any effect that tends to soften the knee of the diode I-V characteristic will reduce the FF and hence the power output from the solar cell. It is difficult to understand why the irradiation should improve the fill factor. We intend to study this aspect in detail by studying the defects and their behavior during irradiation and the subsequent annealing of the cells.

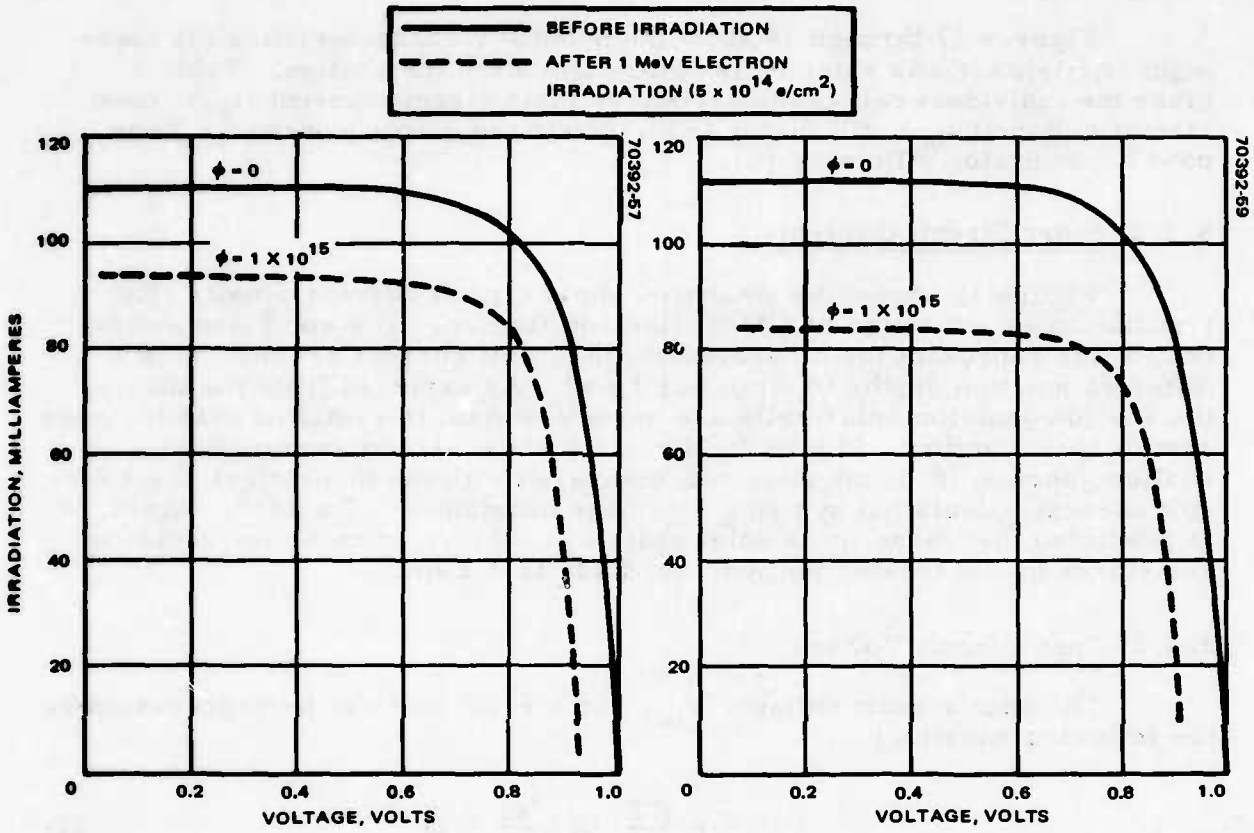

FIGURE 27. CELL 999 PHOTO I-V CHARACTERISTICS

FIGURE 28. CELL 1047 PHOTO I-V CHARACTERISTICS

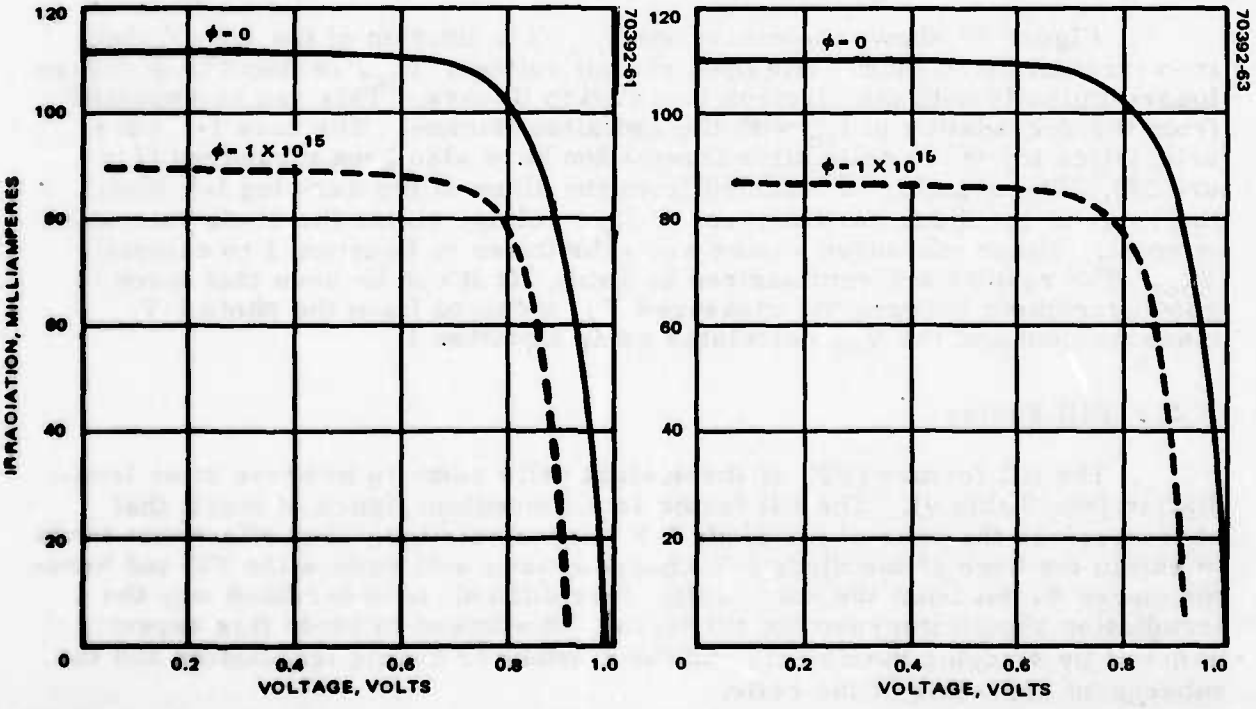

FIGURE 29. CELL 1008 PHOTO I-V CHARACTERISTICS

FIGURE 30. CELL 1011 PHOTO I-V CHARACTERISTICS

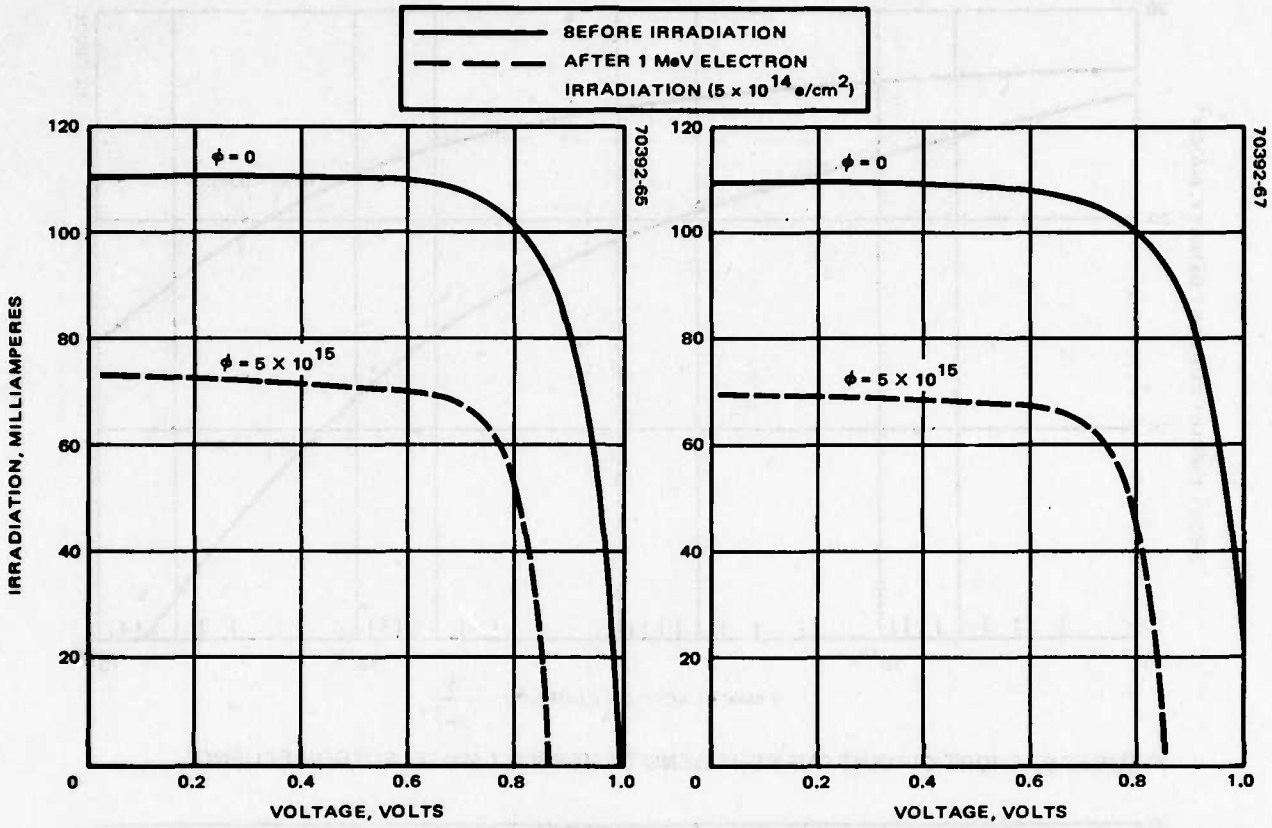

FIGURE 31. CELL 1020 PHOTO I-V CHARACTERISTICS

FIGURE 32. CELL 1010 PHOTO I-V CHARACTERISTICS

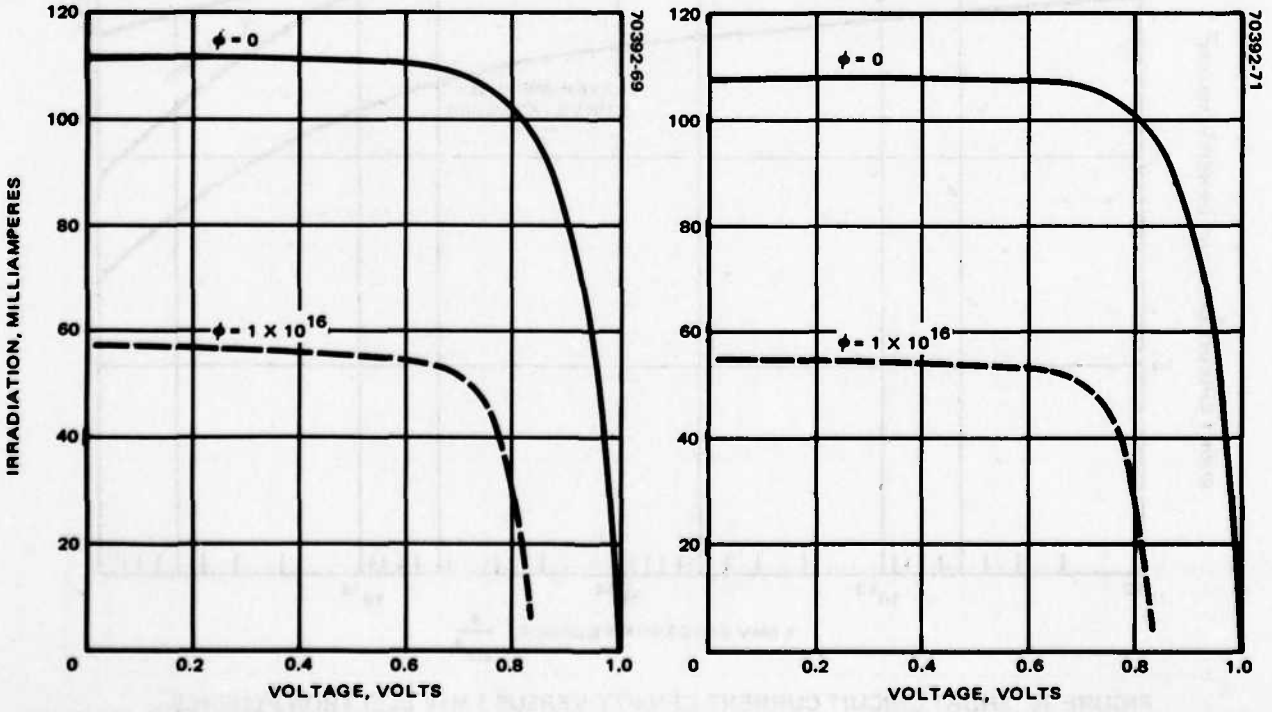

FIGURE 33. CELL 1006 PHOTO I-V CHARACTERISTICS

FIGURE 34. CELL 1002 PHOTO I-V CHARACTERISTICS

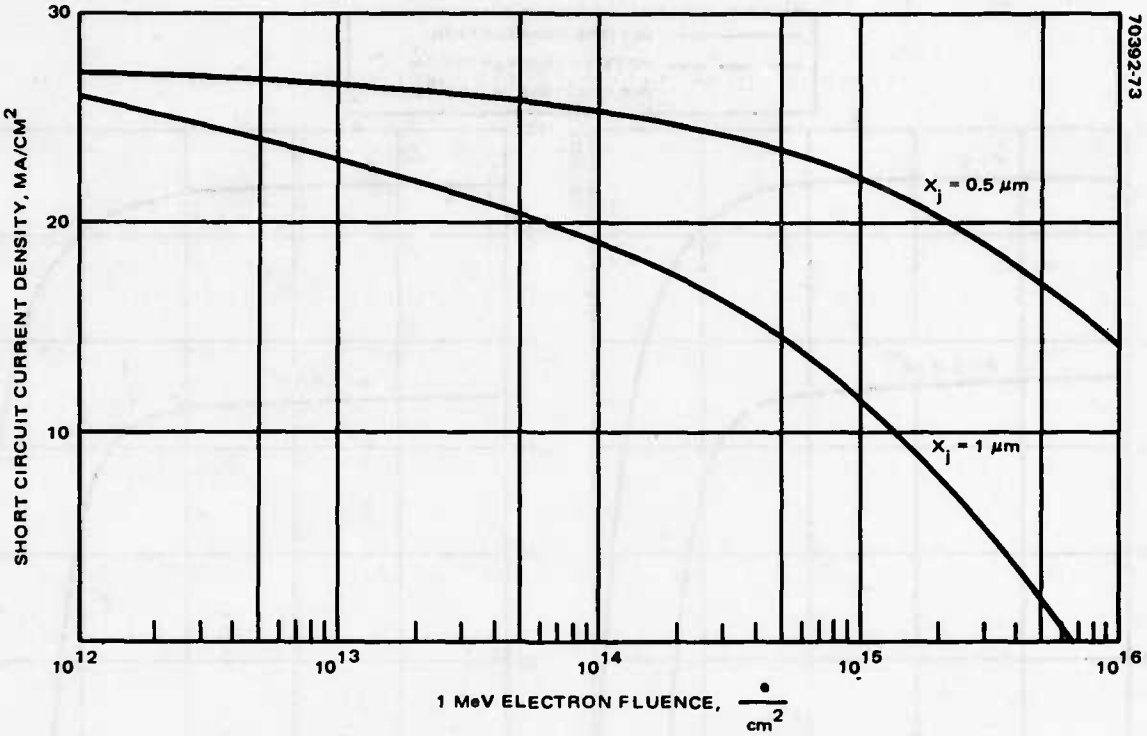

FIGURE 35. SHORT CIRCUIT CURRENT DENSITY VERSUS 1 MeV ELECTRON FLUENCE

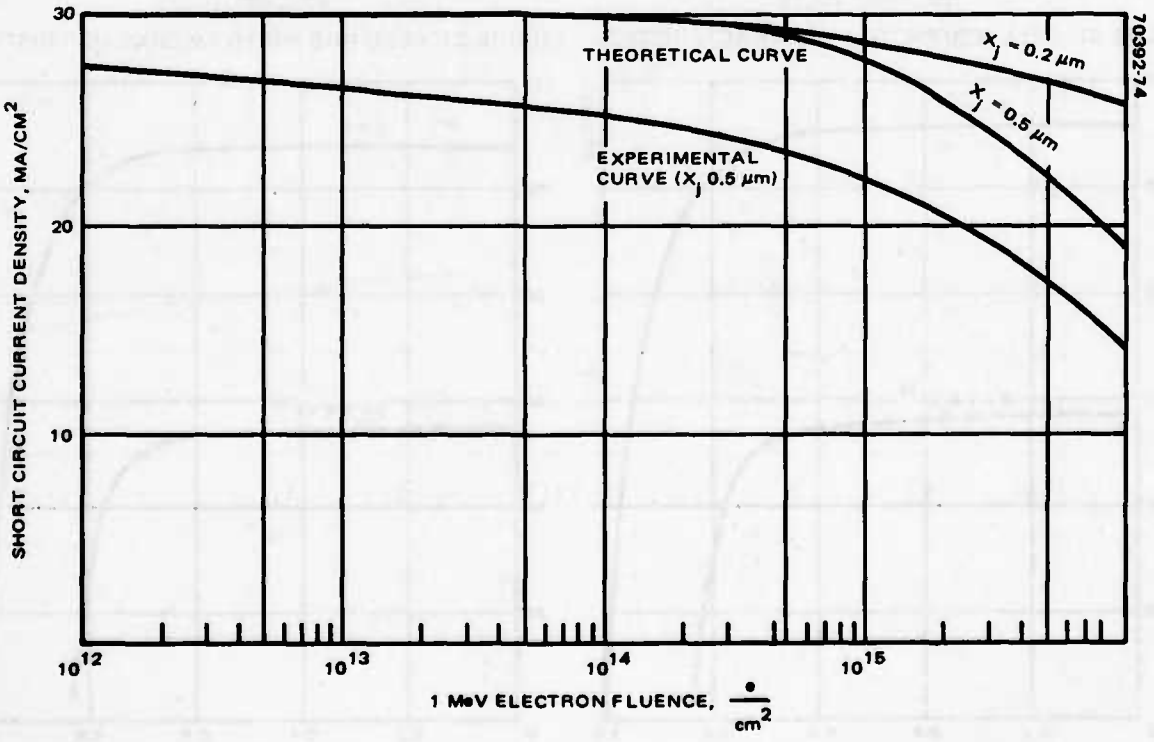

FIGURE 36. SHORT CIRCUIT CURRENT DENSITY VERSUS 1 MeV ELECTRON FLUENCE– THEORETICAL VERSUS EXPERIMENTAL CURVE

TABLE 10. SOLAR CELL: COMPARISON BETWEEN MEASURED AND CALCULATED V_{oc}

Cell No.	Fluence Level	I_{sc}, mA.	η	I_0, A	V_{oc}, V	
					Calculated	Measured
999	5×10^{14}	94.0	2.0	2×10^{-9}	0.919	0.94
1047	1×10^{15}	85.0	2.06	3.6×10^{-9}	0.909	0.91
1008	1×10^{15}	89.5	2.01	3.0×15^{-9}	0.922	0.92
1011	1×10^{15}	87.5	2.0	3.5×10^{-9}	0.92	0.925
1010	5×10^{15}	70.0	1.91	2×15^{-9}	0.86	0.87
1020	5×10^{15}	74.0	1.87	2.8×10^{-9}	0.83	0.85
1002	1×10^{16}	56.0	2.0	4.5×10^{-9}	0.85	0.84
1006	1×10^{16}	58.0	–	–	–	0.84

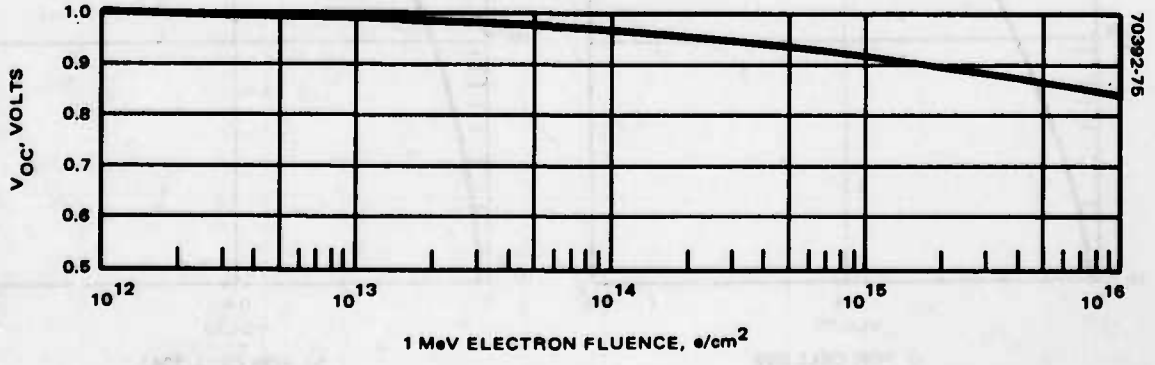

FIGURE 37. OPEN CIRCUIT VOLTAGE VERSUS 1 MeV ELECTRON FLUENCE

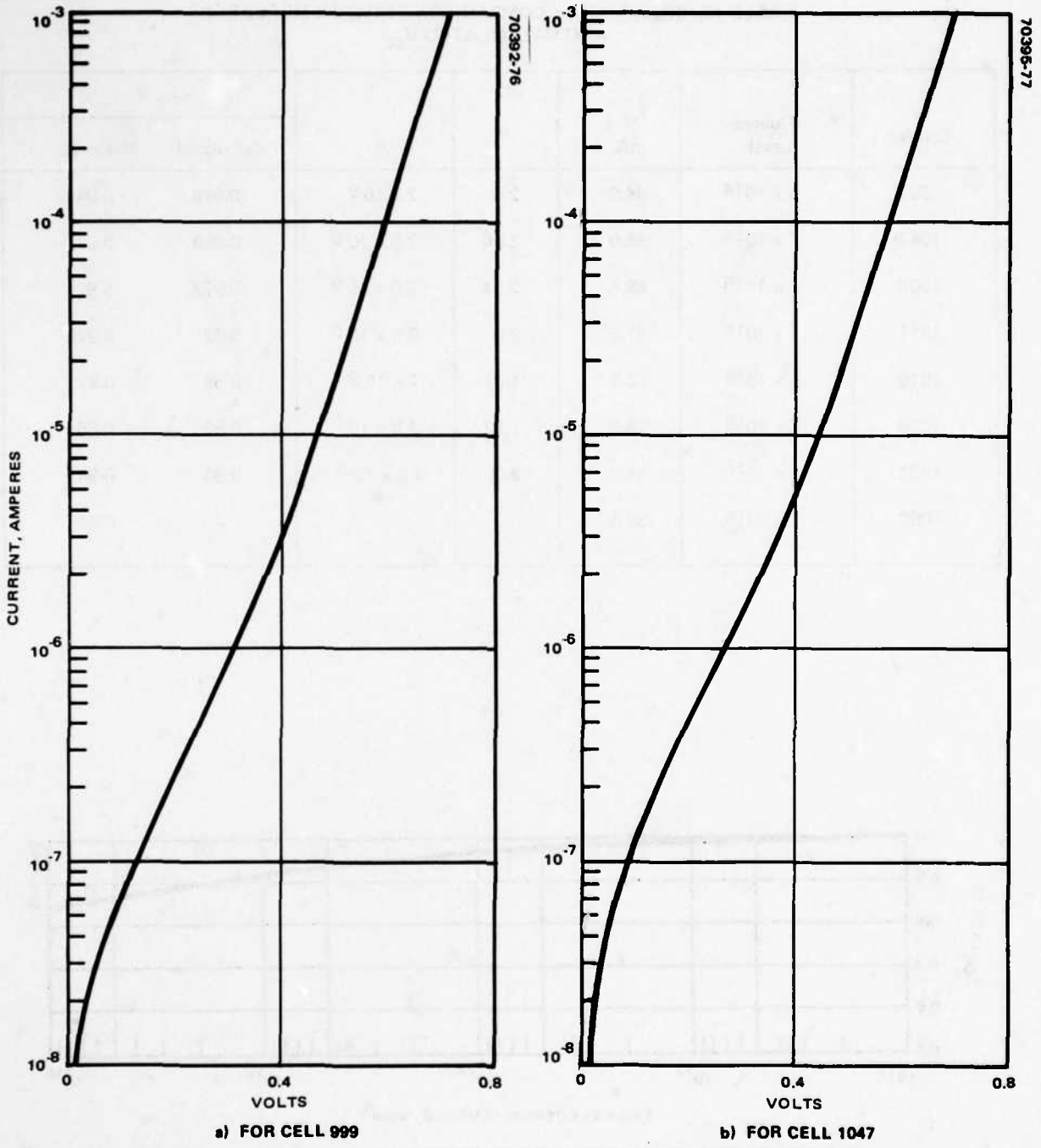

a) FOR CELL 999

b) FOR CELL 1047

FIGURE 38. POSTIRRADIATION DARK I-V CHARACTERISTICS

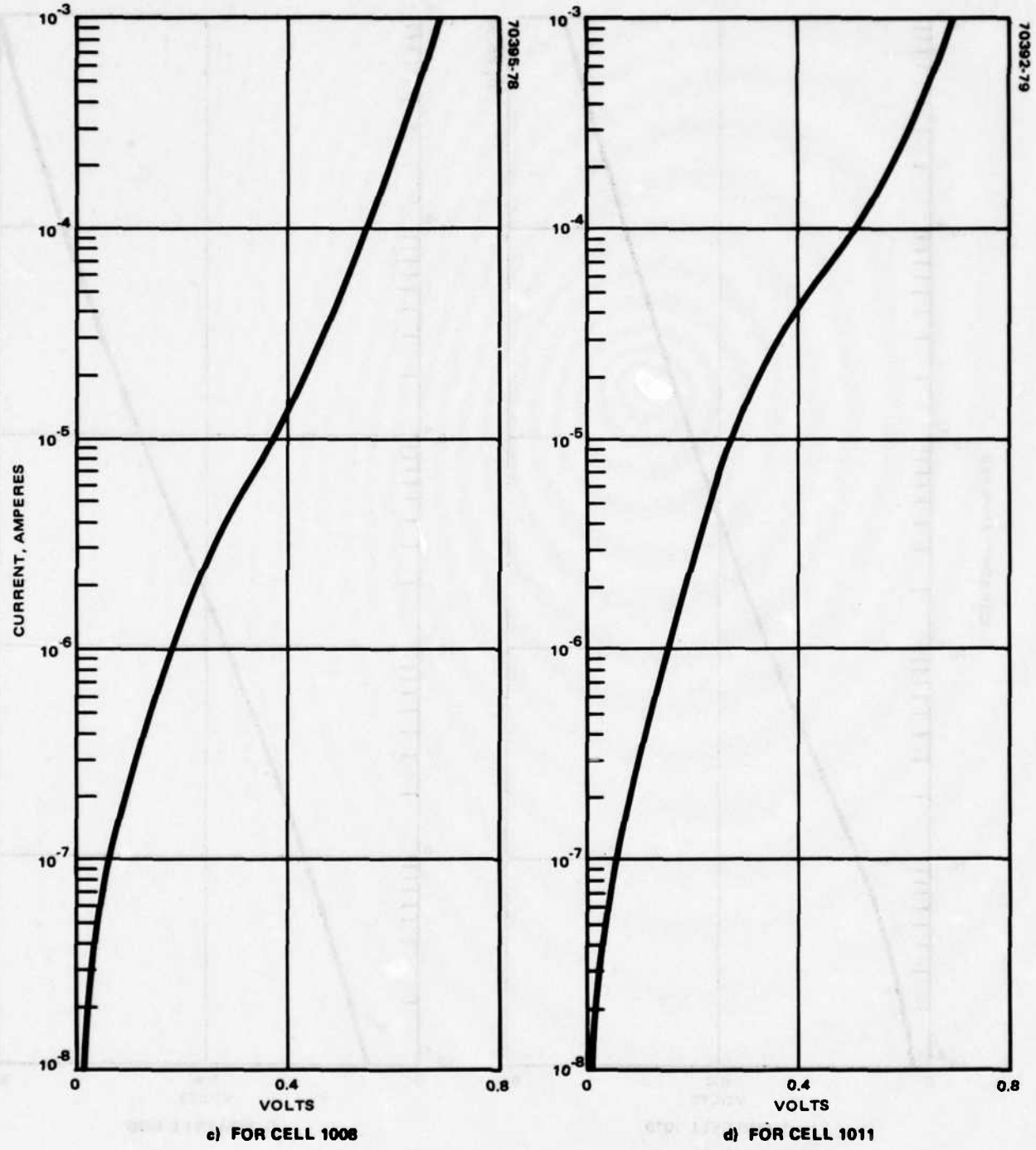

c) FOR CELL 1008

d) FOR CELL 1011

FIGURE 38 (CONTINUED). POSTIRRADIATION DARK I-V CHARACTERISTICS

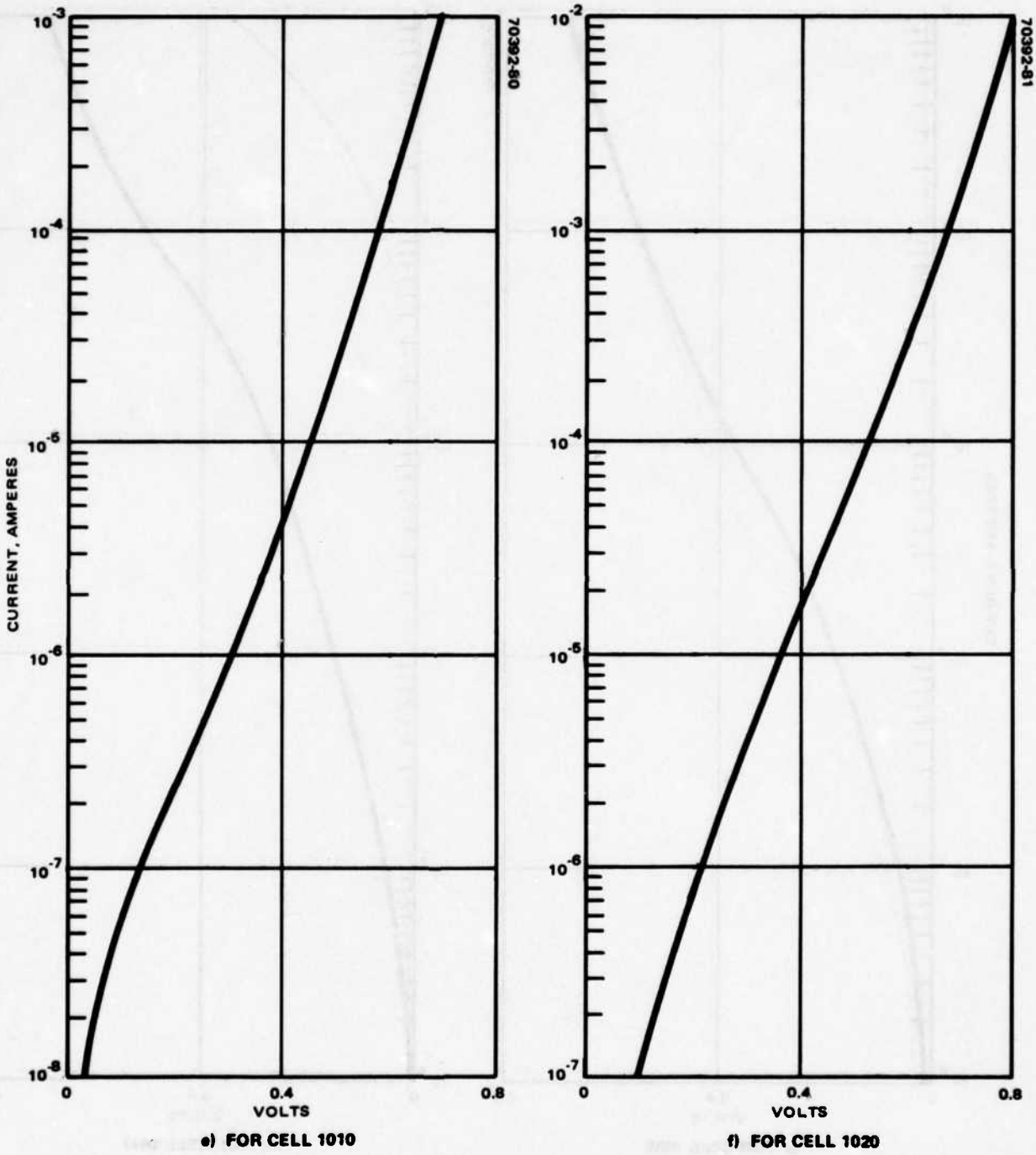

e) FOR CELL 1010

f) FOR CELL 1020

FIGURE 38 (CONTINUED). POSTIRRADIATION DARK I-V CHARACTERISTICS

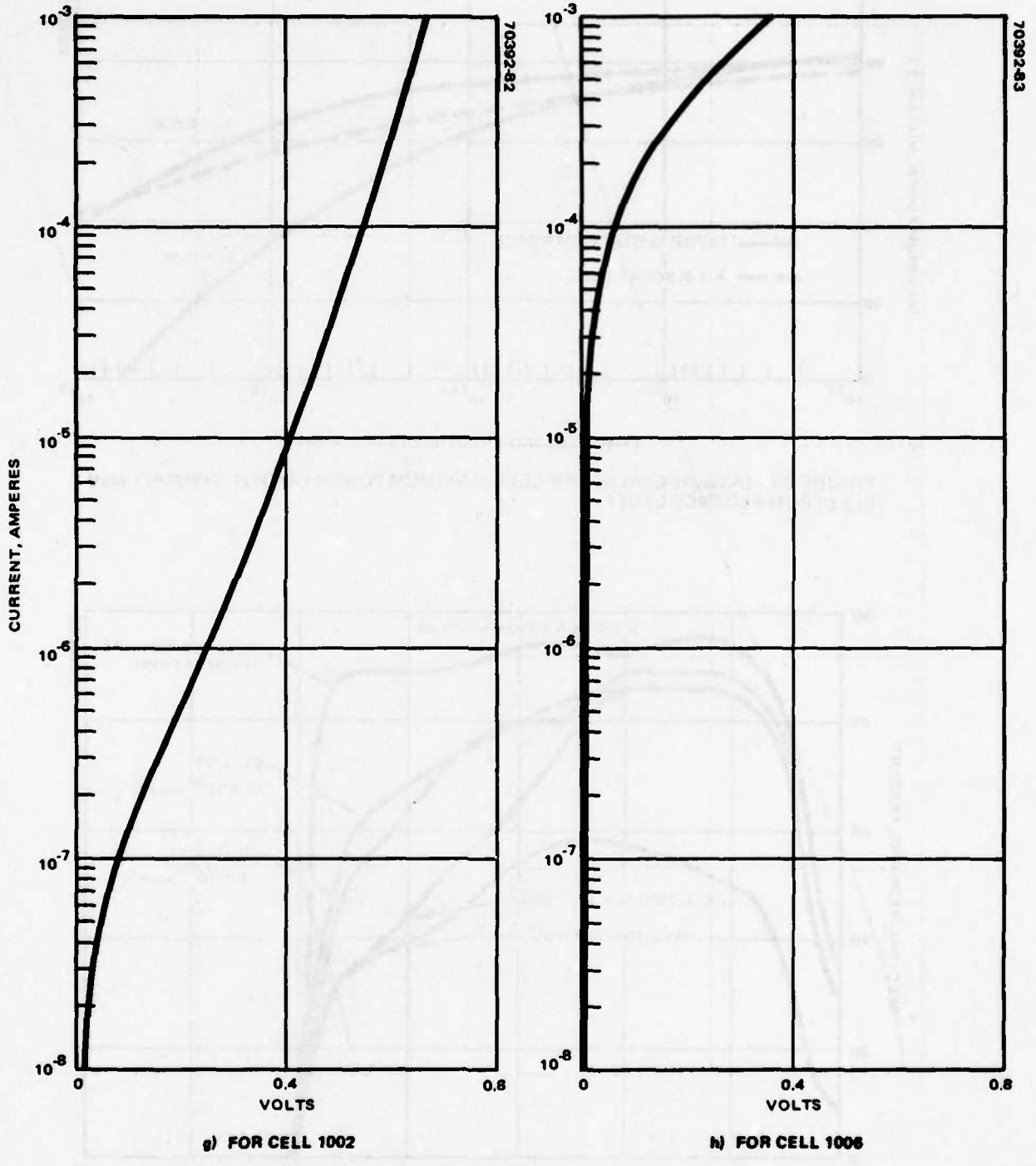

g) FOR CELL 1002

h) FOR CELL 1006

FIGURE 38 (CONTINUED). POSTIRRADIATION DARK I-V CHARACTERISTICS

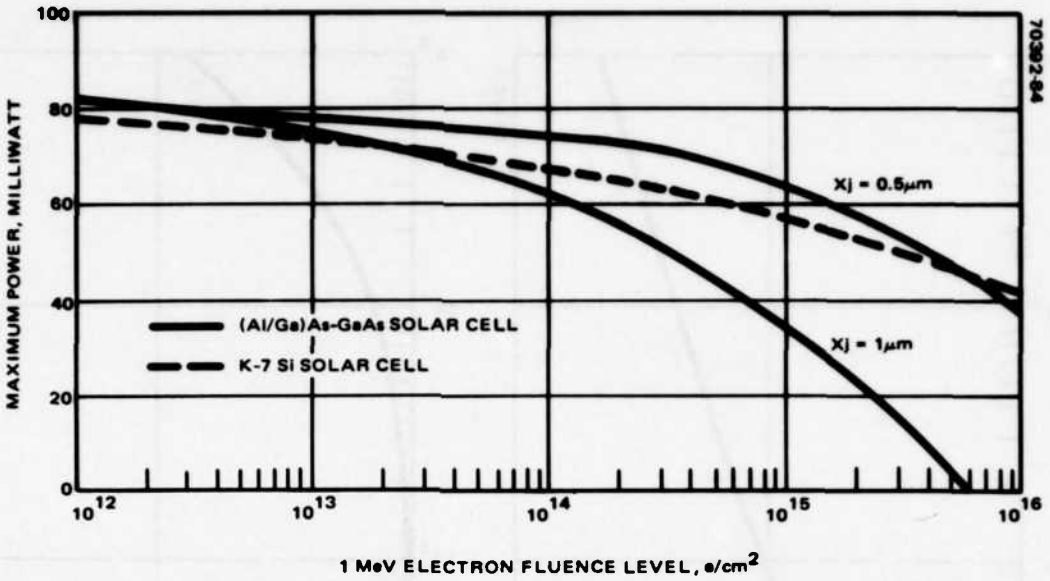

FIGURE 39. (AlGa)As-GaAs SOLAR CELL MAXIMUM POWER OUTPUT VERSUS 1 MeV ELECTRON FLUENCE LEVEL

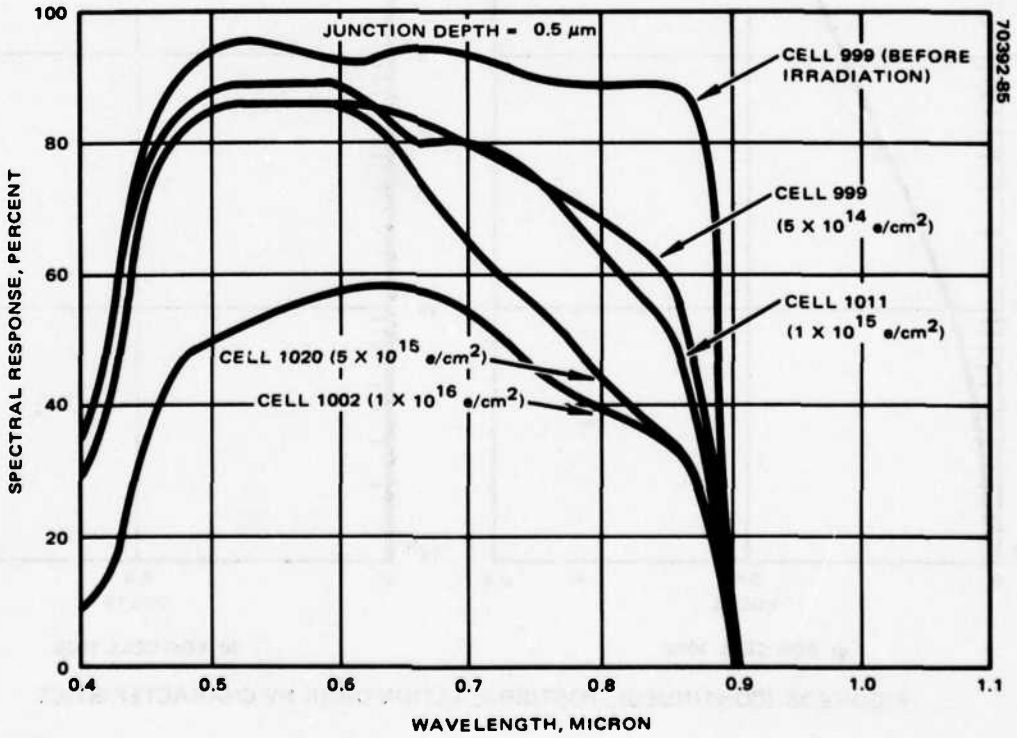

FIGURE 40. (AlGa)As-GaAs SOLAR CELL SPECTRAL RESPONSE VERSUS 1 MeV ELECTRON FLUENCE

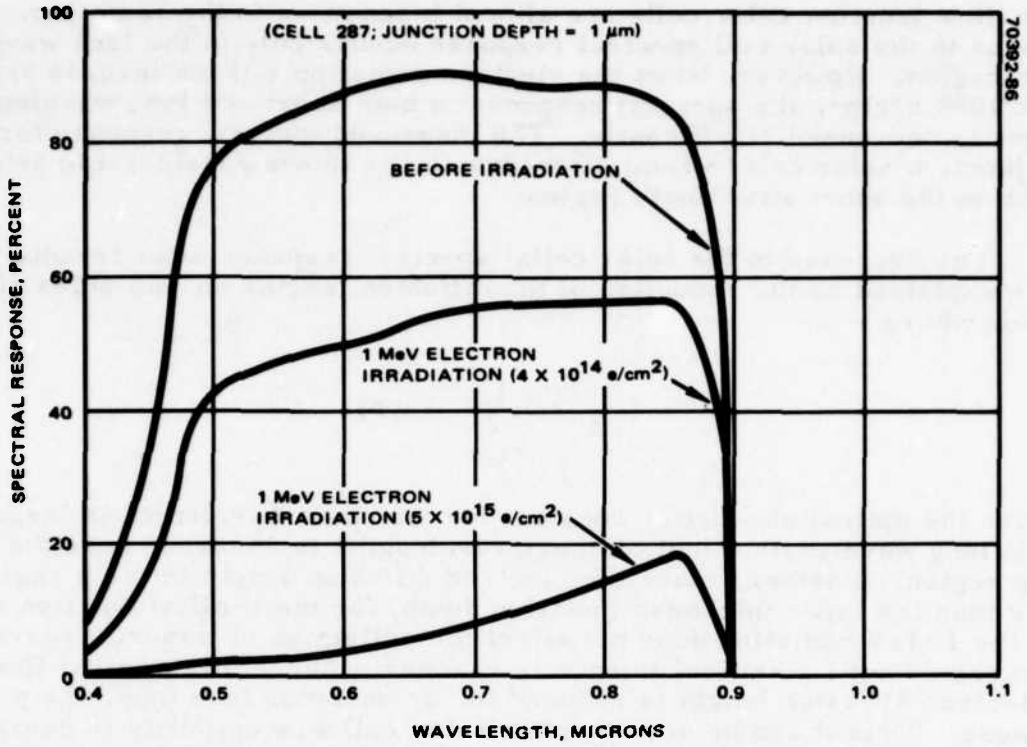

FIGURE 41. (AlGa)As-GaAs SOLAR CELL SPECTRAL RESPONSE VERSUS 1 MeV ELECTRON FLUENCE

3.2.4 Maximum Power

Figure 39 shows the experimental results for both GaAs solar cells and newly developed high efficiency K-7 Si solar cells as a function of 1 MeV electron irradiation. Also shown here are the results of our previously irradiated GaAs deep junction solar cells. It can be seen that the rate of degradation of shallow junction GaAs cells is comparable to K-7 silicon cells. However, since the GaAs cells start off with higher output power, they also have a higher end of life power even after being subjected to a fluence of 5×10^{15} e/cm^2. Further improvement of the GaAs cell is possible by optimizing the carrier concentrations on the two sides of the junction and by reducing the junction depth even more (possibly to 0.2 μm). This offers the exciting possibility of considerable improvement beyond the K-7 silicon cell.

3.2.5 Spectral Response

Figures 40 and 41 show the spectral response as a function of 1 MeV electron radiation fluence for shallow junction (~0.5 μm) and deep junction (~1.0 μm) solar cells, respectively. In the short wavelength region,

the shallow junction solar cells are almost insensitive to the radiation. The decrease in the solar cell spectral response occurs only in the long wavelength region. However, when the electron radiation fluence level is as high as 1×10^{16} e/cm^2, the spectral response in both short and long wavelength regions is decreased significantly. The measured spectral response for the deep junction solar cell ($\sim 1\mu m$) after irradiation shows considerable deterioration in the short wavelength region.

The decrease in the solar cells' spectral response after irradiation can be explained by the reduction of the diffusion lengths on both sides of the junction where

$$\left(\frac{1}{L^2} = \frac{1}{L_o^2} + K\Phi\right)$$

Because the optical absorption constant for the short wavelength is larger than for the long wavelength, light of short wavelengths is absorbed near the surface p region. Further, since the electron diffusion length in the p region is longer than the layer thickness (junction depth) for the shallow junction solar cell, the 1 MeV radiation does not affect the collection of minority carriers in this region until a critical fluence is reached. Above this critical fluence, the electron diffusion length is reduced to, or becomes less than, the p layer thickness. Thus it can be seen that the solar cell susceptibility to damage in the short wavelength region can be minimized by using shallower junctions. As the junction depth is reduced, an increasing part of the spectrum becomes less affected by the 1 MeV radiation. Since the solar spectrum in space peaks in this region, beneficial effects of this happy circumstance can be easily appreciated. We intend to study this aspect of the problem in greater detail in our future work.

3.3 ANNEALING EXPERIMENTS

We have started annealing experiments on the irradiated solar cells. During the last few weeks we have followed the photo I-V behavior of the cells at room temperature, and peculiar effects have been noted similar to what was observed with silicon cells (see Technical Report AFAPL TR-77-36, June-July 1977). It is important to follow these cell characteristics in detail to elucidate the mechanisms that govern cell damage if we wish to minimize and control the damage. We also plan to study the annealing behavior both as a function of temperature and under injection annealing conditions. These studies are essential to optimize the cells for applications in space, for which long term reliable operation with the highest power output is most desirable. The results to date are sufficiently exciting to warrant continued studies on an expanded scale. This work will be pursued in part on the High Efficiency GaAlAs Solar Cell program.

SECTION IV

CELL INTERCONNECT WELDING

4.1 WELDING APPARATUS

A simplified block schematic of the ultrasonic wheel welder and supporting equipment is shown in Figure 42. Here the welding tool is a 0.71 inch diameter wheel machined from drill rod and attached to a 6 inch long tapered horn rigidly connected to a magnetostrictive (ferromagnetic) transducer. This entire unit is spring mounted to a block in such a way that the spring tension and thereby the contact force, F_c, of the wheel against the device can be increased or decreased in the vertical direction by means of set screws (not shown). The block, in turn, can be motor driven along a track in the horizontal plane at a selected speed.

The transducer is controlled by a signal generator equipped with both power and tuning adjustments. Relative scales associated with each ensures reproducibility of settings. Tuning is further facilitated using an oscilloscope displaying a Lissajous pattern resulting from simultaneously monitoring the current and voltage through the transducer.

The vacuum stage supports both the solar cell and tabs during welding, while the calibration stage is used to determine the contact force, F_c, of the wheel by means of a simple switch circuit.

4.2 TAB CHARACTERISTICS

Tabs were constructed from 99.99 percent Ag foil 50 to 60 mils thick. Units prepared for welding were made up of six tabs each originally connected (see Figure 43) but later individually separated following the welding operation. Thus, attached to the completed cell were 12 independent tabs each approximately 1.1 by 6.5 mm in area.

4.3 PROCEDURE

4.3.1 Equipment Parameters

The first step toward producing repeatably reliable bonds entails preliminary trial and error test operations involving sensitive adjustment of equipment and techniques in order to determine the proper settings for the

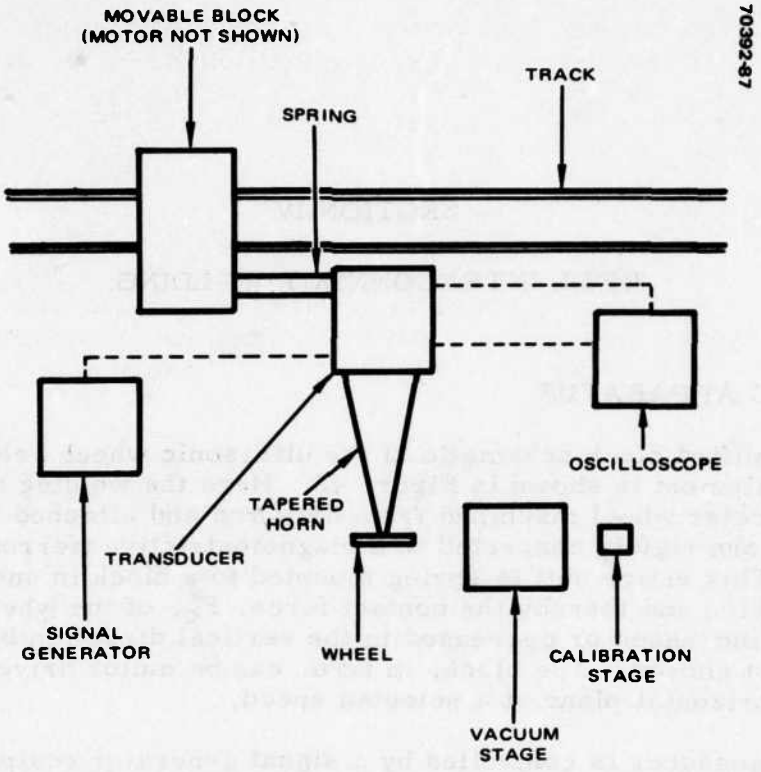

FIGURE 42. TOP VIEW SCHEMATIC OF ULTRASONIC WHEEL WELDER AND SUPPORTING EQUIPMENT

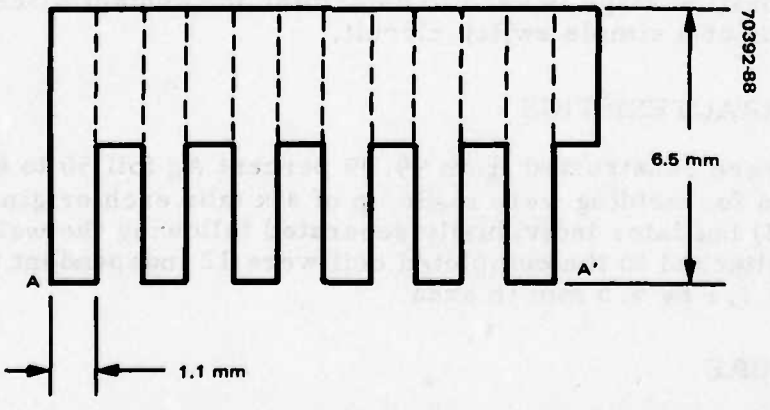

FIGURE 43. SILVER FOIL PATTERN CONSISTING OF SIX TABS

particular substrate/contact/tab system to be welded. At this stage, a minimum of four parameters are of great significance (other variables are discussed in detail in subsection 4.5). Notably, all address themselves to the amount and mode of energy delivery to the interface between the tab and the contact surface of the cell:

1) F_c, the contact force. As already explained, this is the force the wheel exerts upon the tab cell combination during welding. The greater the force, the greater the transmission of energy to the weld area. F_c is determined by measuring directly the force, in grams, necessary to lift the weld wheel from the calibration stage, and is adjustable through a range from zero to well over 450 grams.

2) P, relative power output of the signal generator. This parameter controls the amplitude of the electrical signal converted to mechanical energy through the transducer. Settings are repeatable by means of a relative unitless scale provided on the instrument.

3) T, tuning of the signal generator. For maximum energy delivery to the wheel and minimum feedback vibrations, the frequency of the electrical, and thereby mechanical, signals must match the natural resonant frequency of the horn/wheel/substrate assembly. This is accomplished in unitless values by a meter monitoring directly the coil impedance.

4) V, the velocity of the wheel during the welding operation. The longer the wheel rests on any given area of the weld, the more energy delivered to that bond. Too slow a velocity, however, causes undesirable abrading through both tab and solar cell contacts. Velocity is adjusted reproducibly using a relative but scaled control.

4.3.2 Sample Selection

Silicon solar cells were used to adjust the above setting to optimum welding values and to eliminate equipment- and technique-related problems. It was not expected that the values determined would be precisely applicable to the GaAs cells because of differences between the two semiconductors. For GaAs cells, fine tuning was necessary; for economy, cells exhibiting imperfect electrical characteristics were used. It was anticipated that destructive pull testing of these mechanical cells would reliably determine the strengths of tabs to the electrical cells.

Using the parameters and techniques found to be successful for the imperfect units, a limited number of electrically sound cells were welded and the tabs pulled. This test provided accurate tab pull strength data and allowed final adjustments where needed. Finally, a larger group of electrically sound cells was welded, and each individual weld was examined. From this group, the five best cells were selected.

4.4 TAB PULL RESULTS

All cells tested and the tabs of each were indexed for future reference and saved for possible further experimentation. After welding, tabs were separated and individually tested using a commercial force gauge to determine the pull stregth, in fractions of a pound. In addition to reference number and pull force, the weld condition and that of the metal area beneath the weld were tabulated for each bond. Examinations were visual, by optical microscopy and, when necessary, by SEM. Since the minimum acceptable pull strength was designated to be 2.5 Newtons or 0.56 pound, this became the criterion of failure. The cause of failure for each pull below this value was assigned either to a faulty weld condition or to substandard metallization.

4.4.1 Tests on Substitute Cells

As noted above, welding and pull tests began with silicon and progressed to mechanical GaAs cells. Initial work with the former revealed inadequacies in the determination of F_c. Methods used to date could not repeatably and accurately pinpoint the true force in the real case situation. The solution necessitated construction of a simple indicator device similar to the one already connected to the calibration stage but designed to measure the force of the wheel on the actual solar cell mounted on the vacuum stage itself. By means of this technique, pull forces were easily repeatable to within ± 10 grams.

Again using silicon, a family of values for optimum welding was determined which formed a basis for subsequent determination of the same for GaAs cells. However, early results were far from acceptable. Besides a failure rate of over 50 percent, a great spread in values for pull strengths was observed even between tabs welded side by side and therefore supposedly welded under identical conditions. For example, forces differing by as much as 0.55 pound were commonly recorded for consecutive tabs. Such behavior was taken to indicate localized differences in solar cell contact metallization. Contamination was immediately suspected, and a solvent cleaning procedure was initiated but led to little improvement. Thus, in addition, both cell contacts and tabs were first abraded using a number of techniques and directions of abrasion. As a result, bond pull strengths increased significantly. Eventually, values as high as 1.10 pounds were realized, and the failure rate was reduced to 16 percent. Significantly, in no case was failure due to insufficient adhesion of the cell's contact metallizations.

The improved F_c determination, as well as cleaning and abrading techniques, was carried as testing progressed to the mechanically sound GaAs cells. As expected, the parameter settings and the mechanical surface treatment developed for silicon devices were found inadequate. This was attributed to a variety of differences between the semiconductors including different thicknesses, hardnesses, metallization compositions, and geometries.

As a result, adjustments were made to accomodate the new cells. F_c was gradually increased from 200 grams to 260 grams which resulted in ever increasing pull strengths. Final parameter settings were:

$$F_c = 260 \text{ grams}$$
$$P = 8.0$$
$$V = 35$$
$$T = 0.49$$

Typical results are shown in Table 11. An explanation of the codes adopted here is given below

AO — Already Off: The weld was a total failure in that the tab did not adhere and was not available for pulling. AO always implies a pull force of zero.

TO — Tab Off: Upon testing, the entire tab (the parts on both sides of the weld area) became totally dislodged. TO indicates a successful weld only for pulls ≥ 0.56 pound. For strengths less than this, TO implies:

a) Weld failure - if the metal under the weld area is completely intact (OK)

b) Metal failure - if the metal under the weld area is less than completely intact (NG).

BAW — Broke At Weld: Upon testing the tab breaks at the weld so that the pulled section is removed while the other portion remains. BAW indicates a successful weld only for pulls ≥ 0.56 pound. For strengths less than this, BAW implies a weld failure most likely due to excessive wheel force causing extraordinary deformation of the metals.

TB — Tab Broke: Upon testing, the tab itself broke. This may happen either because the weld was excessively strong or because there was a defect in the tab before pulling. Therefore, by means of the associated pull force, TB can indicate an exceptionally good weld but, on the other hand, can never imply anything negative about weld or metal conditions.

In this and subsequent tables, unacceptable pull strengths (<0.56 pound) are indicated by underscoring as is the assigned cause of failure - either the weld or the metal. Thus, results for the two cells exhibit eleven failures. Five are attributed to metal failure and six to weld problems. Most importantly, there is no discernible pattern. With cell 2M928, the back metallization is poor and the front is excellent, while in 2M1098, the reverse is true.

TABLE 11. TAB PULL RESULTS FOR MECHANICAL (SECOND SET)
GaAs SOLAR CELLS

Record: I35 Date: 9/6/77

F_c = 260 grams
P = 8.0
V = 35
T = 0.49

Front Contact				Back Contact			
Tab No.	Pull Force, lb	Weld Condition	Metal Condition	Tab No.	Pull Force, lb	Weld Condition	Metal Condition
CELL 2M928							
1	0.90	TO	OK	1	0.50	TO	NG
2	0.80	BAW	OK	2	0.0	AO	OK
3	0.90	BAW	OK	3	0.30	BAW	OK
4	0.20	TO	OK	4	0.35	TO	NG
5	0.80	TO	OK	5	0.40	BAW	OK
6	0.95	TO	OK	6	0.40	BAW	NG
CELL 2M1098							
1	0.85	TO	NG	1	1.00	TO	OK
2	0.0	AO	NG	2	0.95	BAW	OK
3	0.90	TO	NG	3	0.80	BAW	OK
4	0.85	TO	NG	4	1.05	BAW	OK
5	0.50	TO	NG	5	0.0	AO	OK
6	0.60	TO	NG	6	0.35	TO	OK

4.4.2 Tests on Electrically Sound Cells

The totality of data from the GaAs investigation suggested that an increase in F_c might decrease the excessive number of failures assigned to welding. Accordingly, the parameters were readjusted to the following:

F_c = 290 grams
P = 8.0
V = 35
T = 0.45

Results are shown in Table 12 for cells 1E981, 1E1021A, and 1E1036. (As indicated, tabs to 1E1021A were welded to the front side only). As demonstrated, unacceptable pull strengths due to weld failure were reduced to about one in fifteen. However, problems with the cells' contact metallizations remained. In general, the back contact proved worse than the front. This was due in part to the fact that during back bonding only, the cells in all cases moved about considerably due to insufficient vacuum seal to the cover glass (none of the mechanical cells had been equipped with covers). No combination of vacuum ports and available stays satisfactorily eliminated the problem without damaging the tabs either previously or subsequently attached to the front side. As a result, a special beryllium copper spring was designed to provide additional support only where needed. With this modification, movement was completely eliminated.

Besides movement during welding, differences in the degree of integrity of metallizations are attributed to subtle differences in fabrication techniques, since at this stage in the development of GaAs cells no two were processed in the same run. This very fact, that cells differ slightly from one another, became the key in hand-picking the more dependable cells from a body of units welded by means of careful visual examination. Accordingly, 12 cells were welded, each weld was scrutinized, and the observations were recorded. Subsequently, the best five were chosen. Except for some lateral shifting of the back tabs under the forward motion of the wheel (caused by the excessive height of the cell and cover glass combination), all welds appeared to be excellent.

4.5 CONCLUSIONS

4.5.1 Summary

Using silicon and GaAs cells, preliminary welding tests were conducted. Such experiments proved extremely useful in establishing and adjusting sensitive welding parameters, selecting additional processing techniques, and modifying equipment to produce the highest yield of acceptable bonds. More specifically, the vacuum stage was improved and a technique was developed for the direct measurement of F_c in situ. In

TABLE 12. TAB PULL RESULTS FOR ELECTRICAL GaAs SOLAR CELLS

Record: 139 Date: 9/9/77

F_c = 290 grams
P = 8.0
V = 35
T = 0.45

Front Contact				Back Contact			
Tab No.	Pull Force, lb	Weld Condition	Metal Condition	Tab No.	Pull Force, lb	Weld Condition	Metal Condition
CELL 1E981							
1	0.68	TO/BAW	OK	1	0.0	TO	NG
2	1.01	TO	OK	2	0.24	TO	NG
3	1.11	TO	NG	3	0.01	TO	NG
4	0.64	TO	NG	4	0.02	TO	NG
5	0.64	TO/BAW	OK	5	0.0	TO	NG
6	0.13	TO	NG	6	0.51	TO	NG
CELL 1E1021A							
1	0.60	TO/BAW	NG	1			
2	0.94	BAW	OK	2			
3	1.00	TB	OK	3	(tabs were not welded to the back contact)		
4	0.91	BAW	NG	4			
5	0.86	BAW	OK	5			
6	0.87	BAW	OK	6			
CELL 1E1036							
1	0.07	TO	OK	1	0.38*	TB	OK
2	0.44	TO	NG	2	0.89	TO	NG
3	0.60	TO	NG	3	0.28	TO	NG
4	0.49	TO/BAW	NG	4	0.16	TO	NG
5	0.47	TO	NG	5	0.76	BAW	OK
6	0.57	BAW	OK	6	0.45	TO	OK

*This failure was due to a defective tab and so it was assigned as neither a weld nor a metal problem.

addition, attachments were designed for complementing the vacuum force to accommodate the thicker, heavier GaAs cells. Also, cleaning and mechanical surface treatments were initiated, and parameters were fine-tuned. As a result of these measures the rate of acceptable welds increased dramatically to the point where weld-related failures - those associated with handling and equipment deficiencies - were almost entirely eliminated for the cells tested. The improvements and experience gained via this preliminary effort was then applied to GaAs cells exhibiting good electrical characteristics.

4.5.2 Present Involvement

Modifications are being incorporated in an improved version of the ultrasonic welder to facilitate handling and optimize weld yields. In addition, good progress is being made in tracing metallization problem to the fabrication steps responsible in order to increase adhesion and eliminate metal-related failure entirely.

SECTION V

CONCLUSIONS

Some major conclusions can be drawn from the present study that lead us to believe that GaAs solar cells offer significant advantages for space applications at low solar concentrations.

1) A 2 μm (AlGa)As window layer is sufficient for low concentration applications to provide low series resistance for the cells. This implies that the spectral response of the cells is not seriously affected by absorption in the blue region of the spectrum and an overall efficiency of > 16 percent AMO can be expected from these cells for the concentrated power supply.

2) Concentrator design - In our limited studies, concentrator designs were found to offer no advantage for satellites in near earth orbits. This was partially due to pointing accuracy requirements.

3) The radiation damage data on the GaAs cells is extremely encouraging. With a junction depth of 0.5 μm, we have shown that the GaAs cell is superior to silicon cells (K-7) under 1 MeV electron irradiation up to a fluence of 5×10^{15} e/cm^2. Indications are that even further gains can be made by further optimization of the cell, both in junction depth and in carrier concentrations on the two sides of the p-n junction.

4) The weakest area of array fabrications for GaAs cells seems to be the mechanical integrity of the ohmic contacts. Solutions to the problem are under study, and the technology to meet the needs for improved contact integrity is presently being developed under separate contract.

APPENDIX A

TEMPERATURE COEFFICIENT TEST OF GaAlAs SOLAR CELLS, CONCENTRATOR DESIGN

BACKGROUND AND TEST TECHNIQUE

Four GaAlAs solar cells representing recent improvements in the state of the art fabrication technology have been tested over a wide range of temperatures in order to obtain data on the temperature coefficients of the principal electrical parameters. These cells, serial numbers 576, 578, 584, and 594, were randomly drawn from the deliverable lot of 12 cells. The technique and equipment used for the test sequence is described in detail below. The test temperatures were -160, -100, -50, 0, +50, +100, +150, +200 and +250°C. One GaAlAs test cell and one silicon control cell, both solderless and of the 2 x 2 cm size, were subjected to the temperature excursion in each run. Four runs were made. The same silicon control cell was used in each run. The reference copperconstantin thermocouple was located in between the two cells. Liquid nitrogen was used as the cooling medium; the temperature was first brought down to -160°C, and the other temperatures were obtained in ascending order by means of the heating elements located in the block underneath the test cells. At each specified test temperature, the AMO light source from the X-25 simulator was unshuttered, and an eight-point I-V characteristic was measured and electronically recorded using the Hughes 2500-1 data acquisition system.

TEST RESULTS

The raw I-V curve data was computer-reduced and each of the significant electrical output parameters, open circuit voltage, V_{oc}, maximum power voltage, V_{mp}, short circuit current, I_{sc} and maximum power current, I_{mp} was then plotted as a function of temperature. Figures A-1a and b contain, respectively, the V_{oc}/V_{mp} versus temperature plots and the I_{sc}, I_{mp} versus temperature plots for the average of the various GaAlAs cells at each temperature. In a similar manner, Figures A-2a and b contain respectively the V_{oc}, V_{mp} versus temperature plots and the I_{sc}, I_{mp} versus temperature plots for a typical measurement sequence of the silicon control cell.

The trend of the data indicates general improvements in V_{oc}, I_{sc} and curve factor of the GaAlAs cells since measurements of similar nature on prototype cells were taken early in the program. The data on the silicon cell is presented to illustrate the inherent superiority of the GaAlAs at high temperature, particularly with respect to the voltage parameters.

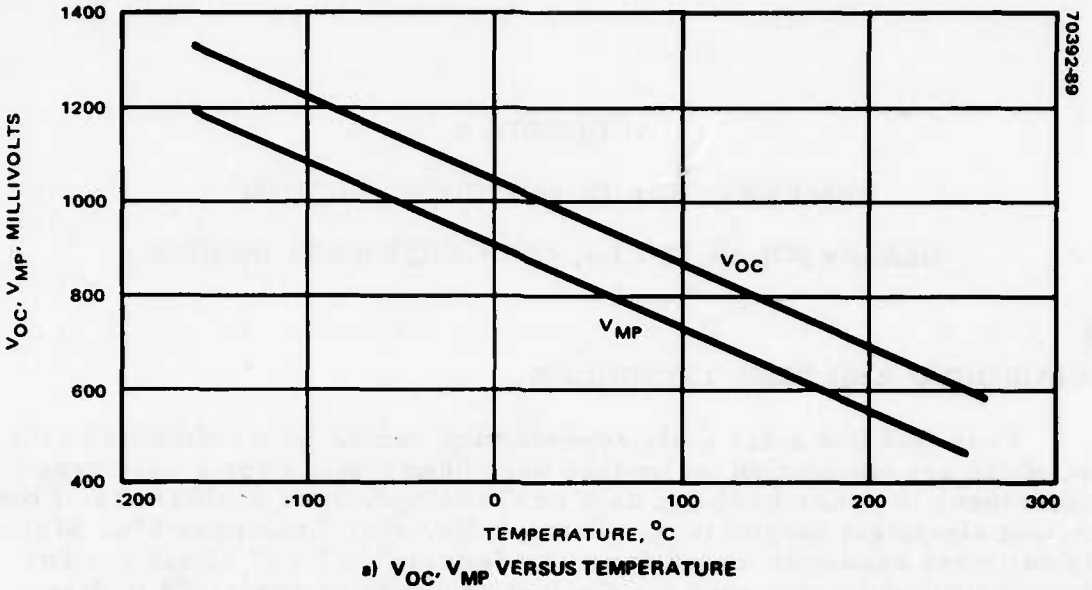

a) V_{OC}, V_{MP} VERSUS TEMPERATURE

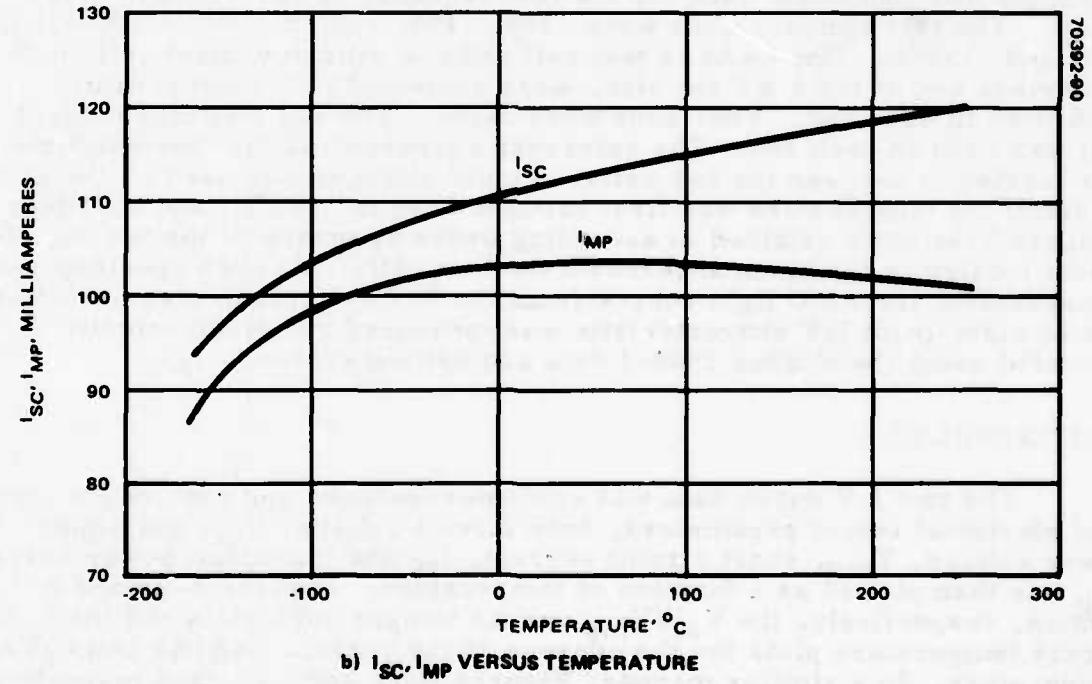

b) I_{SC}, I_{MP} VERSUS TEMPERATURE

FIGURE A-1. (AlGa)As-GaAs SOLAR CELLS

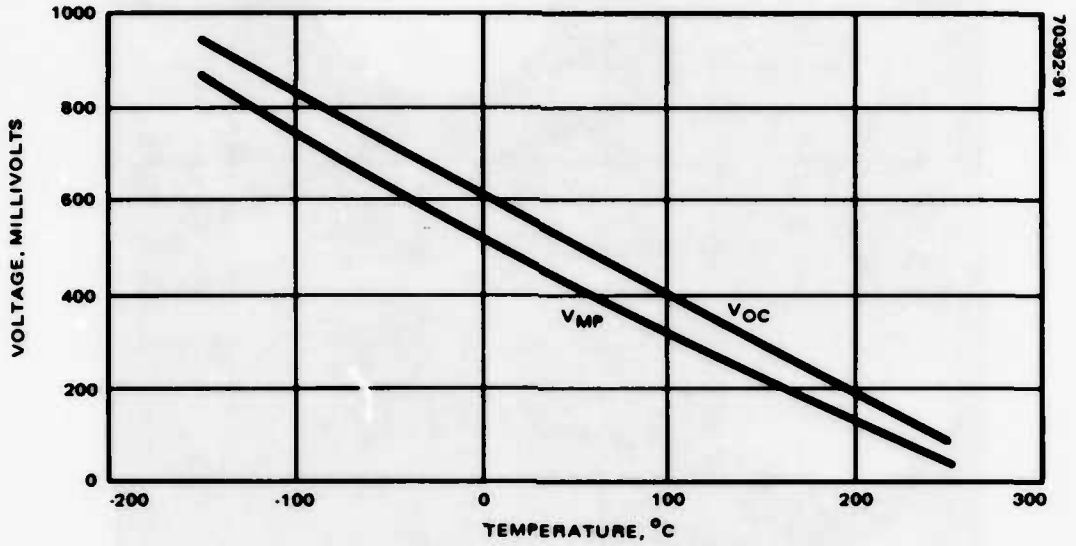

a) V_{OC}, V_{MP} VERSUS TEMPERATURE

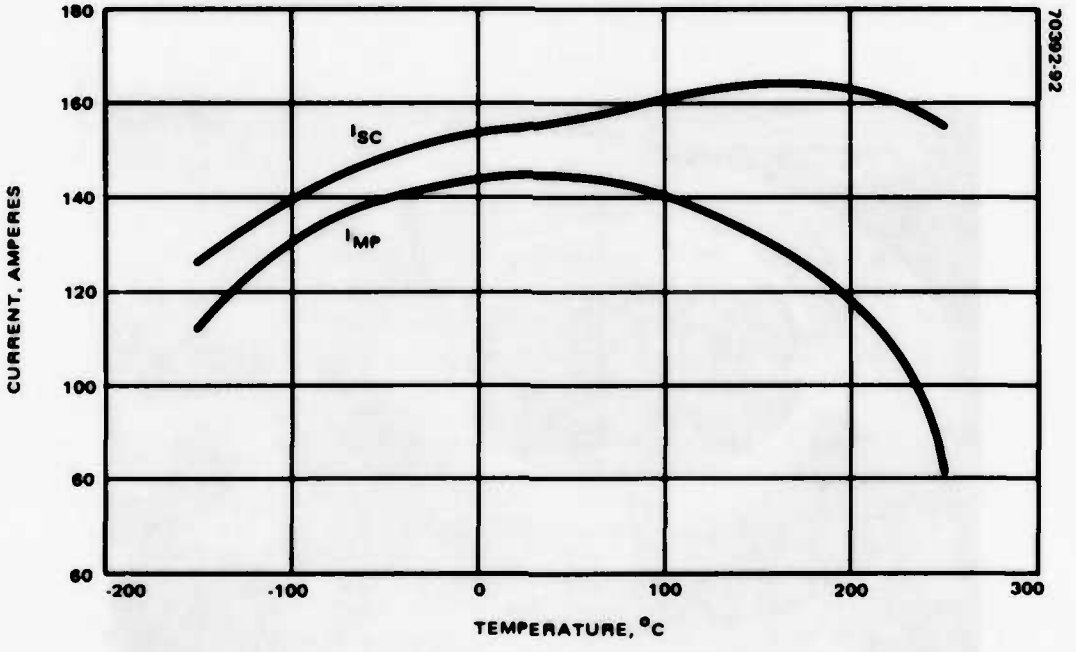

b) I_{SC}, I_{MP} VERSUS TEMPERATURE

FIGURE A-2. SILICON CONTROL CELL (PV-K6)

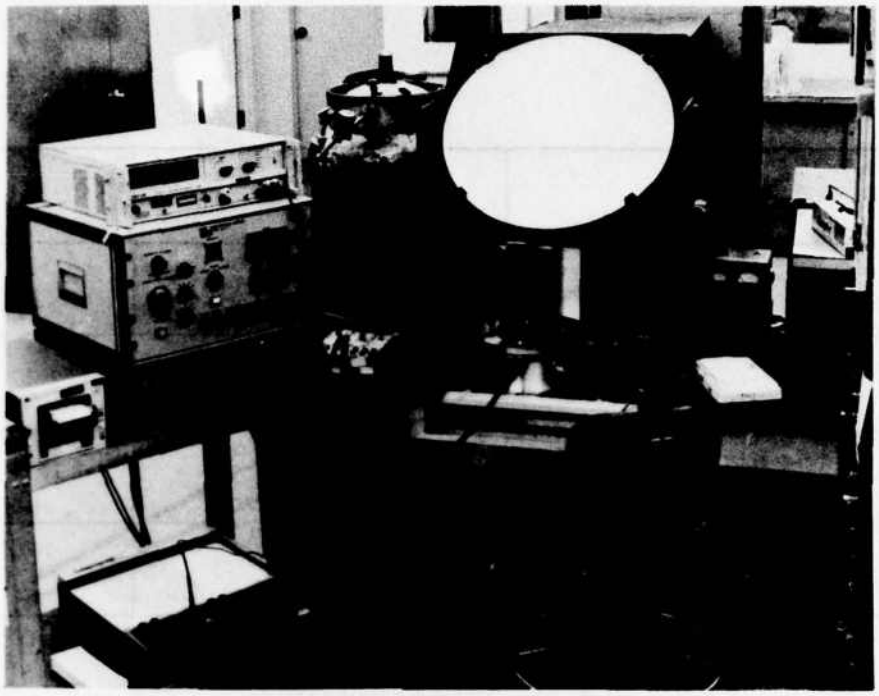

70392-93

FIGURE A-3. TEMPERATURE COEFFICIENT MEASUREMENT SYSTEM

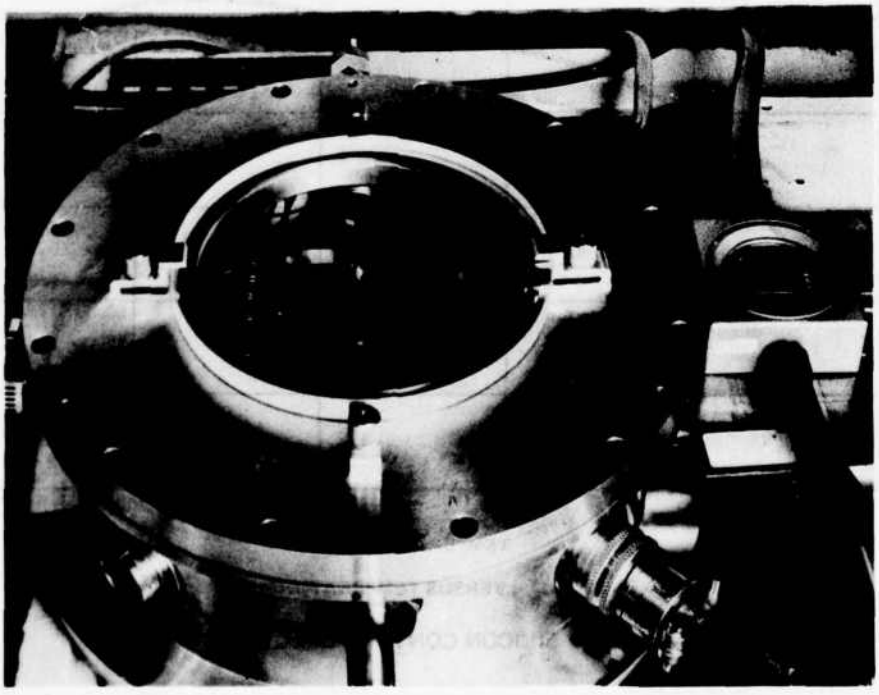

70392-94

FIGURE A-4. TEMPERATURE COEFFICIENT MEASUREMENT FIXTURE

MEASUREMENT METHOD

Introduction And Background

The equipment and method used for the temperature coefficient measurement of solar cell assemblies are described below. Solar cell assembly characteristics were measured at temperatures from -160 to +250°C in 50°C increments. To accomplish these measurements, a fixture/data acquisition apparatus and test technique was used which allows a large number of measurements to be made accurately in a very short period of time. Other important considerations included the elimination of frost below 0°C and temperature drift at the time of the solar cell output measurement.

Test Equipment

Categories

The test equipment necessary for temperature coefficient measurements of photovoltaic devices comprises three basic categories: 1) equipment for simulating the thermal environment (i.e., providing the capability of reaching and maintaining a specified temperature above or below room ambient); 2) equipment for simulating air mass zero light; 3) data acquisition equipment (i.e., equipment for measuring and recording cell output).

Test Fixture (for temperature variation)

To simulate the thermal environment, a fixture was used from which the moisture could be excluded in order to prevent frost formation on the test cells at temperatures below 0°C. This was accomplished by using a fixture enclosed by a chamber in which the atmosphere can be excluded by either pumping a vacuum or by substitution with flowing dry nitrogen. Inside the chamber, the test cells are located on a thermally controlled test block. Thermal control is accomplished by flow of liquid cooling medium (LN_2) through the block and by electrical cartridge heaters mounted in the block. The highly transparent Supersil II window on the top of the fixture allows AMO light to reach the active surfaces of the test cells. Thermocouples attached to the block by positive tension spring probes, which make the electrical contact to the top of the cell. The electrical and thermal contact to the cells is made to the back of the cells by pressure contact to the test block. The temperature coefficient fixture is shown in Figure A-3, where the fixture is shown together with the X-25 and Hughes Aircraft Company data acquisition system. A close-up photo, taken through the fixture window of test cells mounted on the thermally controlled block, is shown in Figure A-4.

Solar Simulator

The Hughes Aircraft Company X-25 solar simulator, Hughes Aircraft Company ID H946269, was used as the AMO light source for the tests. Test

solar cells mounted in the fixture are calibrated relative to a secondary standard solar cell of a similar design type. The secondary standard in turn was calibrated relative to a primary balloon standard of a similar type cell.

Data Acquisition System

The Hughes 2500-1 data acquisition system, Hughes Aircraft Company ID H328309, was used to measure the characteristic outputs of the solar cells at the different temperatures. With this system, the solar cell output curve is measured during a nominal 525 μs interval with an electronic eight-step moving load. The first step is always the short circuit current condition, and the eighth point is normally set for open circuit voltage. The eight readings of the characteristic curve are then printed out on a paper tape by an auxiliary high speed printer. Each of the data points consists of three lines of printed information channels; the first is the reading of the intensity standard cell; the second is the test cell load point voltage; the third is the test cell load point current. The printed current value is automatically corrected by the ratio of the AMO I_{sc} value of intensity standard cell to the actual measured I_{sc} of the intensity standard.

This type system was used rather than an electronic continuous sweep load because of the extremely short measurment time, 1/2 ms versus approximately 8 seconds. This reduced the amount of error due to temperature drift while the measurement of output is being taken.

METHOD

The basic test method consisted of the following: two 2 x 2 cm cells were placed in each of the test positions. The cells were measured at -160, -100, -50, 0, +50, +100, +150, +200 and +250°C under constant AMO illumination from the X-25. The two cells were measured at each of the temperatures in an ascending or descending sequence depending on the last temperature of measurement of the previous two cells. This was done to average out possible thermal lag effects. The six termocouples at the extremities of each cell, top-right, center and left, bottom-right, center and left, were read in parallel so that an average temperature was obtained for each output characteristic.

LH_2 was used as the coolant and was bucked by a constant current setting on the heater to approach and dwell at a particular measurement temperature. The time of the dwell was long enough to enable the taking of three separate measurements of the test cell output characteristic, approximately 15 to 60 seconds.

APPENDIX B

CONCENTRATED AND FILTERED ILLUMINATION GaAlAs SOLAR CELL OPERATION

INTRODUCTION

Photovoltaic solar cells are unable to utilize photons less energetic than their bandgap energy. The unused photons that are absorbed result in cell heating and no power production. Larger bandgap energy photovoltaic materials (i.e., GaAlAs) are under development that use even less of the solar spectrum than current silicon solar cells. A significant increase in the conversion efficiency in terms of reduced heat load is possible by the use of filtered light for these materials.

In January 1976, experiments were done with a GaAlAs solar cell using concentrated solar illumination. The purpose of this work was to demonstrate the reduced solar cell heat burden possible by selective filtration of the incident irradiation. The short circuit current of the solar cell was measured for incident fluxes of up to 500 mW/cm^2 for filtered and unfiltered light. The short circuit current was found to be directly proportional to the incident flux.

EXPERIMENTAL

The GaAlAs solar cell (No. 54) was mounted on a copper block calorimeter using a silver loaded conductive paint. An external 0.1 ohm resistor was used as an electrical load for the solar cell to measure the short circuit current. A biased and linearized 5,000 ohm thermistor was used to monitor the temperature of the copper block. Styrofoam and aluminum foil tape was used to insulate the sides and back of the copper block, while a multiple sheet aluminum foil/felt was used to mask around the solar cell area on the front side. A 102 mm biconvex glass lens (Edmund No. 94330, 250 mm focal length) was used to concentrate the solar energy. Different concentration ratios were achieved by changing the solar cell to lens spacing on an optical bench. A column of sunlight was tracked and positioned for the optics by a 12 inch square second surface plane glass mirror heliostat. The sky was clear and was approximately AM2 (air mass two). The temperature of the copper block and the solar cell short circuit current were strip chart recorded while a cardboard shutter was removed to expose the solar cell to different illumination levels. A minute of data was strip chart recorded before and after each exposure to allow for the graphic extrapolation of the temperature data to eliminate the heat diffusion time delay. A dichroic

filter (Edmund No. 30,635) was also used (at 45 degrees) for some of the exposures to remove a portion of the longer wavelength radiation in order to demonstrate the higher efficiency solar cell operation.

The data was analyzed by combining the caloric heat with the joule heating of the current sense resistor to obtain the energy input. The power output of the solar cell was approximated by multiplying the short circuit current by a factor (0.65) which is typical of a GaAlAs solar cell power to short circuit current ratio (Figure B-1). The results of the runs are shown in Table B-1. The solar cell efficiency is the ratio of output power to input power. A plot of the efficiency versus the short circuit current for all of the runs is shown in Figure B-2. Here it can be seen that the solar cell efficiency is independent of the concentration ratio up to the levels tested. In other words the solar cell short circuit current output is proportional to the concentrated solar power input. The filtered light runs show a higher conversion efficiency, as was expected. The filter used was not ideal, and its transmission is shown in Figure B-3.

CONCLUSIONS

Due to the unused light energy and other losses, the overall conversion efficiency in terms of total system intercepted area would not be higher for a filtered light system than for an unfiltered light system. The advantage of filtering is that less heat has to be removed from the solar cells. The unused concentrated solar energy may be discarded, used for silicon solar cells, and/or used for a high temperature heat application, such as a heat engine.

The lower heat input to the filtered light solar cell system allows for simpler heat removal and lower temperature operation. Lower temperature of operation results in higher output voltages and higher conversion efficiencies. Short wavelength reflecting dielectric filters are inexpensive and, thus, filtered light should be considered in any concentrated solar cell system using mirror optics.

TABLE B-1. CONCENTRATED AND FILTERED ILLUMINATION
GaAlAs SOLAR CELL OPERATION – TEST RESULTS

Run No.	t(s)	I(A)	H(J)	I^2Rt	ΣH	It	It/ΣH	x (0.65)
	Filter							
1	111.45	0.5416	160.6	3.3	163.9	60.4	0.369	0.240
2	98.0	0.568	141.4	3.2	144.6	55.7	0.385	0.250
3	70.6	0.568	105.6	2.3	107.9	40.1	0.372	0.242
4	101.0	0.452	120.0	2.1	122.1	45.1	0.374	0.243
5	109.4	0.328	106.0	1.2	107.2	35.9	0.335	0.218
6	93.4	0.260	66.0	0.6	66.6	24.3	0.365	0.237
7	128.0	0.188	68.4	0.5	68.9	24.1	0.350	0.228
								Average: 0.237 ± 0.010
	No Filter							
8	69.6	0.1216	34.0	0.1	34.1	8.46	0.248	0.161
9	105.6	0.1936	78.0	0.4	78.4	20.44	0.261	0.170
10	105.6	0.2768	104.0	0.8	104.8	29.2	0.279	0.181
11	96.0	0.4192	137.0	1.7	138.7	40.24	0.290	0.189
12	64.8	0.5904	122.6	2.3	124.9	38.3	0.307	0.200
13	49.4	0.5888	96.0	1.7	97.7	29.1	0.298	0.194
14	105.0	0.592	208.0	3.7	211.7	62.2	0.294	0.191
15	69.6	0.0496	12.4	0.02	12.42	3.45	0.278	0.181
								Average: 0.183 ± 0.013

LEGEND:

- t(s) Illumination period, seconds
- I(A) Solar cell short circuit current, amperes
- H(J) Calorimetric heat input, joules
- I^2Rt Resistor heat, joules
- ΣH Total heat input (H(J) + I^2Rt), joules
- It Total short circuit charge, coulombs
- It/ΣH Short circuit current to power input, amperes/watt
- x(0.65) (It/ΣH) x 0.65: Approximated conversion efficiency

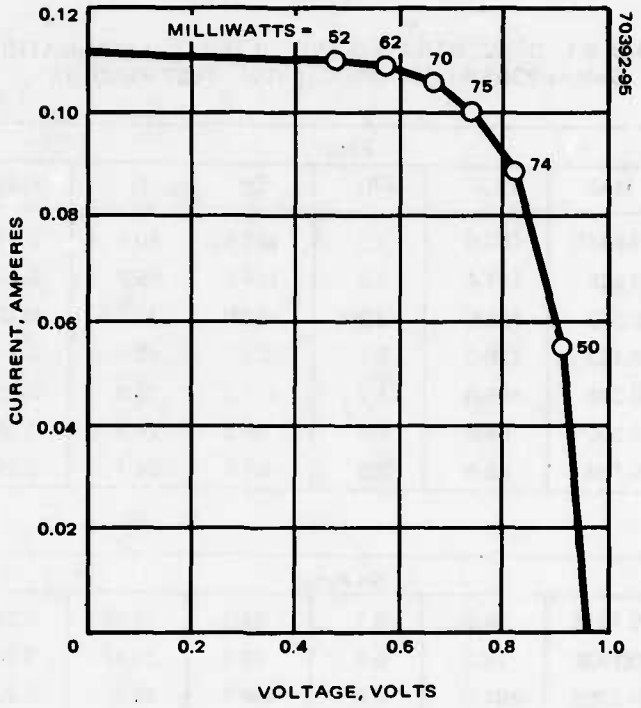

FIGURE B-1. GaAlAs SOLAR CELL POWER OUTPUT (CELL NO. 365)

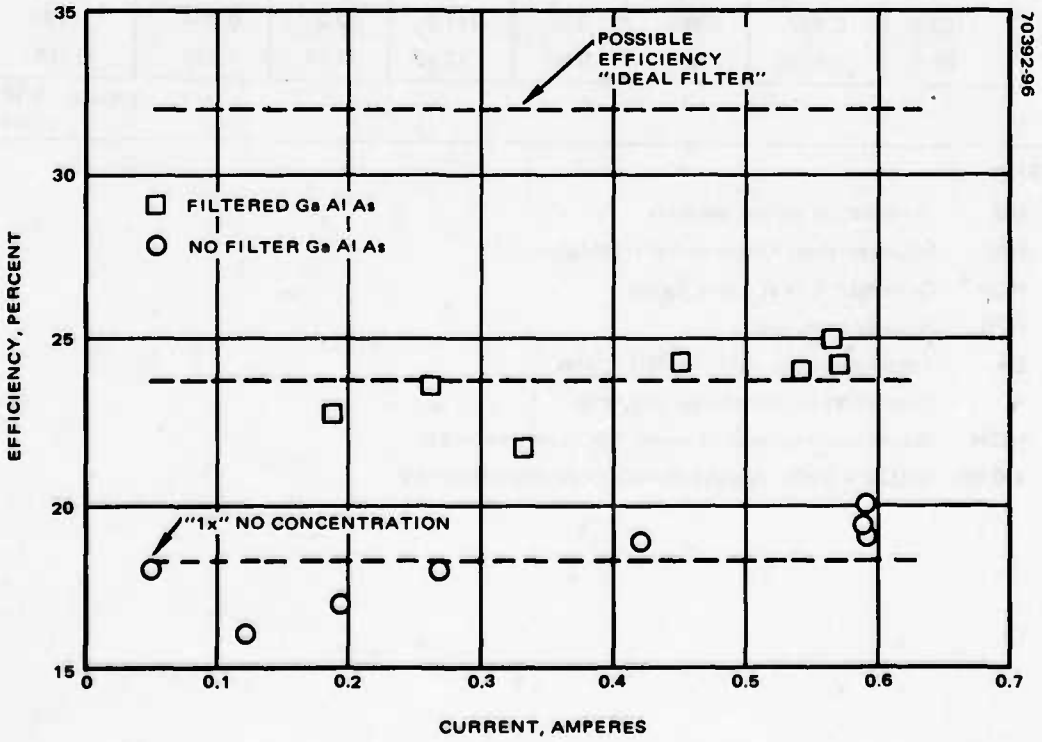

FIGURE B-2. EFFICIENCY VERSUS SHORT CIRCUIT CURRENT – ALL RUNS

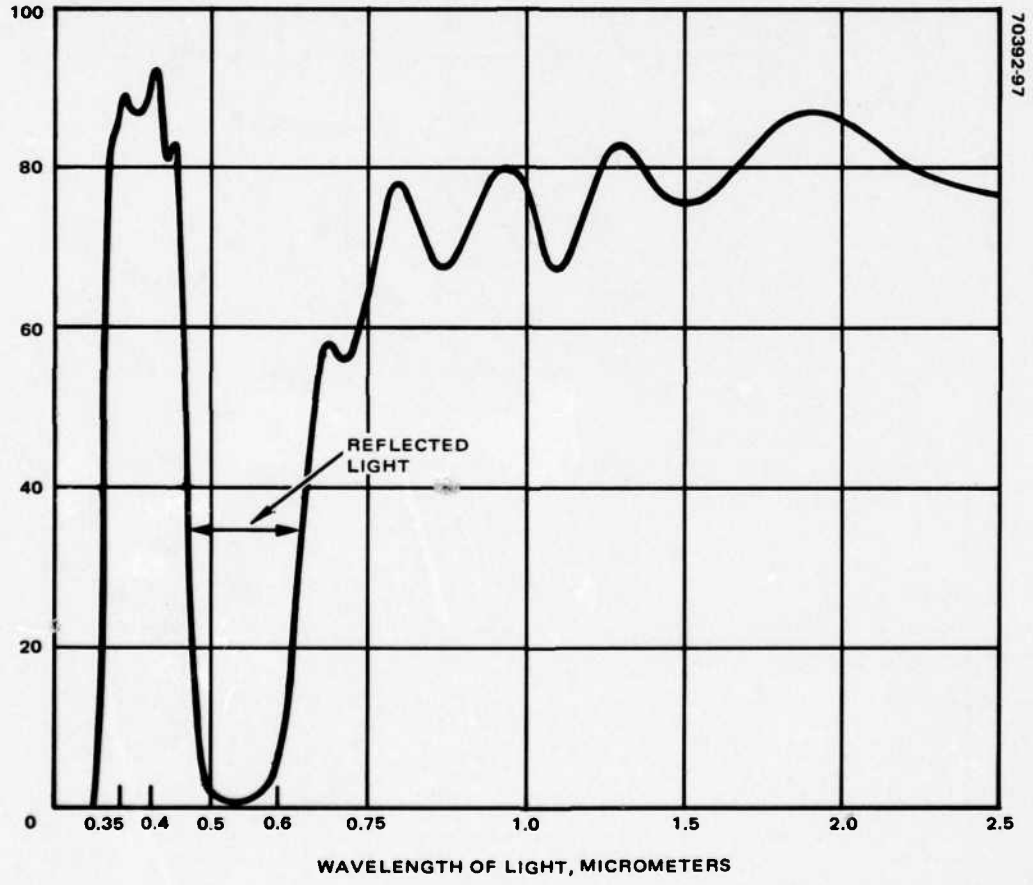

FIGURE B-3. EDMUND NO. 30,635 DICHROIC FILTER TRANSMISSION

APPENDIX C

CASSEGRAINIAN CONCENTRATOR

THERMAL ANALYSIS

DISCUSSION

Solar concentrators, while enhancing the solar cell output, also increase the thermal load on the cell. A multi-element concentrator allows the use of various dielectric coatings to reduce this thermal load. A long wavelength pass coating or cold mirror reflects the incident energy of wavelengths shorter than its cut-on wavelength and trasmits the long wavelength energy. A short wavelength pass or hot mirror reflects energy at wavelengths longer than its cut-off wavelength. Figure C-1 illustrates how by selecting appropriate cut-on and cut-off wavelengths, a selected band of wavelengths can be reflected onto the cell. Limiting the incident energy to the solar cell response reduces the thermal load at the cell.

The GaAs solar cell parameters are listed in Table C-1. The thermal load on the cell can be reduced by limiting the incident energy to 0.4 to 0.9 microns. As Figure C-2 illustrates, roughly 15 percent of the in band energy is reflected; the remainder is either absorbed or converted into electricity. That energy outside the cell response not reflected is absorbed.

The absorption of the cell over its active region can be calculated from its efficiency. For a GaAs cell, 15 percent of the incident solar energy is converted into electrical energy. Output from a 2 x 2 cm cell:

$$0.15 \times 4\ \text{cm}^2 \times 0.135\ \text{W/cm}^2 = 0.081\ \text{watts}$$

where $0.135\ \text{W/cm}^2$ is the solar constant. An alternate calculation using the maximum cell current of 0.098 amperes at 0.8 volts yields 0.078 watts. Table C-2 lists values of the solar constant in various spectral bands. Since the cell only responds in the 0.4 to 0.9 micron band, its inband efficiency is:

$$\frac{0.081}{4 \times 0.074} = 0.27$$

Since 15 percent of the inband energy is reflected and 27 percent is converted into electrical energy, the remainder of the energy in the 0.4 to 0.9

TABLE C-1. GaAs SOLAR CELL PARAMETERS

Size	2 x 2 cm
Response	0.4 to 0.9
α_S	0.75
ϵ_{TH}	0.82
Efficiency	0.15
Efficiency derating	0.025%/°C
Maximum temperature	200°C

TABLE C-2. SOLAR CONSTANT = 0.135 W/cm^2

Wavelength Region	Fraction of Solar Constant	Energy Density, W/cm^2
0.4	0.087	0.012
0.4 to 0.9	0.547	0.074
0.9	0.366	0.049

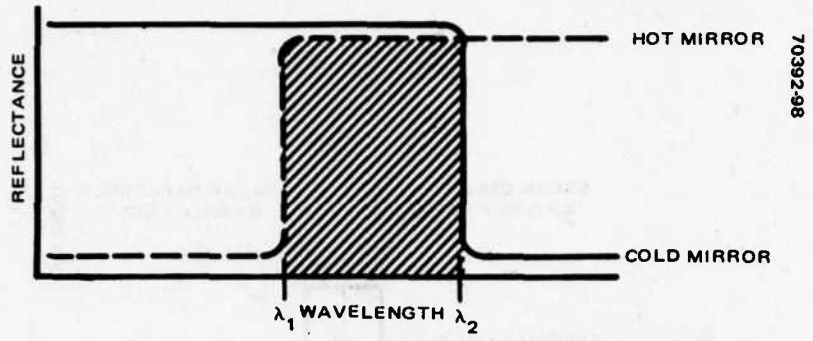

FIGURE C-1. COMBINING HOT AND COLD MIRRORS

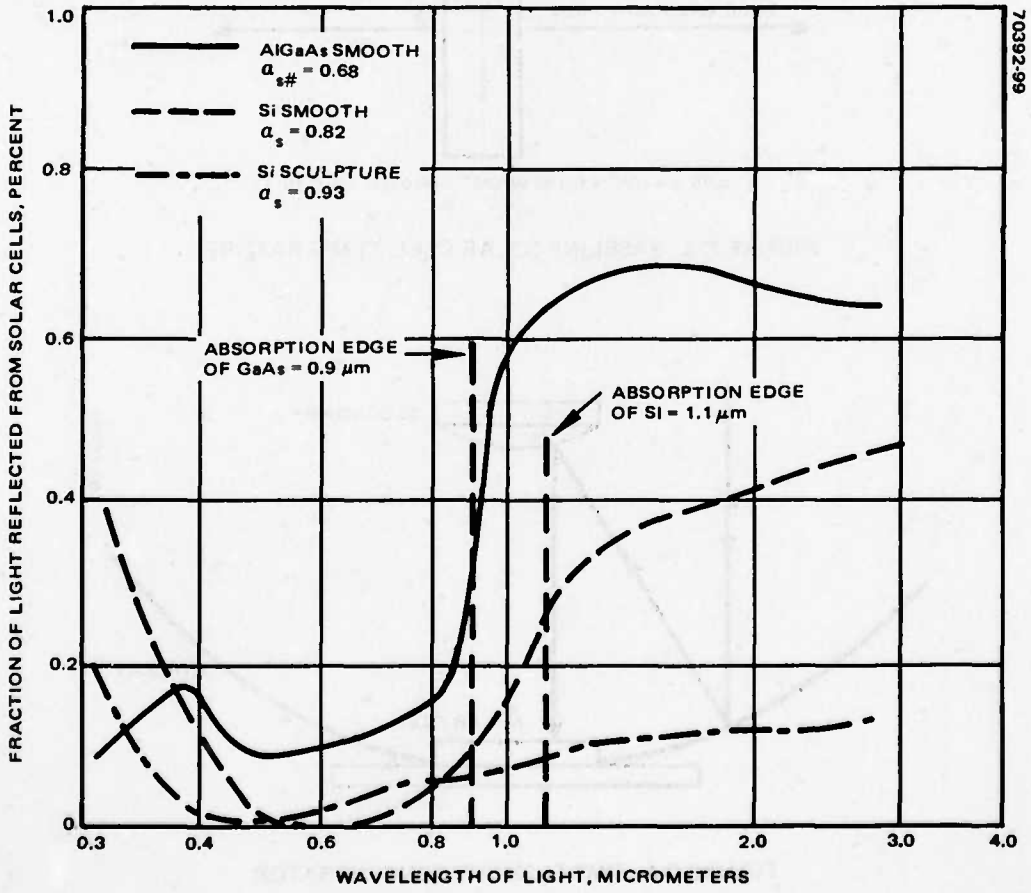

FIGURE C-2. SOLAR ABSORPTIVITY OF SOLAR CELLS

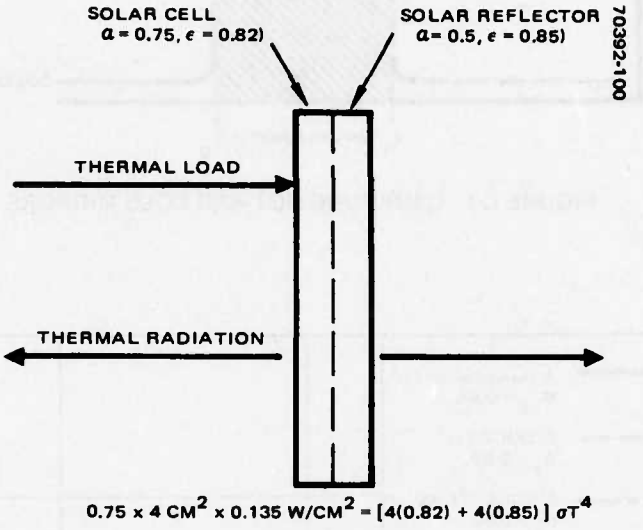

FIGURE C-3. BASELINE SOLAR CELL TEMPERATURE

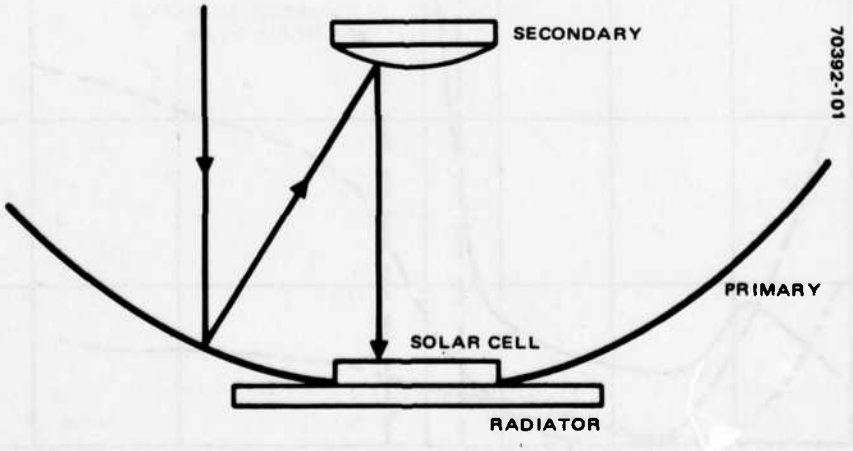

FIGURE C-4. TWO-ELEMENT CONCENTRATOR

micron region is absorbed, that is 0.58 x 4 x 0.074 = 0.172 watts per cell is absorbed. Of the inband energy not reflected, 32 percent is converted into electricity:

$$\frac{0.081}{4 \times 0.074 \times 0.85} = 0.32$$

If the cell were perfectly anti-reflection coated, its output would increase by 5 percent since 0.32 x 0.15 = 0.05.

One of the simplest means of removing heat in space is through a passive radiator. These passive radiators physically are dielectric coatings on a thin quartz substrate. The coatings are designed to have low solar absorptance ($\alpha = 0.05$) and high emittance ($\epsilon = 0.85$). An example best illustrates what this low α/ϵ ratio implies. Consider two 2 x 2 cm samples bonded together, in space, one side looking at the sun, the other into deep space. The heat load is just:

$$\alpha_s \times \text{area} \times \text{solar constant} = \text{heat load}$$

$$0.05 \times 4\ \text{cm}^2 \times 0.135\ \text{W/cm}^2 = 0.027\ \text{watts}$$

Since two surfaces are available for radiating this heat, the thermal balance equation yields:

$$0.027\ \text{watts} = 2 \times \text{area} \times \sigma\, T^4$$

$$0.027\ \text{watts} = 2 \times 4\ \text{cm}^2 \times 0.85 \times 5.67 \times 10^{-12}\ \text{W/cm}^2/\text{K}^4 \times T^4$$

Solving for T, the equilibrium temperature of the structure

$$T = 163^\circ\text{K} = -110^\circ\text{C}$$

The baseline solar cell temperature can be derived in a similar manner. A solar cell, backed with a solar reflector as shown in Figure C-3, reaches an equilibrium temperature of 322°K or 49°C.

Typical of multi-element concentrators is the Cassegrainian type reflector drawn in Figure C-4. This structure has two elements, a primary and a secondary mirror; this allows two different dielectric coatings to be used. The solar reflector panels are used in two locations, one on the sun side of the secondary and the other on the solar cell radiator.

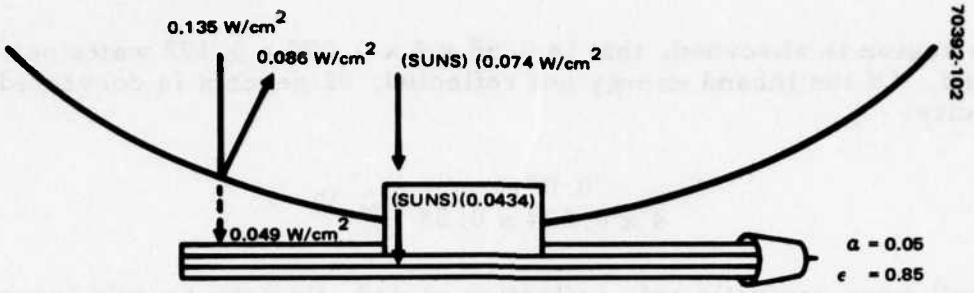

FIGURE C-5. SOLAR CELL RADIATOR THERMAL LOAD

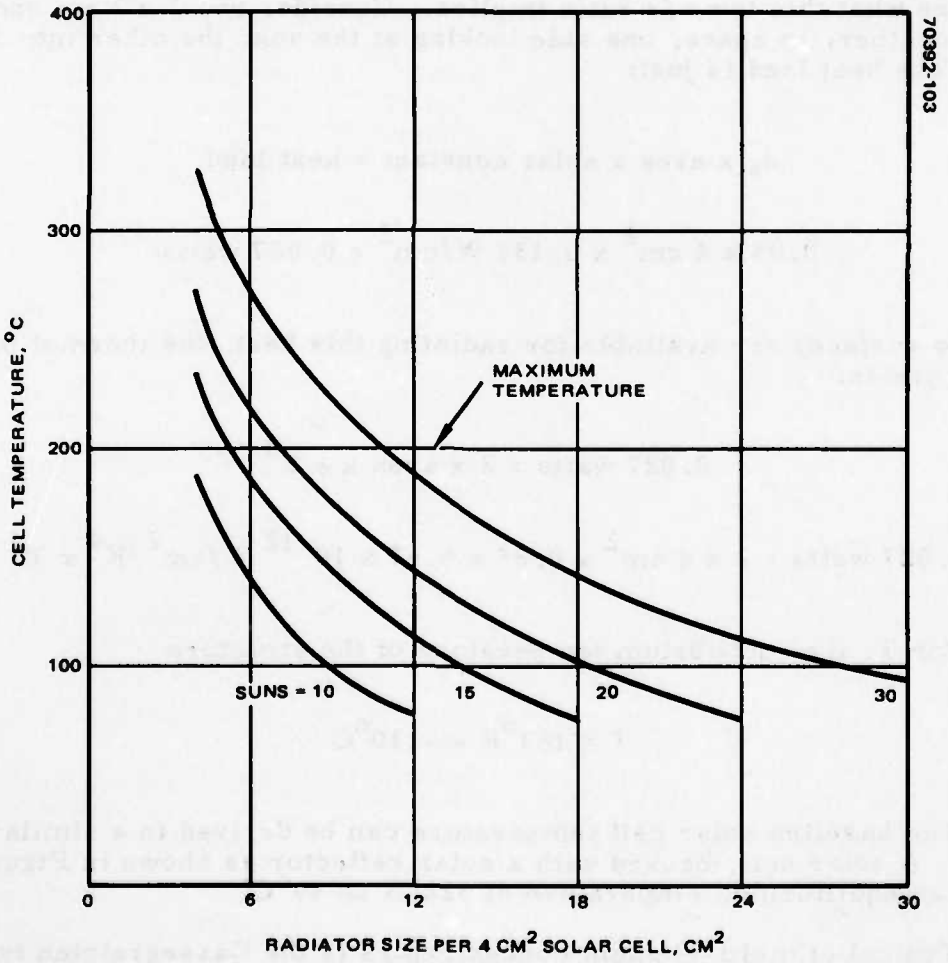

FIGURE C-6. CELL TEMPERATURE VERSUS RADIATOR SIZE

An option exists for the primary to use either a hot or cold mirror. For the GaAs cell, a hot mirror reflects 88 percent of the solar constant to the secondary, while a cold mirror reflects 63 percent. To reduce the heat load on the secondary, a cold mirror is used on the primary with a cut-on at 0.9 micron. This allows 63 percent of the solar constant to be reflected into the secondary with the remainder "transmitted" through the primary. In reality, depending on the coating used on the back surface of the primary, only a fraction of the energy would actually be radiated behind the primary. However, for a worse case of back loading on the solar cell radiator, it is assumed that all this energy is radiated.

At the secondary, a hot mirror is used with a cut-off at 0.4 micron. Energy of wavelengths shorter than 0.4 micron is absorbed by the secondary. The energy from 0.4 micron to 0.9 micron (reflected by the primary) is reflected to the solar cell. In this fashion, only energy between 0.4 and 0.9 micron will reach the solar cells.

From Figure C-5, there are two sources of thermal loading on the radiator, the energy absorbed by the solar cell (0.172 W/cm^2 per cell per sun) and the energy transmitted by the primary (0.050 W/cm^2). It is assumed that the cell is thermally isolated from the primary. The thermal input side of the heat balance equation then becomes:

$$(\text{no. of suns}) \times 0.043\ W/cm^2 \times 4\ cm^2 + 0.049\ W/cm^2 \times 0.05 \times (X - 4\ cm^2)$$

where X is the area of the radiator (back-surface). The radiative side has three contributions:

$$[4\ cm^2 \times 0.82 + X \times 0.85 + (X - 4\ cm^2) \times 0.85]\ \sigma \times T^4$$

The first term is radiation by the cell itself; the second, by the side of the radiator away from the primary; the third, by the side of the radiator facing the primary.

The equilibrium temperature of the cell is plotted as a function of the radiator size parametric with solar concentration in Figure C-6. The smallest radiator size is 4 cm^2, just covering the back of the cell. To stay below the 200°C limit with a 15X concentrator requires a 5 cm^2 radiator, while 30X requires 11 cm^2. The thermal loading caused by the primary is negligible in comparison to the solar cell load. Thermal loading of the solar cell radiator is therefore independent of the type of coating on the primary.

The radiator areas are not significantly larger than the cells themselves and are much smaller than the primary required for the various concentrations. Depending on how the primary is actually constructed, it may be feasible to allow a thermal path between the cells and the primary. The

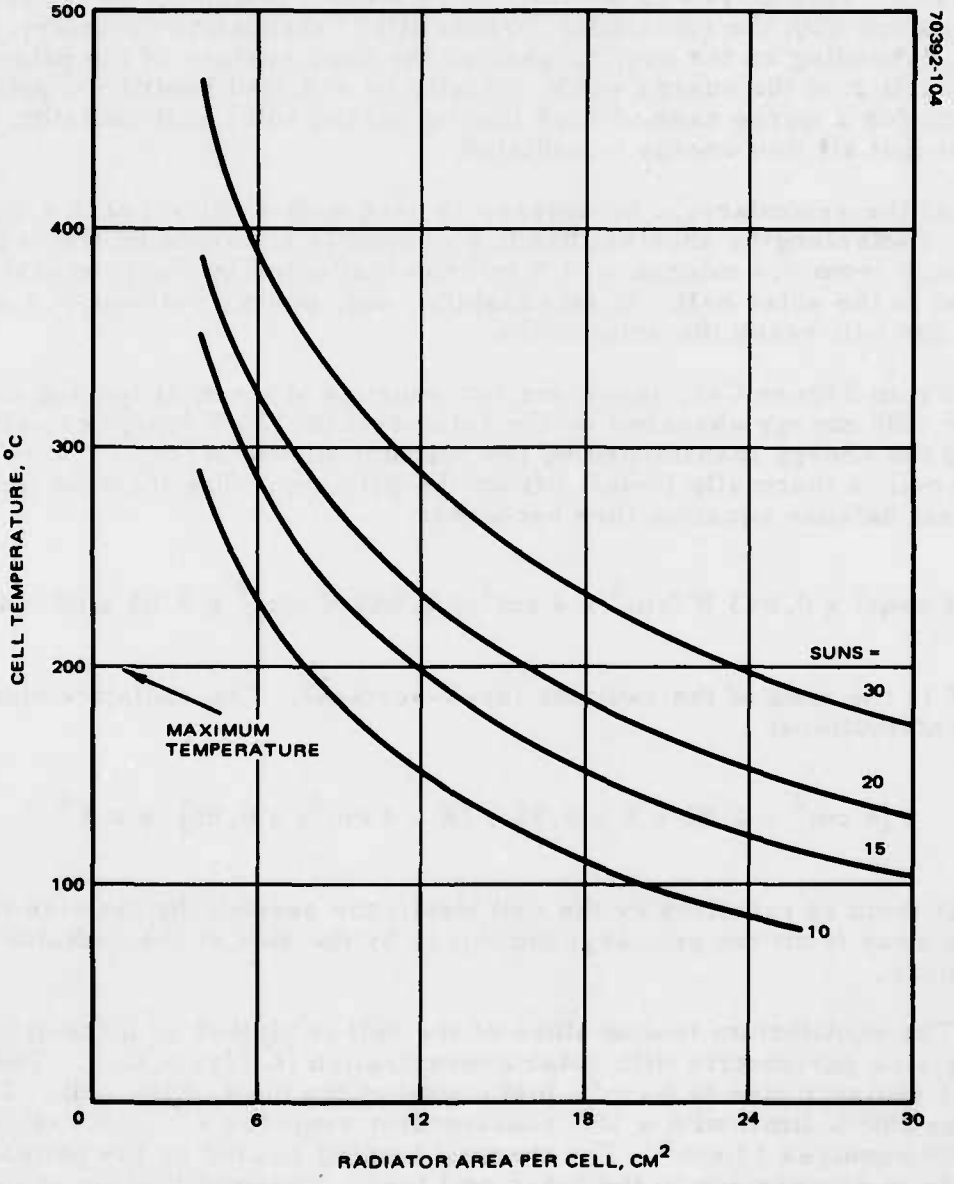

FIGURE C-7. CELL TEMPERATURE WITHOUT DIELECTRIC COATINGS

primary, with solar reflector panels bonded to its back surface, then also acts as radiator. Such an approach minimizes the weight and reduces packaging requirements.

The advantage of using dielectric coatings is demonstrated by assuming that the total concentrated solar energy is incident on the cell. The radiative side of the balance equation remains the same, while the load side becomes:

$$(\text{no. of suns}) \times 0.135\ \text{W/cm}^2 \times 4\ \text{cm}^2 \times 0.72$$

where 0.72 is the solar absorptance of the solar cell. Figure C-7 gives the radiator sizes as in Figure C-6, but without the use of wavelength selective coatings. A 15X concentrator, to keep the cell below 200°C, requires a radiator of 12 cm^2 and a 30X concentrator 24 cm^2.

The secondary uses a hot mirror with a cut-off at 0.4 micron. An analysis was made of the secondary taking into account the dielectric coating, quartz substrate, and solar reflector as shown in Figure C-8. The thermal load per unit area is divided into three terms:

Mirror:	(absorption) x (no. of suns) x 0.63 x 0.135
Substrate:	0.012 x (no. of suns) x 0.135
Solar reflector:	0.05 x 0.135

The dielectric materials used in the mirror coating have some absorption ranging from 1 to 6 percent. With a cold mirror on the primary, 63 percent of the solar constant is incident of the secondary. The cold mirror reflects energy above 0.4 micron, and the substrate absorbs the transmitted energy, that is energy below 0.4 micron. From Table C-2, this is 1.2 percent of the solar constant. The solar reflector ($\alpha = 0.05$) will be looking directly at the solar constant.

Thermal radiation is possible from both the coating and the solar reflector:

$$(0.85 + 0.8)\ \sigma\ T^4$$

The equilibrium temperature of the secondary is plotted in Figure C-8 against solar concentration for various coating absorptions. Assuming 6 percent coating absorption and a solar magnification of 10 at the secondary yields 35°C as an operating temperature, well within thermal limits of the structure.

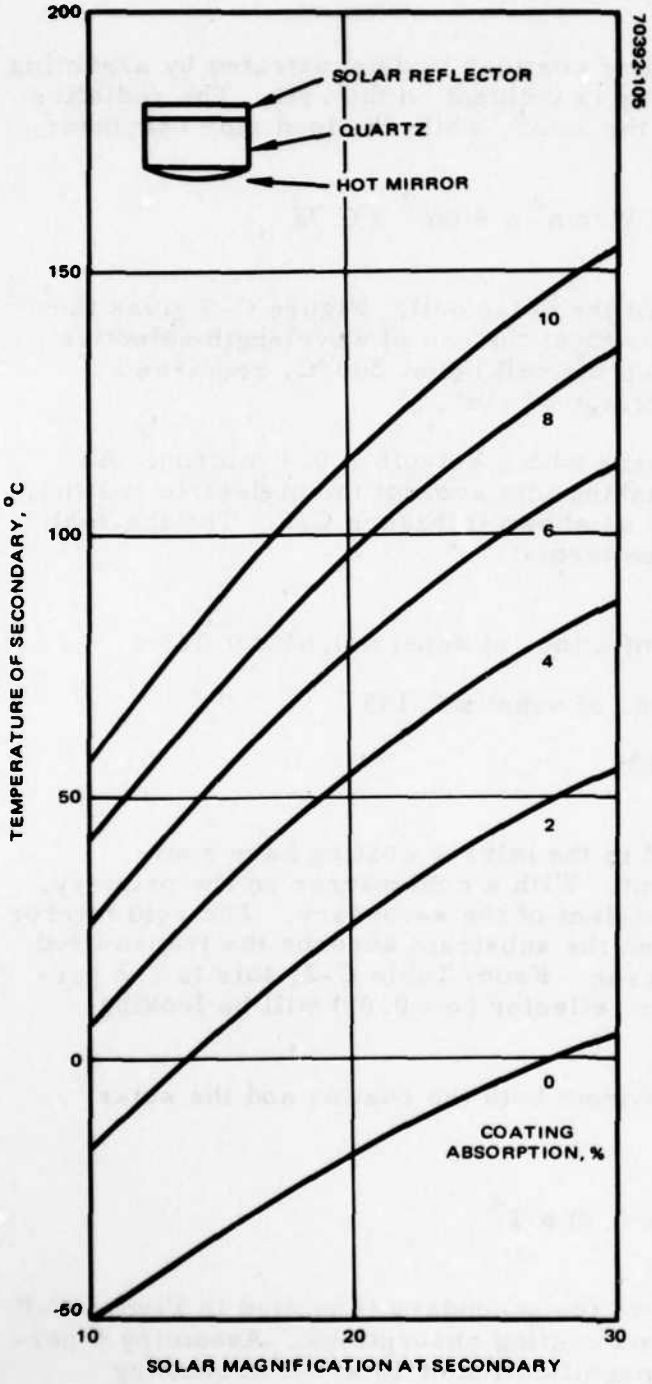

FIGURE C-8. SECONDARY TEMPERATURE (COLD MIRROR PRIMARY)

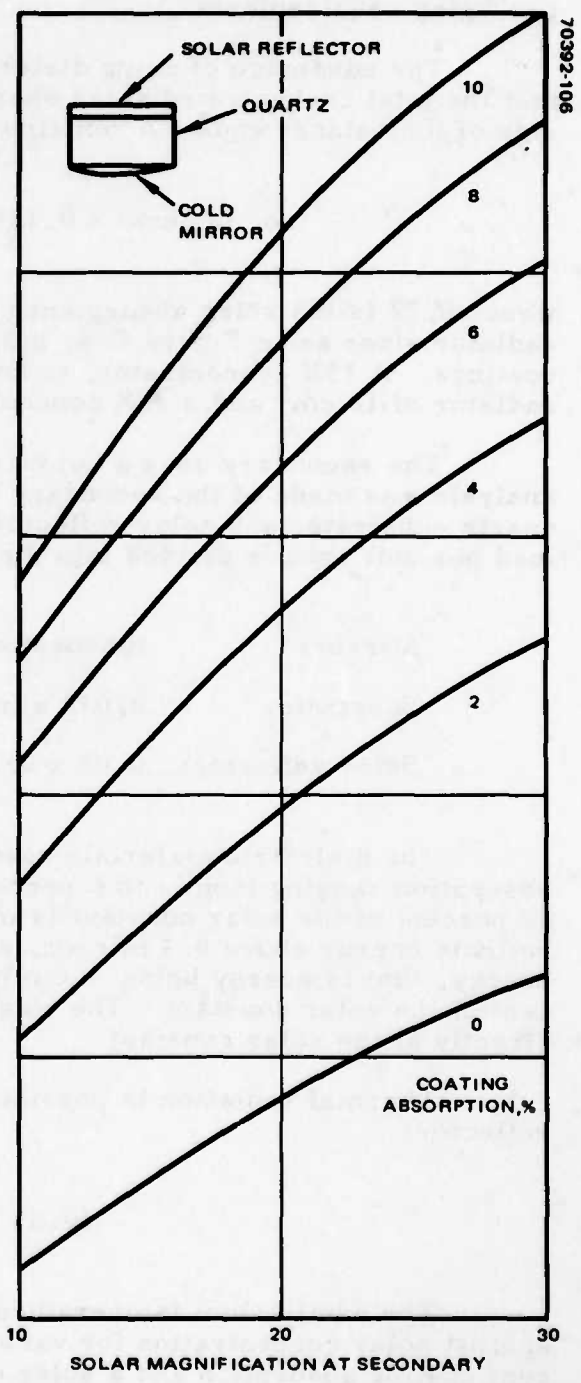

FIGURE C-9. SECONDARY TEMPERATURE (HOT MIRROR PRIMARY)

For comparison, Figure C-9 is the same data for a hot mirror on the primary and a cold mirror on the secondary. For 6 percent coating absorption and a solar magnification of 10, the secondary temperature is 55°C.

SUMMARY

This analysis has presented thermal tradeoffs on various dielectric coatings and passive radiator. On the basis of this analysis, a cold mirror is recommended for the primary and a hot mirror for the secondary, with passive radiators on the secondary. The GaAs solar cell can be operated well below its 200°C limit in a high concentration environment with current technology. Depending on final cost/weight tradeoff, it may be feasible to use a high emissivity paint on the cell radiator in place of solar reflectors. A cost/weight saving may also be realized by mechanical packaging to allow the primary to double as the radiator for the solar cells.

APPENDIX D

CASSEGRAINIAN CONCENTRATOR

OPTICAL ANALYSIS

It is desired to image the sun onto a solar energy panel approximately 2 cm wide by 10 cm long, each solar energy cell being 2 cm square. Since the sun subtends approximately $1/2^{o}$ at the earth, an optical system of 230 cm focal length will form a 2 cm diameter image of the solar disk. However, a cylindrical optical system is required, as the image of the sun should be 2 cm by 10 cm. To achieve a 15:1 optical gain, the width of the optics should be at least 30 cm in the plane of optical power and 10 cm in the perpendicular plane (width equal to solar panel length); in the plane of optical power, this is an f/7.7 optical system.

One obvious possiblity for the optical system would be a refractive lens; to minimize weight, a plastic Fresnel lens would be used. Low-cost, aspheric Fresnel lenses are readily available that would be more than adquate from an image quality standpoint. Figure D-1a is a 1/5 scale computer drawing of typical f/7 Fresnel lens system.

From Figure D-1a, it is apparent that one obvious drawback to using a single refracting element is the extreme length of the system. To significantly shorten the system, a Cassegrain optical system can be used. If an f/1 primary mirror is used and the image formed by the Cassegrainian lies at the plane of the primary mirror, an optical system such as that shown in Figure D-1b results; this is an f/6.2 Cassegrain. Both optical systems shown in Figure D-1 have a 15:1 optical gain after transmittance, and obscuration losses have been taken into account. The compactness of the Cassegrainian is quite dramatic as compared to the Fresnel lens.

In production, the two conic mirrors used in the Cassegrain can be replicated optics, thereby keeping their cost down. Being more compact than the Fresnel lens system, the Cassegrainian should be easier to deploy and track the sun better, although positioning tolerances on the secondary mirror will be relatively tight due to the magnification of this element. Table D-1 gives optical parameters of the Cassegrainian; Table D-2 is a computer listing of this lens.

A. f/7.0 FRESNEL LENS

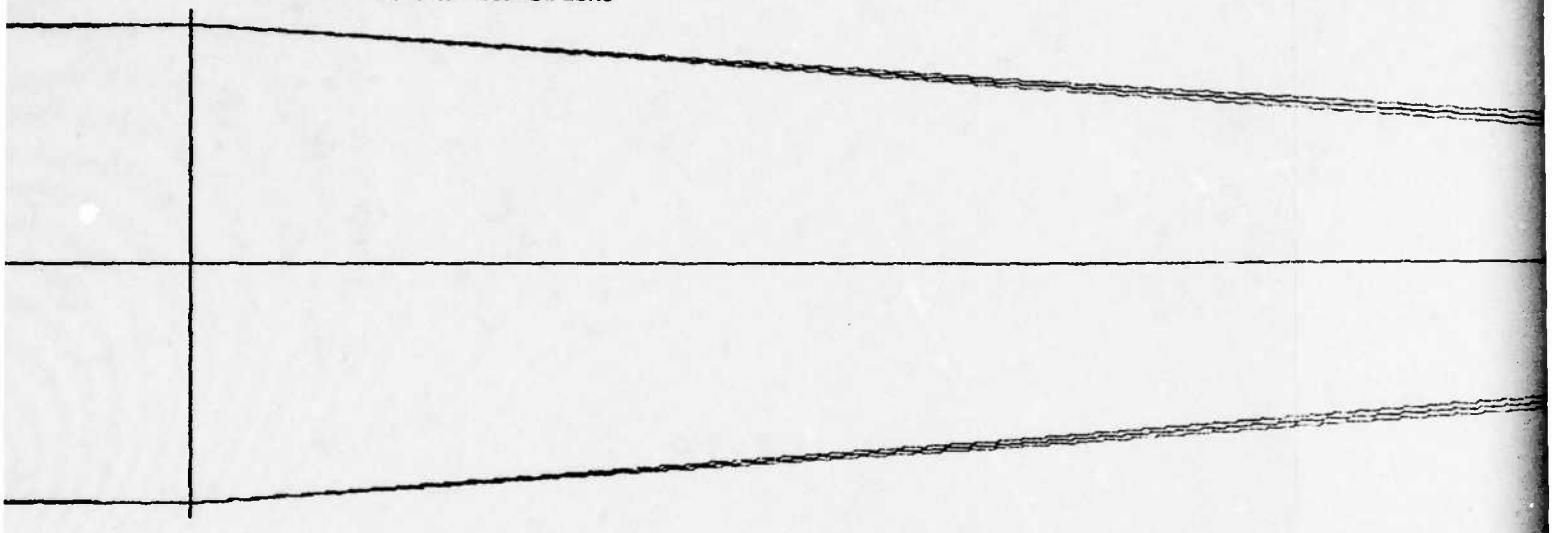

X SCALE 1 IN. = 12.7000
Y SCALE 1 IN. = 12.7000

FIGURE D-1. SCHEMATICS OF POSSIBLE CASSEGRAIN OPTICAL SYSTEMS

AD-A051 851 HUGHES AIRCRAFT CO EL SEGUNDO CALIF SPACE AND COMMUN--ETC F/G 10/2
GAAS CONCENTRATOR PHOTOVOLTAIC POWER SYSTEM FEASIBILITY INVESTI--ETC(U)
DEC 77 S KAMATH, R C KNECHTLI, S SCHWARTZ F33615-76-C-2142

UNCLASSIFIED SCG-70392P AFAPL-TR-77-80 NL

2 OF 2
AD
A051851

END
DATE
FILMED
4-78
DDC

70392-107

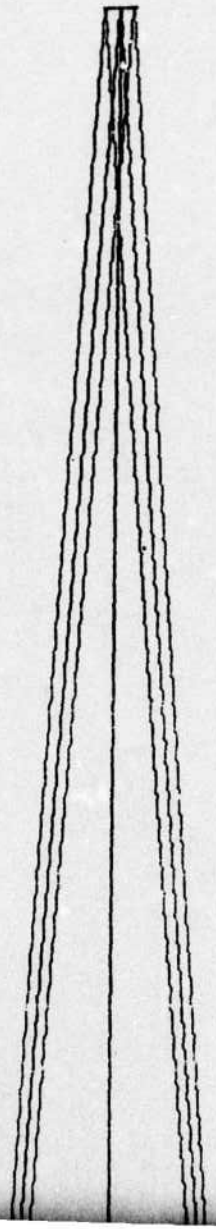

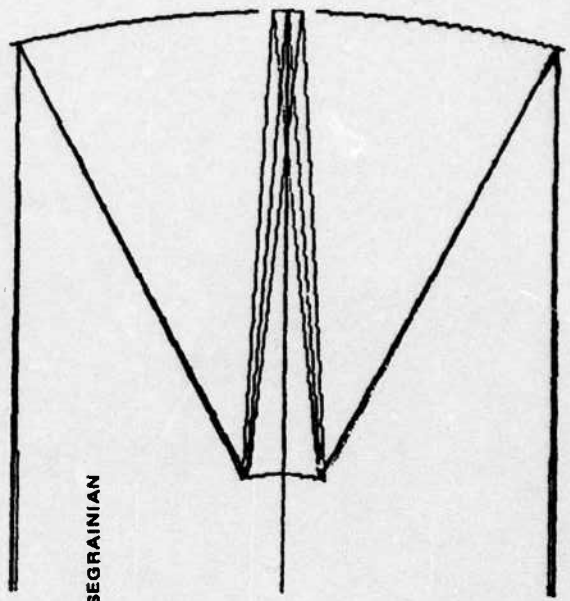

B. 1/6.2 CASSEGRAINIAN

TABLE D-1. CASSEGRAINIAN PARAMETERS

Parameter	Value
Effective focal length	230.0 cm
Entrance aperture diameter	37.0 cm
f/number	f/6.2
Field of view	1/2° circular
Radius of curvature and f/number of primary parabolic mirrors	74.0 cm, f/1.0
Radius of curvature and conic constant of secondary hyperbolic mirror	12.22 cm, cc = -1.914
Linear obscuration ratio	0.16
Primary - secondary axial spacing (equal to secondary-to-image spacing)	31.87 cm

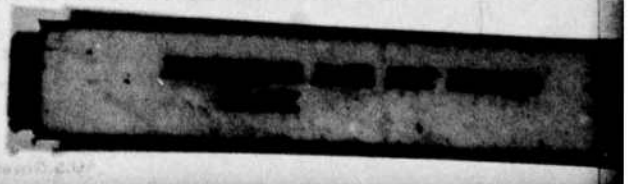

TABLE D-2. COMPUTER PRINTOUT OF CASSEGRAIN

```
   TESCO CASSEGRAIN

BASIC LENS DATA

SURF          RD                TH          MEDIUM                RN          DF
  0           .0          .1000000D+20       AIR

  1      -71.0000          -31.8727          MIRROR

  2      -13.2235           31.8727          MIRROR

  3           .0                .0          AIR


CC AND ASPHERIC DATA

SURF        CC              AD              AE              AF              AG
  1   -1.0000
  2   -1.9138          .0              .0              .0              .0

PICKUPS

SURF    TYPE        J          A              B
  2     TH          1   -1.000          .0

SOLVES

SURF    TYPE    PARAMETER       VALUE       SLV DATUM
  2     PUY         CV          -.6162690D-01 -.6043480D-01

 REF OBJ HT                     REF AP HT    OBJ SURF   REF SURF   IMG SURF
 -.4966335D+17(    6.25 IG)     18.50000          0          1          3

         EFL             BF              F/NO            LENGTH          DIM
     230.00000          .0              6.2162162          .0           1.0635707

LENS IS CURRENTLY IN CFG 1

WAVL NBR            1          2          3          4          5
WAVELENGTH      0.60000    0.60000    1.00000    0.0        0.0
SPECTRAL WT      1.0000     0.5000     0.5000     0.0        0.0

APERTURE STOP AT SURF   1

LENS UNITS ARE CM'S

EVALUATION MODE IS FOCAL

PRIMARY CHROMATIC WAVELENGTHS ARE 2 - 3

SECONDARY CHROMATIC WAVELENGTHS ARE 2 - 1
```


*U.S.Government Printing Office: 1978 — 757-080/389

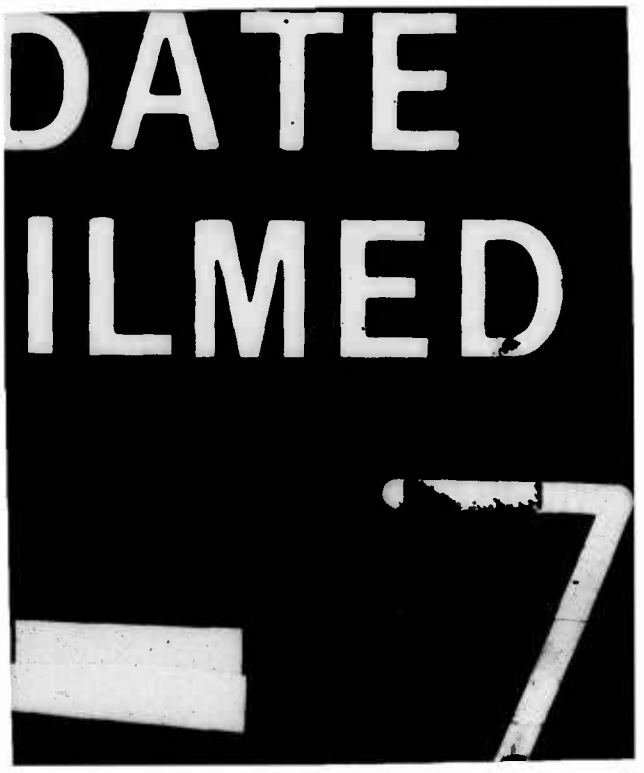
DATE
ILMED